

**Ground-Water Resources Program
National Cooperative Geologic Mapping Program**

Simulation of Ground-Water Flow in the Shenandoah Valley, Virginia and West Virginia, Using Variable-Direction Anisotropy in Hydraulic Conductivity to Represent Bedrock Structure



Scientific Investigations Report 2008–5002

Cover. Photograph showing aerial view looking eastward toward the Blue Ridge Mountains with the South Fork Shenandoah River in the foreground. Photograph by David L. Nelms, U.S. Geological Survey.

**Ground-Water Resources Program
National Cooperative Geologic Mapping Program**

**Simulation of Ground-Water Flow in
the Shenandoah Valley, Virginia and
West Virginia, Using Variable-Direction
Anisotropy in Hydraulic Conductivity to
Represent Bedrock Structure**

By Richard M. Yager, Scott Southworth, and Clifford I. Voss

Scientific Investigations Report 2008–5002

**U.S. Department of the Interior
U.S. Geological Survey**

U.S. Department of the Interior
DIRK KEMPTHORNE, Secretary

U.S. Geological Survey
Mark D. Myers, Director

U.S. Geological Survey, Reston, Virginia: 2008

For product and ordering information:

World Wide Web: <http://www.usgs.gov/pubprod>

Telephone: 1-888-ASK-USGS

For more information on the USGS--the Federal source for science about the Earth, its natural and living resources, natural hazards, and the environment:

World Wide Web: <http://www.usgs.gov>

Telephone: 1-888-ASK-USGS

Any use of trade, product, or firm names is for descriptive purposes only and does not imply endorsement by the U.S. Government.

Although this report is in the public domain, permission must be secured from the individual copyright owners to reproduce any copyrighted materials contained within this report.

Suggested citation:

Yager, R.M., Southworth, Scott, and Voss, C.I., 2008, Simulation of ground-water flow in the Shenandoah Valley, Virginia and West Virginia, using variable-direction anisotropy in hydraulic conductivity to represent bedrock structure: U.S. Geological Survey Scientific Investigations Report 2008-5002, 54 p.

Contents

Abstract.....	1
Introduction	2
Purpose and Scope	2
Previous Investigations.....	2
Hydrogeology of the Shenandoah Valley.....	2
Physiography.....	5
Bedrock Geology.....	5
Stratigraphy.....	5
Structure.....	6
Surficial Geology.....	8
Hydrology	8
Ground-Water Discharge	10
Ground-Water Withdrawals.....	10
Recharge	10
Transmissivity	14
Anisotropy in Inclined, Fractured Sedimentary Rocks.....	14
Simulation of Flow in Inclined, Fractured Sedimentary Rocks	16
Representation of Bedrock Structure in Shenandoah Valley	18
Conceptual Fracture Framework	18
Form Lines, Form Surfaces, and Computation of Conductivity Tensor	20
Ground-Water Flow Model.....	22
Model Design.....	22
Mesh and Layering	22
Boundary Conditions.....	22
Hydraulic Conductivity.....	24
Model Calibration.....	29
Observations.....	29
Parameters.....	29
Model Fit.....	33
Model Applications.....	36
Ground-Water Age Distributions.....	36
Capture Zones of Well Fields	38
Summary.....	44
Acknowledgments	45
References Cited.....	46
Appendix 1. Modifications to SUTRA.....	49

Figures

1–3.	Maps showing—	
	1.	Geologic and physiographic provinces in eastern North America showing the Great Valley and Mesozoic Rift basins.....3
	2.	Geographic features of the Shenandoah Valley, Virginia and West Virginia4
	3.	Bedrock geology of the Shenandoah Valley, Virginia and West Virginia.....7
	4.	Photograph showing bedrock surface exposed near quarry operation in Cambrian-Ordovician carbonate rock, Shenandoah Valley, Virginia and West Virginia9
	5.	Graph showing long-term water-level hydrographs for two observation wells in the Shenandoah Valley in Augusta and Rockingham Counties, Virginia9
	6.	Map showing watersheds and streamflow-gaging stations where base flow was estimated, and locations of wells with long-term hydrographs11
	7.	Graph showing relation between base flow estimated from streamflow measurements and computed as a function of the percentages of the basin area underlain by rock unit15
8–14.	Diagrams showing—	
	8.	Box plots of transmissivity values by rock unit estimated from specific capacity of pumped wells15
	9.	Schematic diagram showing alternative designs to represent ground-water flow through inclined fractured sedimentary rocks with an orthogonal finite-difference grid.....17
	10.	Formation of fractures in response to contractional deformation and folded bedding.....19
	11.	Generalized geologic sections showing rock units and form lines of bedding and faults in rocks underlying the Shenandoah Valley, Virginia and West Virginia.....21
	12.	Model domain showing map view of finite-element mesh and four rock units represented by the model.....23
	13.	Generalized section D–D’ showing units used to define model layers24
	14.	Perspective three-dimensional views along sections C–C’ and E–E’ showing attitude of bedding represented in ground-water flow models A and B: (A) strike direction (maximum conductivity direction, K_{max}), and (B) dip angle (medium conductivity direction, K_{med}).....27
	15.	Graph showing estimated relations used to compute maximum hydraulic conductivity with depth in carbonate, clastic, and metamorphic rocks in model A30
16–18.	Diagrams showing—	
	16.	Block diagrams along sections C–C’ and E–E’ showing spatial distribution of maximum hydraulic conductivity (K_{max}) used in models A and B.....31
	17.	Block diagrams along sections C–C’ and E–E’ showing spatial distribution of simulated ground-water velocity in model A32
	18.	Box plots of hydraulic conductivity values by rock unit estimated from specific capacity of pumped wells and through calibration with model A.....33
19–21.	Graphs showing—	
	19.	Residual plots for simulated heads in model A: (A) relation between simulated and observed values, and (B) relation between simulated values and residuals.34
	20.	Residual plots for simulated flows in model A: (A) relation between residuals

	and drainage-area size, and (B) relation between simulated and observed base flow and drainage-area size	35
21.	Composite-scaled sensitivities of optimal parameters in model A. [K _{max} : maximum hydraulic conductivity, K _{med} : medium hydraulic conductivity, K _{min} : minimum hydraulic conductivity].....	37
22–26.	Diagrams showing—	
22.	Block diagram along section D–D' showing spatial distribution of simulated ground-water age and flow directions with (A) model A (variable strike and dip), and (B) model C (uniform strike).....	39
23.	Capture zones (plan view of contributing area) delineated with model A (variable strike and dip) to (A) the Martinsburg water supply in Berkeley County, W.Va., and (B) industrial well fields in Rockingham County, Va	40
24.	Capture zones (plan view of contributing area) delineated with model C (uniform strike) to (A) the Martinsburg water supply in Berkeley County, W.Va., and (B) industrial well fields in Rockingham County, Va.....	41
25.	Three-dimensional perspective views of capture zones to the Martinsburg water supply in Berkeley County W.V. delineated with (A) model A (variable strike and dip), and (B) model C (uniform strike)	42
26.	Capture zones (plan view of contributing area) delineated with model A (variable strike and dip) with recharge decreased by one-half to simulate drought conditions at (A) the Martinsburg water supply in Berkeley County, W.Va., and (B) industrial well fields in Rockingham County, Va.....	43

Tables

1.	Lithologic units in the Shenandoah Valley	6
2.	Ground-water withdrawals from the Shenandoah Valley	10
3.	Base flow and basin characteristics for streamflow-gaging stations used in linear regressions.....	12
4.	Recharge rates for different rock units in the Shenandoah Valley estimated by linear regression of base flow.....	14
5.	Finite-difference models constructed to simulate ground-water flow through inclined, fractured sedimentary rocks	16
6.	Parameter values in alternative models of ground-water flow in the Shenandoah Valley specified or estimated through nonlinear regression	25
7.	Standard error in meters in ground-water flow models of the Shenandoah Valley	33
8.	Parameter error ratios associated with variations of model A	37

Conversion Factors, Datum, and Abbreviations

Multiply	By	To obtain
Length		
centimeter (cm)	0.3937	inch (in.)
millimeter (mm)	0.03937	inch (in.)
meter (m)	3.281	foot (ft)
kilometer (km)	0.6214	mile (mi)
Area		
square meter (m ²)	0.0002471	acre
square kilometer (km ²)	247.1	acre
square meter (m ²)	10.76	square foot (ft ²)
square centimeter (cm ²)	0.1550	square inch (ft ²)
square kilometer (km ²)	0.3861	square mile (mi ²)
Volume		
liter (L)	0.2642	gallon (gal)
cubic meter (m ³)	264.2	gallon (gal)
cubic meter (m ³)	0.0002642	million gallons (Mgal)
cubic centimeter (cm ³)	0.06102	cubic inch (in ³)
cubic meter (m ³)	35.31	cubic foot (ft ³)
cubic meter (m ³)	0.0008107	acre-foot (acre-ft)
Flow rate		
cubic meter per second (m ³ /s)	70.07	acre-foot per day (acre-ft/d)
cubic meter per year (m ³ /yr)	0.000817	acre-foot per year (acre-ft/yr)
meter per second (m/s)	3.281	foot per second (ft/s)
meter per day (m/d)	3.281	foot per day (ft/d)
meter per year (m/yr)	3.281	foot per year (ft/yr)
cubic meter per second (m ³ /s)	35.31	cubic foot per second (ft ³ /s)
cubic meter per day (m ³ /d)	35.31	cubic foot per day (ft ³ /d)
liter per second (L/s)	15.85	gallon per minute (gal/min)
cubic meter per day (m ³ /d)	264.2	gallon per day (gal/d)
cubic meter per second (m ³ /s)	22.83	million gallons per day (Mgal/d)
millimeter per year (mm/yr)	0.03937	inch per year (in/yr)
Specific capacity		
liter per second per meter [(L/s)/m]	4.831	gallon per minute per foot [(gal/min)/ft]
Hydraulic conductivity		
meter per day (m/d)	3.281	foot per day (ft/d)
Hydraulic gradient		
meter per kilometer (m/km)	5.27983	foot per mile (ft/mi)
Transmissivity*		
meter squared per day (m ² /d)	10.76	foot squared per day (ft ² /d)
Leakance		
meter per day per meter [(m/d)/m]	1	foot per day per foot [(ft/d)/ft]
millimeter per year per meter [(mm/yr)/m]	0.012	inch per year per foot [(in/yr)/ft]

Vertical coordinate information is referenced to the North American Vertical Datum of 1988 (NAVD 88).

Horizontal coordinate information is referenced to the North American Datum of 1983 (NAD 83).

Altitude, as used in this report, refers to distance above the vertical datum.

*Transmissivity: The standard unit for transmissivity is cubic foot per day per square foot times foot of aquifer thickness $[(\text{ft}^3/\text{d})/\text{ft}^2]\text{ft}$. In this report, the mathematically reduced form, meter squared per day (m^2/d), is used for convenience.

List of Acronyms

CSS	Composite-scaled sensitivities
DEM	Digital elevation model
FD	Finite difference
FE	Finite element
JMU	James Madison University
NWIS	National Water Information System
USGS	U.S. Geological Survey

This page has been left blank intentionally.

Simulation of Ground-Water Flow in the Shenandoah Valley, Virginia and West Virginia, Using Variable-Direction Anisotropy in Hydraulic Conductivity to Represent Bedrock Structure

By Richard M. Yager, Scott Southworth, and Clifford I. Voss

Abstract

Ground-water flow was simulated using variable-direction anisotropy in hydraulic conductivity to represent the folded, fractured sedimentary rocks that underlie the Shenandoah Valley in Virginia and West Virginia. The anisotropy is a consequence of the orientations of fractures that provide preferential flow paths through the rock, such that the direction of maximum hydraulic conductivity is oriented within bedding planes, which generally strike N. 30° E.; the direction of minimum hydraulic conductivity is perpendicular to the bedding. The finite-element model SUTRA was used to specify variable directions of the hydraulic-conductivity tensor in order to represent changes in the strike and dip of the bedding throughout the valley.

The folded rocks in the valley are collectively referred to as the Massanutten synclinorium, which contains about a 5-km-thick section of clastic and carbonate rocks. For the model, the bedrock was divided into four units: a 300-m-thick top unit with 10 equally spaced layers through which most ground water is assumed to flow, and three lower units each containing 5 layers of increasing thickness that correspond to the three major rock units in the valley: clastic, carbonate, and metamorphic rocks. A separate zone in the carbonate rocks that is overlain by colluvial gravel—called the western-toe carbonate unit—was also distinguished.

Hydraulic-conductivity values were estimated through model calibration for each of the four rock units, using data from 354 wells and 23 streamflow-gaging stations. Conductivity tensors for metamorphic and western-toe carbonate rocks were assumed to be isotropic, while conductivity tensors for carbonate and clastic rocks were assumed to be anisotropic. The directions of the conductivity tensor for carbonate and clastic rocks were interpolated for each mesh element from a stack of “form surfaces” that provided a three-dimensional representation of bedrock structure. Model simulations were run with (1) variable strike

and dip, in which conductivity tensors were aligned with the strike and dip of the bedding; and (2) uniform strike, in which conductivity tensors were assumed to be horizontally anisotropic with the maximum conductivity direction parallel to the N. 30° E. axis of the valley (strike of bedding) and the minimum conductivity direction perpendicular to the strike. Simulated flow penetrated deeper into the aquifer system with the uniform-strike tensor than with the variable-strike-and-dip tensor. Sensitivity analyses suggest that additional information on recharge rates would increase confidence in the estimated parameter values.

Two applications of the model were conducted—the first, to determine depth of recent ground-water flow by simulating the distribution of ground-water ages, showed that most shallow ground water is less than 10 years old. Ground-water age distributions computed by variable-strike-and-dip and uniform-strike models were similar, but differed beneath Massanutten Mountain in the center of the valley. The variable-strike-and-dip model simulated flow from west to east parallel to the bedding of the carbonate rocks beneath Massanutten Mountain, while the uniform-strike model, in which flow was largely controlled by topography, simulated this same area as an east-west ground-water divide. The second application, which delineated capture zones for selected well fields in the valley, showed that capture zones delineated with both models were similar in plan view, but differed in vertical extent. Capture zones simulated by the variable-strike-and-dip model extended downdip with the bedding of carbonate rock and were relatively shallow, while those simulated by the uniform-strike model extended to the bottom of the flow system, which is unrealistic. These results suggest that simulations of ground-water flow through folded, fractured rock can be constructed using SUTRA to represent variable orientations of the hydraulic-conductivity tensor and produce a physically realistic flow system that accurately reflects the pattern of bedrock structure.

Introduction

Increasing development in recent years in the Shenandoah Valley in Virginia and West Virginia (fig. 1) has placed additional demands on the water resources of the region. The area has experienced rapid population growth during the past several decades, increasing 30 percent from 1980 to 2000 (Krstolic and Hayes, 2004), mainly because of its proximity to Washington, D.C. Ground water, which provides about two-thirds of the current (2008) water supply, flows through fractures and along bedding planes in the sedimentary and metamorphic rocks that underlie the valley. Ground-water supplies are derived from springs and wells, and are pumped from abandoned quarries. Severe droughts during 1999–2002 limited the supply of ground water, especially from springs. Thorough understanding of ground-water availability, especially in relation to drought and population growth, is needed to effectively manage water supplies in the valley.

A hydrogeologic study of the Shenandoah Valley, an area of 7,100 km², was undertaken to assess the ground-water resources in this region. A three-dimensional ground-water flow model was constructed to estimate the rate and pattern of regional ground-water flow. The model design was complicated, however, by the complex geologic framework. The sedimentary rocks that underlie the Shenandoah Valley have been folded and faulted to form a large synclinal structure in a 5-km-deep basin. Bedding planes and fractures in the rocks are inclined, allowing ground water to penetrate at depth below land surface—freshwater is obtained from wells more than 400 m deep. Hydraulic connections along bedding planes were represented in the model by varying the generalized dip of the bedding. This was accomplished using SUTRA (Voss and Provost, 2002), a finite-element (FE) model that allows directions of the conductivity tensor to vary throughout the model domain independent of the configuration and shape of the finite elements that make up the model mesh. This research was supported by the U.S. Geological Survey (USGS) Ground-Water Resources Program in collaboration with the National Cooperative Geologic Mapping Program.

Purpose and Scope

This report describes the hydrogeology of the Shenandoah Valley, including a discussion of bedrock geology and structure, and presents a conceptual model of the fracture network that transmits water through the aquifer system. The report includes a set of generalized geologic sections that show the principal rock units that underlie the valley and indicate the orientation of bedding in the rocks. The report documents the design and calibration of a three-dimensional model that was used to simulate the pattern and rate of regional ground-water flow, and to estimate values of hydraulic properties of the rocks that control the flow of ground water. The report also presents the results of a linear regression used to estimate

recharge to the aquifer system as a function of rock unit, which was based on measurements of base flow in watersheds of different sizes in the valley. Finally, some applications of the model simulations are presented to show the distributions of ground-water age and delineate capture zones of the most productive well fields.

Previous Investigations

The first study of the hydrogeology of the Shenandoah Valley was conducted by Cady (1938), who summarized the bedrock geology and structure, and described ground-water conditions in six Virginia counties. Additional hydrogeologic studies of ground-water availability were later conducted in Virginia for Rockingham County (Hinkle and Sterrett, 1976), Shenandoah County (Hinkle and Sterrett, 1977), and Augusta County (Hinkle and Sterrett, 1978), and in West Virginia for Jefferson County (Bieber, 1961; Kozar and others, 1991) and Berkeley County (Bieber, 1961; Shultz and others, 1995). More recent hydrogeologic studies that relate ground-water flow to bedrock structure were completed by Harlow and others (2005) for Frederick County, Va.; Kozar and others (2007) for the Leetown area in Jefferson County, W.Va.; and McKoy and others (2005a, 2005b) for Berkeley and Jefferson Counties, W.Va.

Hydrogeology of the Shenandoah Valley

The Shenandoah Valley is part of the Great Valley section of the central Appalachian Valley and Ridge Province. The Great Valley extends from southern New York to central Alabama, a distance of about 1,600 km (fig. 1). That part of the Great Valley south of the Potomac River in northern Virginia is called the Shenandoah Valley. The Great Valley is also called the Hagerstown Valley in Maryland, the Cumberland Valley in Pennsylvania, and the Tennessee Valley in the southern Appalachians. The Great Valley section of the Valley and Ridge Province is bounded on the east by rocks of the Blue Ridge Province and is bounded on the west by the Appalachian Plateaus Province.

The drainage basin of the Shenandoah Valley is bounded on the north by the east-flowing Potomac River, on the east by the crest of the Blue Ridge Mountains, on the west (generally) by the crest of Little North Mountain near the boundary between the Great Valley and Valley and Ridge Province, and on the south by the drainage divide between the Shenandoah and James Rivers (fig. 1 and fig. 2). Therefore, some of the metamorphic rocks of the Blue Ridge Province and some of the rocks of the Valley and Ridge Province are included in the drainage basin. The main tributaries of the Shenandoah Valley are the North and South Forks of the Shenandoah River, which join near Front Royal, Va., to become the Shenandoah River, which flows northeast to the Potomac River at Harpers Ferry, W.Va (fig. 2). The northern

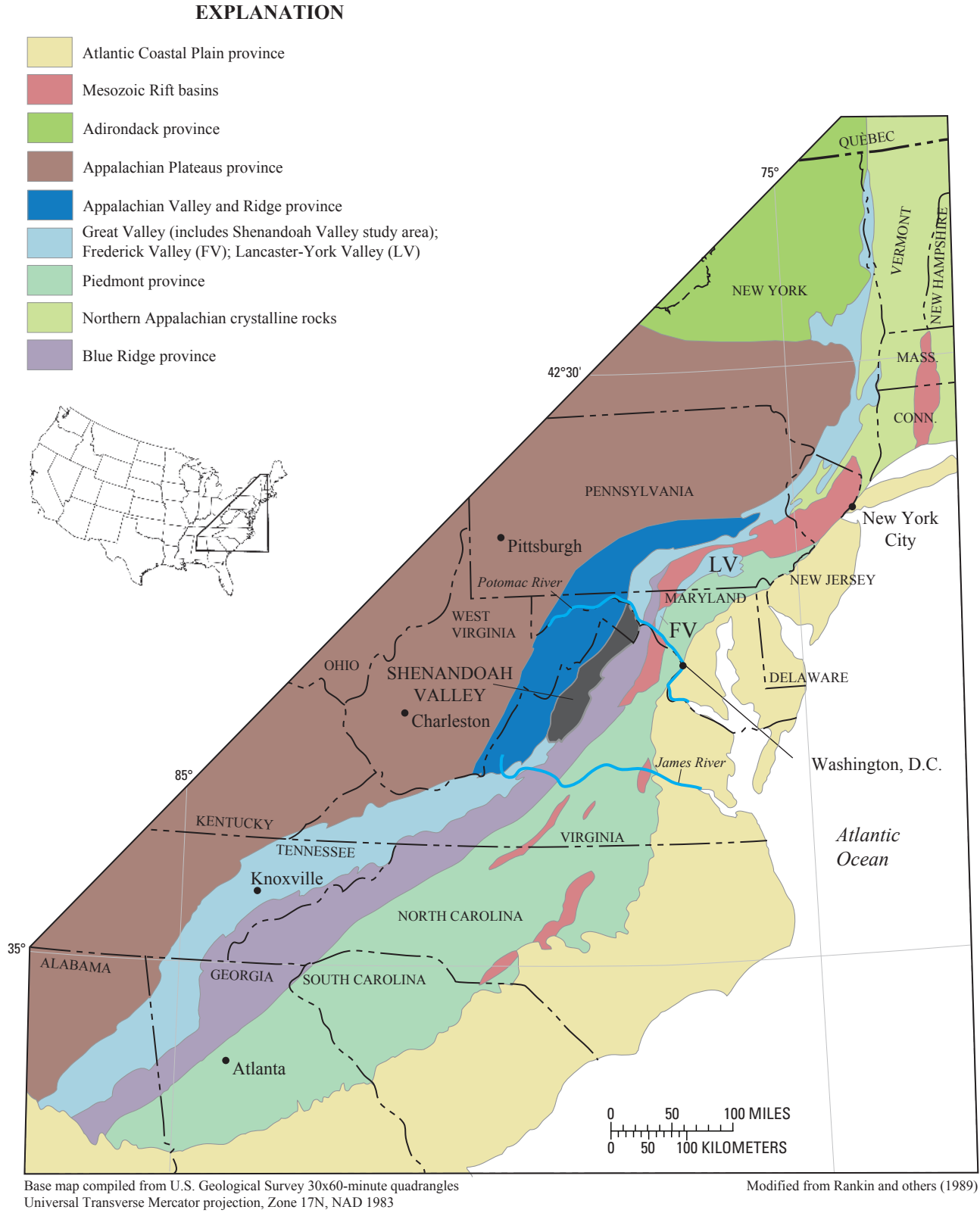
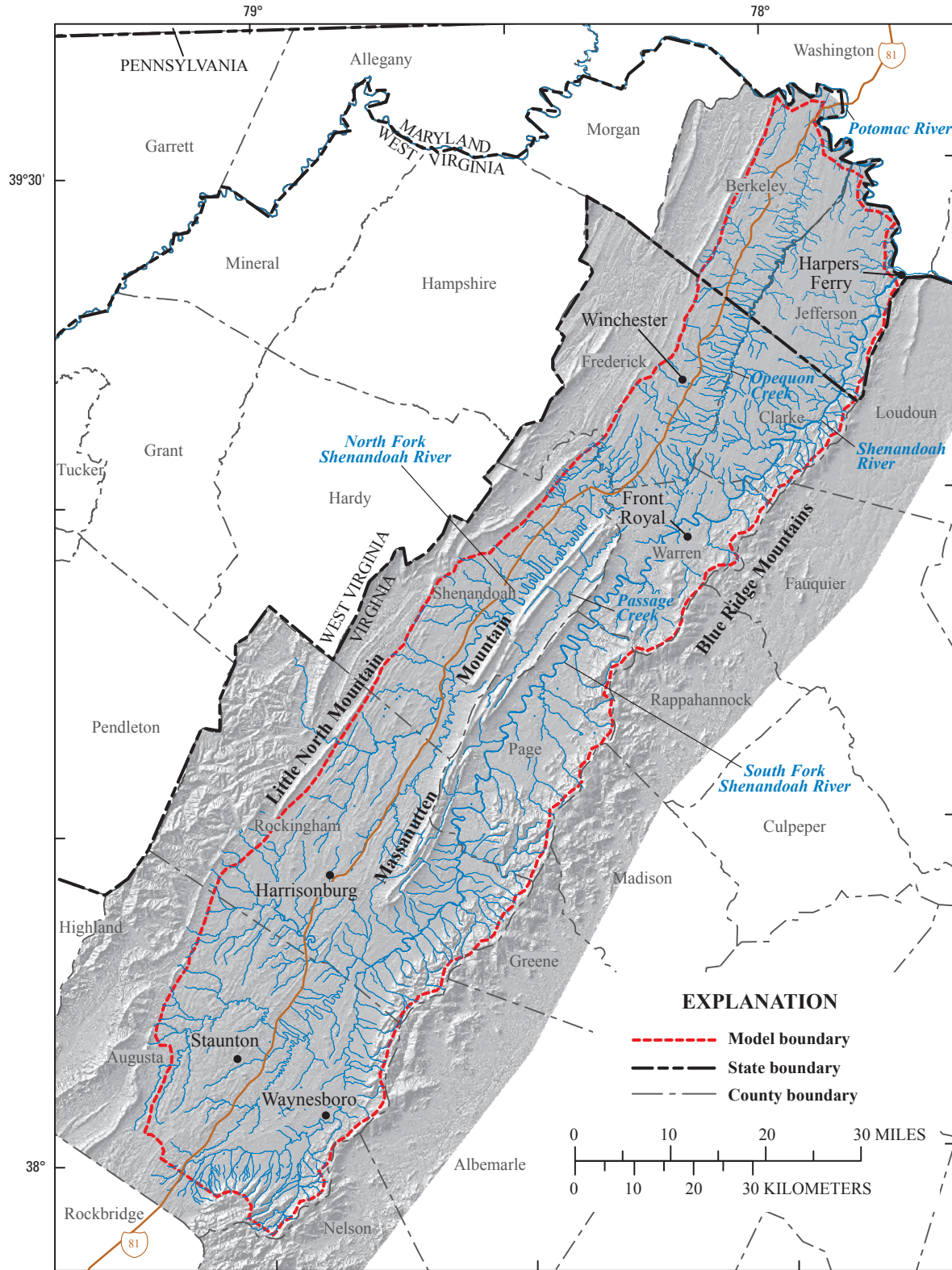


Figure 1. Geologic and physiographic provinces in eastern North America showing the Great Valley and Mesozoic Rift basins.

4 Simulation of Ground-Water Flow in the Shenandoah Valley, Virginia and West Virginia



Base from U.S. Geological Survey, Seamless Data Distribution System
 Accessed in 2006 at URL <http://seamless.usgs.gov>
 Universal Transverse Mercator projection, Zone 17

Figure 2. Geographic features of the Shenandoah Valley, Virginia and West Virginia.

part of the Shenandoah Valley also includes the watershed of the Opequon Creek, which flows north into the Potomac River.

Physiography

The 7,100-km² Shenandoah Valley is a broad, gently rolling landscape that ranges from about 30 to 38 km wide and is about 200 km long. Massanutten Mountain is in the center of the Shenandoah Valley, and the two forks of the Shenandoah River flow around it. The rocks in the footwall of the North Mountain Fault underlie Little North Mountain on the west side of the Shenandoah Valley and form a fairly consistent northeast-southwest-trending boundary. The drainage basin includes rocks west of the Little North Mountain in only a few places. The boundary between the Great Valley and the Blue Ridge Province on the east is the lower slope of a sinuous series of ridges that mark the Blue Ridge Mountains. Topographically, the highest land-surface altitudes, as much as 1,120 m, are along the drainage divide on the eastern side of the basin along the Blue Ridge Mountains, although altitudes of ridges in Massanutten Mountain approach 900 m. In contrast, the altitude of the valley floor ranges from 110 to 660 m, with the highest altitudes at the southern end of the basin and the lowest altitudes near the Potomac River. The South Fork of the Shenandoah River drains the largest part of the valley.

Bedrock Geology

The Shenandoah Valley is underlain by Cambrian to Devonian sedimentary rocks that were contractionally deformed and folded into the regional Massanutten synclinorium. The central part of the synclinorium is underlain by clastic rocks, which are in turn underlain by carbonate rocks. The most extensive clastic rock unit is the shale and sandstone of the Martinsburg Formation (Ordovician), which extends the entire length of the valley. The Massanutten Sandstone (Silurian) underlies the numerous ridges of Massanutten Mountain, and the Mahantango Formation (Devonian) is present in the core of the synclinorium in Passage Creek Valley (fig. 2). The carbonate rocks of the Shenandoah Valley include limestone and dolostone from the Tomstown Formation (Early Cambrian) to the New Market Limestone (Ordovician). Within the broad section of carbonate rocks, the Waynesboro and Conococheague Formations also contain clastic rocks. Mesoproterozoic gneisses, Neoproterozoic metasedimentary and metavolcanic rocks, and Early Cambrian clastic metasedimentary rocks of the west limb of the Blue Ridge-South Mountain anticlinorium are locally thrust onto the non-metamorphosed rocks that underlie the Shenandoah Valley.

Stratigraphy

Bedrock units were classified into four lithologic units based on the dominant type of rock shown on the 1:500,000-scale bedrock map of Virginia (Virginia Division of Mineral Resources, 1993) and the 1:250,000-scale bedrock map of West Virginia (Cardwell and others, 1968) (table 1 and fig. 3). The four rock units include (1) metamorphic rocks of Mesoproterozoic to Early Cambrian age, (2) carbonate rock of Cambrian and Ordovician age, (3) clastic rocks of Ordovician to Devonian age, and (4) carbonate rocks of Cambrian and Ordovician age covered by late Cenozoic gravel deposits, called the western-toe carbonate unit.

1. The metamorphic rock unit consists of Mesoproterozoic granitic gneiss, metaclastic rocks of the Swift Run Formation (Neoproterozoic), metavolcanic rocks of the Catoclin Formation (Neoproterozoic), and the metamorphosed coarse-grained clastic rocks of the Chilhowee Group (Early Cambrian). The Chilhowee Group consists of the Weverton, Harpers, and Antietam Formations. The metamorphic rocks are present in the Blue Ridge Province, on the eastern side of the Shenandoah Valley.
2. The carbonate rock unit consists of, from oldest to youngest, dolostone of the Tomstown Formation (Cambrian); dolostone, shale, limestone, and sandstone of the Waynesboro Formation (Cambrian); dolostone, shale, and limestone of the Elbrook Formation (Cambrian); limestone, dolostone, and calcareous sandstone of the Conococheague Formation (Cambrian and Ordovician); dolostone, limestone, and chert of the Beekmantown Group (Ordovician); limestone and shale of the Edinburg Formation (Ordovician); and the Lincolnshire and New Market Limestones (Ordovician).
3. The clastic rock unit consists of, from oldest to youngest, shale, sandstone, siltstone, and limestone of the Martinsburg Formation (Ordovician); quartzarenite and conglomerate of the Massanutten Sandstone (Silurian); calcareous sandstone, limestone, and calcareous shale of the Ridgely Sandstone (Silurian and Devonian); limestone of the Helderberg and Cayugan Groups (Devonian); and shale and sandstone of the Millboro Shale, Marcellus Formation, Needmore Shale, and Mahantango Formation (Devonian). These rocks underlie the Massanutten synclinorium.
4. The western-toe carbonate unit consists of, from oldest to youngest, dolostone of the Tomstown Formation (Cambrian); dolostone, shale, limestone, and sandstone of the Waynesboro Formation (Cambrian); dolostone, shale, and limestone of the Elbrook Formation (Cambrian); and limestone, dolostone, and calcareous sandstone of the Conococheague Formation (Cambrian and Ordovician). These rocks are overlain by colluvial gravel deposits of late Cenozoic age. The bedrock is deeply weathered due to ground-water recharge through the gravel.

6 Simulation of Ground-Water Flow in the Shenandoah Valley, Virginia and West Virginia

Table 1. Lithologic units in the Shenandoah Valley.

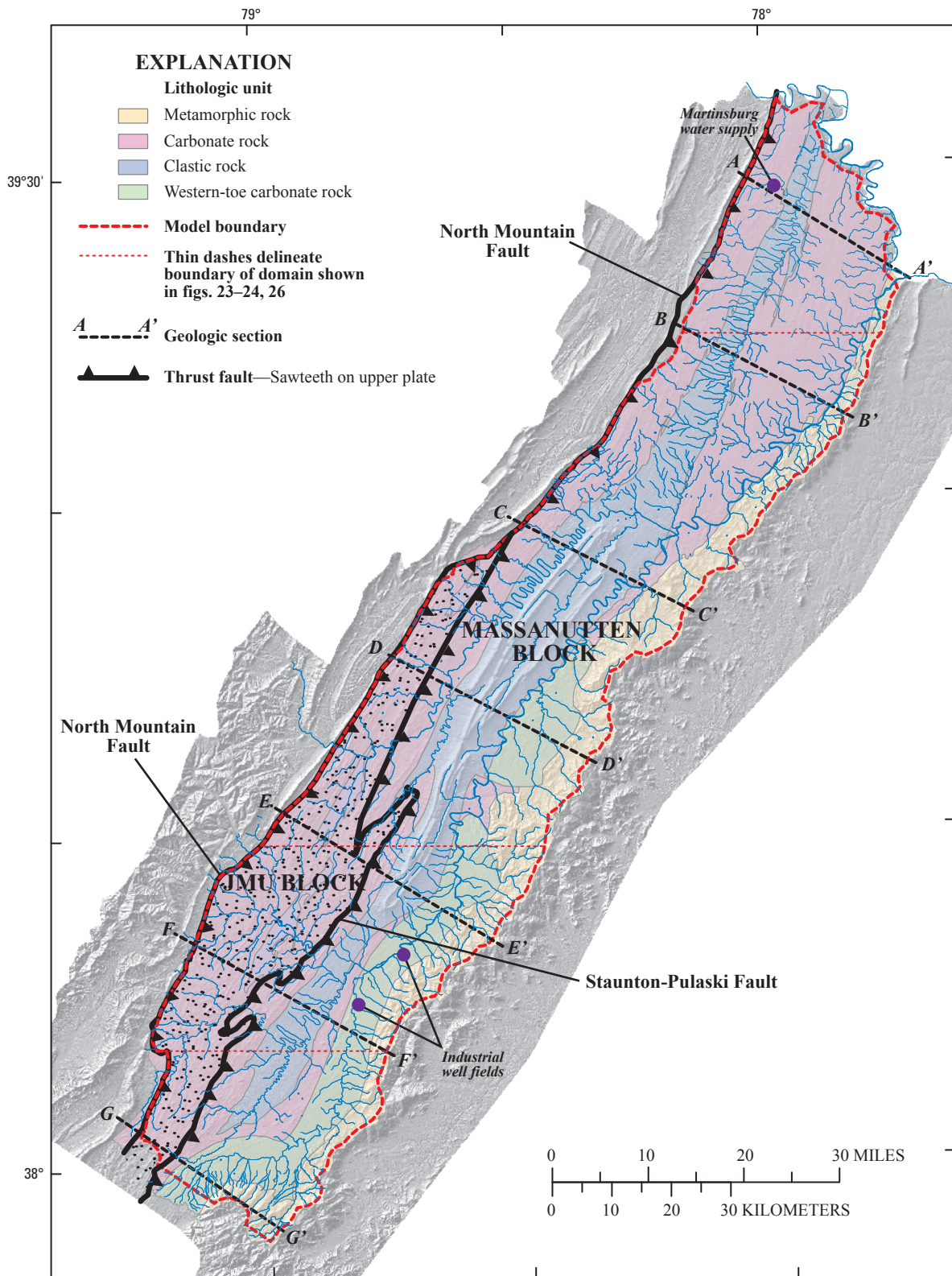
Devonian			
	Mahantango Formation	}	
	Needmore Shale		
	Marcellus Formation		
	Millboro Shale		
Silurian and Devonian	Helderberg Group and Cayugan rocks	}	Clastic rocks
	Ridgeley Sandstone		
Silurian	Massanutten Sandstone		
Ordovician	Martinsburg Formation		
Ordovician	Lincolnshire and New Market Limestone	}	
	Edinburg Formation		
	Beekmantown Group		
Cambrian and Ordovician	Conococheague Formation	}	Carbonate rocks
Cambrian	Elbrook Formation		
	Waynesboro Formation		Western-toe carbonate rocks
	Tomstown Formation		
Cambrian Chilhowee Group	Antietam Formation	}	
	Harpers Formation		
	Weverton Formation		
Neoproterozoic	Catoctin Formation		
	Swift Run Formation		
Mesoproterozoic granitic gneiss			Metamorphic rocks

Structure

The rocks of the Blue Ridge and Valley and Ridge Provinces were folded and faulted during the Alleghanian orogeny about 300 million years ago (Southworth and others, 2007). Continental collision of North America and Africa resulted in westward tectonic transport of a wedge of rock as much as 5 km thick above the North Mountain Fault a distance of hundreds of kilometers. The regional structure of the rocks of the Shenandoah Valley is the first-order Massanutten synclinorium. The rocks of the synclinorium do not form a simple synclinal trough, but instead contain numerous second- and third-order anticlines and synclines that verge up the limbs of the larger synclinorium. The synclinorium has an east limb and a west limb that converge to a core of nearly flat-lying rocks. In general, the rocks of the west limb dip gently southeast, whereas the rocks of the east limb dip to the northwest, are more vertical, and locally are overturned and dip steeply to the southeast.

The Shenandoah Valley can be further subdivided into two structural blocks. The Massanutten block on the east is separated by the Staunton-Pulaski Fault from the JMU block on the west, named after James Madison University (JMU), which is located in Harrisonburg (figs. 2–3). The Massanutten block is a continuous synclinorium from the southern boundary of the basin to the northern boundary of the basin. Both ends of the Massanutten synclinorium plunge toward one another at a low angle. The rocks within the JMU block between the Staunton-Pulaski Fault and the North Mountain Fault form a distinct structural domain that contains a regional synclinorium cored by the Martinsburg Formation, which makes the JMU block distinct from the Massanutten synclinorium to the east. North of the mapped termination of the Staunton-Pulaski Fault (Virginia Division of Mineral Resources, 1993), a regional anticline and local fault are used to define the block boundary.

The dominant foliation in the sedimentary rocks in the Shenandoah Valley is bedding, which generally strikes



Base from U.S. Geological Survey, Seamless Data Distribution System
 Accessed in 2006 at URL <http://seamless.usgs.gov>
 Universal Transverse Mercator projection, Zone 17

Figure 3. Bedrock geology of the Shenandoah Valley, Virginia and West Virginia.

N. 30° E. Most thrust faults strike northeast and dip southeast, whereas local back thrusts dip steeply to the northwest. Locally, southeast-dipping cleavage is associated with folding and faulting, and cross and longitudinal joints related to folding are steep and strike northwest and northeast, respectively. Most ridges and swales are developed along northeast-striking beds. Streams and creeks use cross joints, best demonstrated by the seven bends of the North Fork of the Shenandoah River (Hack and Young, 1959). The dominant foliations in the rocks of the Blue Ridge are gneissic foliation, cleavage, and fractures. These foliations develop partings through which ground water flows, rather than through primary bedding.

Surficial Geology

The carbonate rocks of the Shenandoah Valley chemically weather in the humid temperate climate to form karst features, which include sinkholes, caves and caverns, and overburden of variable thickness (Hack, 1965). Fluvial terraces with deposits of sandstone cobbles are along all major drainages of the rivers in the Shenandoah Valley. Aprons of colluvium are present along lower slopes beneath sandstone ridges. Thin aprons of colluvium blanket shale along Massanutten Mountain, but thicker colluvial aprons, as much as 150 m thick (King, 1950), are along the western toe of the Blue Ridge above carbonate rocks. These colluvial deposits range in thickness and were formed as ground water infiltrated the gravel and the underlying carbonate bedrock was chemically dissolved. These deposits are important recharge areas for ground water and have been referred to as “western toe fans” and “the Elkton aquifer” (Morgan and others, 2004; Swain and others, 2004).

Hydrology

Ground water flows from topographic highs in the Shenandoah Valley toward stream channels that drain to the Shenandoah River and Opequon Creek. The highest points are in the center of the valley on Massanutten Mountain and along ridges that form the eastern and western boundaries of the valley. The density and pattern of drainage is controlled by the underlying bedrock. Areas underlain by metamorphic rock are generally steep, and the drainage pattern is dendritic and highly developed. Areas underlain by clastic rocks can either be steep, as on Massanutten Mountain, or gently rolling, as in areas to the north or south of the mountain. The drainage in clastic-rock areas is a well-developed trellis pattern that generally follows the predominant fractures in the rock parallel and perpendicular to the strike of the bedding. Areas underlain by carbonate rocks are generally low-lying, and the drainage is less developed. Numerous karst features, such as sinkholes and springs, occur in the carbonate-rock areas, and their occurrence is partly controlled by fractures and faults (Harlow and others, 2005). The density of sinkholes

approaches two per square kilometer in parts of Jefferson County, W.Va., with an average sinkhole diameter of 2 m, although sinkholes larger than 10 m in diameter occur near the Potomac River where the hydraulic gradient is steep (Kozar and others, 1991).

Water enters fractures in the bedrock by infiltration through the overburden, which serves as a reservoir of recharge for the underlying carbonate-rock aquifers. The overburden thickness generally ranges from 1 to 30 m above carbonate areas where it is best developed, except along the western toe of the Blue Ridge, where the thickness can exceed 150 m. The bedrock surface is highly irregular in carbonate areas (fig. 4) and the depth to bedrock is difficult to determine. The overburden is less developed in clastic-rock areas, where the bedrock surface appears to be more uniform and is closer to the land surface.

Anisotropic ground-water flow was noted in the Shenandoah Valley by Jones (1991), who conducted tracer tests in Jefferson and Clarke Counties and found that the movement of tracers was often parallel to the strike of the bedding. Jones also mapped potentiometric surfaces that displayed elongated troughs parallel to strike, suggesting preferential flow along bedding planes, and concluded that ground-water flow was not dominated by discrete karst features (Jones, 1991). Burbey (2003) simulated municipal ground-water withdrawals from an abandoned quarry in carbonate rock in Frederick County. He mapped a large zone of influence created by pumping that extended more than 3 km along strike, and estimated an anisotropy ratio of 3:1 in strike-parallel to strike-normal hydraulic conductivity from the simulation results.

Long-term hydrographs from observation wells completed in carbonate rock in the southern part of the Shenandoah Valley do not indicate any trend in water levels, suggesting that the aquifer system is near equilibrium (fig. 5). The hydrograph for the Augusta County well (107–00127) displays numerous peaks that are associated with large recharge events, whereas the hydrograph for the Rockingham County well (182–00096) displays a much different behavior. Water levels in the Rockingham well typically range between 18 and 21 m below land surface, but drop sharply once the depth to water exceeds 21 m. The water levels then recover rapidly to the previous range following a recharge event. This behavior suggests that at least two fracture zones intersect the well bore. The upper fracture zone is probably more transmissive and controls the water level in the well during wet conditions. When the upper fracture zone is dewatered during dry conditions, the water level in the well falls rapidly to a level controlled by the lower fracture zone. Similar behavior has been observed in wells in carbonate rocks in the Valley and Ridge Province in Pennsylvania (D.W. Risser, U.S. Geological Survey, oral commun., 2007).



Figure 4. Bedrock surface exposed near quarry operation in Cambrian-Ordovician carbonate rock, Shenandoah Valley, Virginia and West Virginia. (Photograph by Randall Orndorff, U.S. Geological Survey.)

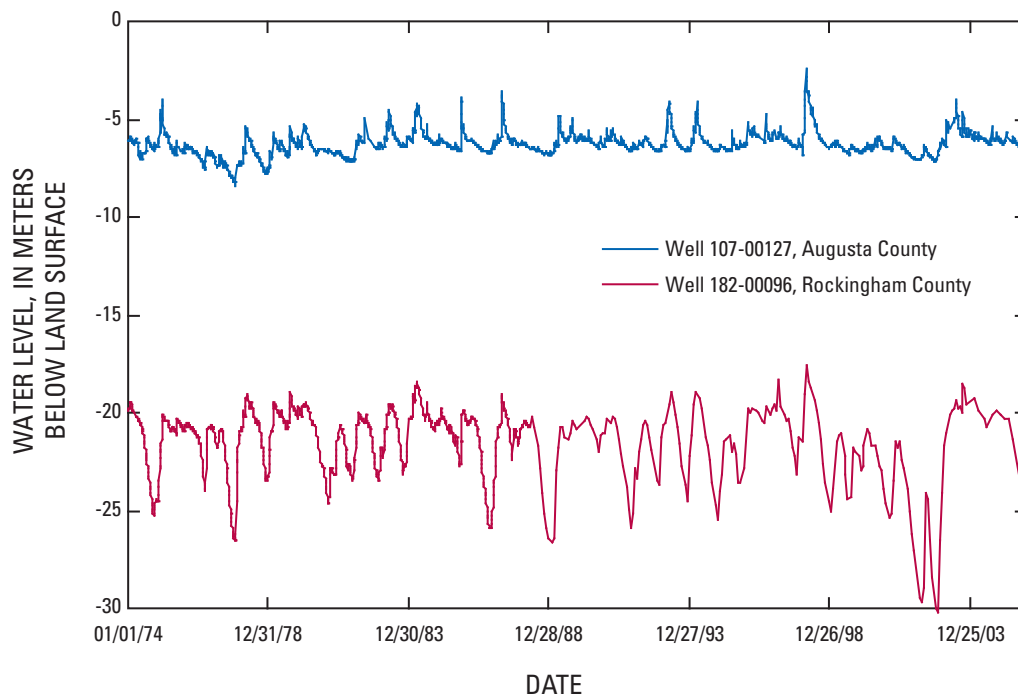


Figure 5. Long-term water-level hydrographs for two observation wells in the Shenandoah Valley in Augusta and Rockingham Counties, Virginia. Well locations shown in figure 6. Data from Ground-Water Site Inventory maintained by USGS.

Ground-Water Discharge

In areas underlain by carbonate rock, ground water discharges principally through springs along stream channels, and the headwaters of many streams begin at a spring (Harlow and others, 2005). Large springs serve as water supplies for a number of municipalities (table 2), and spring discharges exceeding 420 L/s have been measured in Augusta County (Hinkle and Sterrett, 1978). Although springs also occur in areas underlain by clastic rock, ground-water discharge there typically is more dispersed along stream channels than in carbonate-rock areas. Ground-water discharge (base flow) to streams has been estimated for a number of watersheds of different sizes in the Shenandoah Valley (Nelms and others, 1997) (fig. 6 and table 3). The base-flow estimates were computed from measured daily discharges using a hydrograph-separation method (Rutledge, 1993). Average base flow discharged from the Shenandoah Valley, including the Shenandoah River and Opequon Creek, is estimated as 4.5×10^6 m³/d. Ground water also discharges directly to the Potomac River, but the magnitude of streamflow in the Potomac River is too large to allow estimation of the rate of direct discharge from the Shenandoah Valley.

Ground-Water Withdrawals

Ground-water withdrawals from the principal municipal and private well fields total approximately 112,000 m³/d and provide about two-thirds of the water supply in the Shenandoah Valley (table 2), and an additional 10,000 m³/d was pumped for irrigation in 2004. The largest withdrawals are from Rockingham and Augusta Counties in Virginia and Berkeley County in W.Va. (fig. 2). The most productive wells

are in carbonate-rock areas, especially in the western toe of the Blue Ridge where yields can exceed 200 L/s (Golder Associates Inc., 2005). The most productive wells (more than 6 L/s) are 60 to 150 m deep, although two wells each produce about 3 L/s from depths exceeding 400 m in Augusta and Rockingham Counties (Hinkle and Sterrett, 1978; 1976). Wells in clastic-rock areas typically produce less water; yields in the clastic Martinsburg Formation can exceed 6 L/s (Hinkle and Sterrett, 1976; 1977; and 1978).

Recharge

Ground-water withdrawals from wells and springs are equal to 2.4 percent of the measured base flow discharged from the Shenandoah Valley, suggesting that the aquifer system is near equilibrium and not greatly stressed at a regional scale. No major interbasin transfers of water from the valley take place and consumptive use of water resulting from irrigation is assumed to be negligible. Under these conditions, nearly all the recharge that enters the aquifer system discharges through base flow, and the recharge rate can be computed by dividing the estimated base flow by the area of the drainage basin. The mean recharge rate for the entire Shenandoah Valley is about 19 cm/yr, but the recharge rate in local areas varies as it is controlled by the topography, precipitation, and the underlying bedrock. A linear regression was conducted using the base flows presented by Nelms and others (1997) to determine the relative contributions of these factors.

Recharge, expressed as base flow per basin area, was computed in the linear regression as a function of several variables. The following basin characteristics were included in the regression: (1) mean precipitation, (2) mean elevation, and (3) mean slope. The precipitation values were scaled from Nelms and others (1997, fig. 4), and the elevations and slopes were computed using digital elevation models (DEMs) with 30-m resolution. The percentages of the basin area underlain by the four major rock units also were included in the regression because of their differing effect on recharge and discharge from underlying aquifers (see fig. 3 and table 3).

The linear regression used base flows measured for 20 of the 25 streamflow-gaging stations listed in table 3. Four of the stations were not included in the regression because the period of record was less than 10 years. A fifth station, Abrams Creek near Winchester (01616000), was omitted as an outlier because the base flow was much larger than flows for other stations with basins of comparable size. Underflow from an adjacent ungaged basin and (or) the occurrence of several perennial springs in the 42.7-km² basin may account for the larger flow to Abrams Creek (G.E. Harlow, Jr., U.S. Geological Survey, oral commun., 2007). The percentages of the basin area underlain by the rock units were the only significant variables found by regression, indicating that the variation in precipitation and topography is reflected by the rock unit. Recharge (*Rch*, in cm/yr) can be computed with the following expression:

Table 2. Ground-water withdrawals from the Shenandoah Valley.

[Based on data from Hutson and others (2004). Values in cubic meters per day. --, not applicable]

State	County	Water supply, m ³ /d	
		Wells	Springs
Va.	Augusta	27,313	24,179
W. Va.	Berkeley	20,313	--
Va.	Clarke	95	322
Va.	Frederick	855	--
W. Va.	Jefferson	6,992	--
Va.	Page	3,512	3,478
Va.	Rockingham	45,897	5,235
Va.	Shenandoah	7,086	519
Va.	Warren	519	--
Total		112,581	33,732

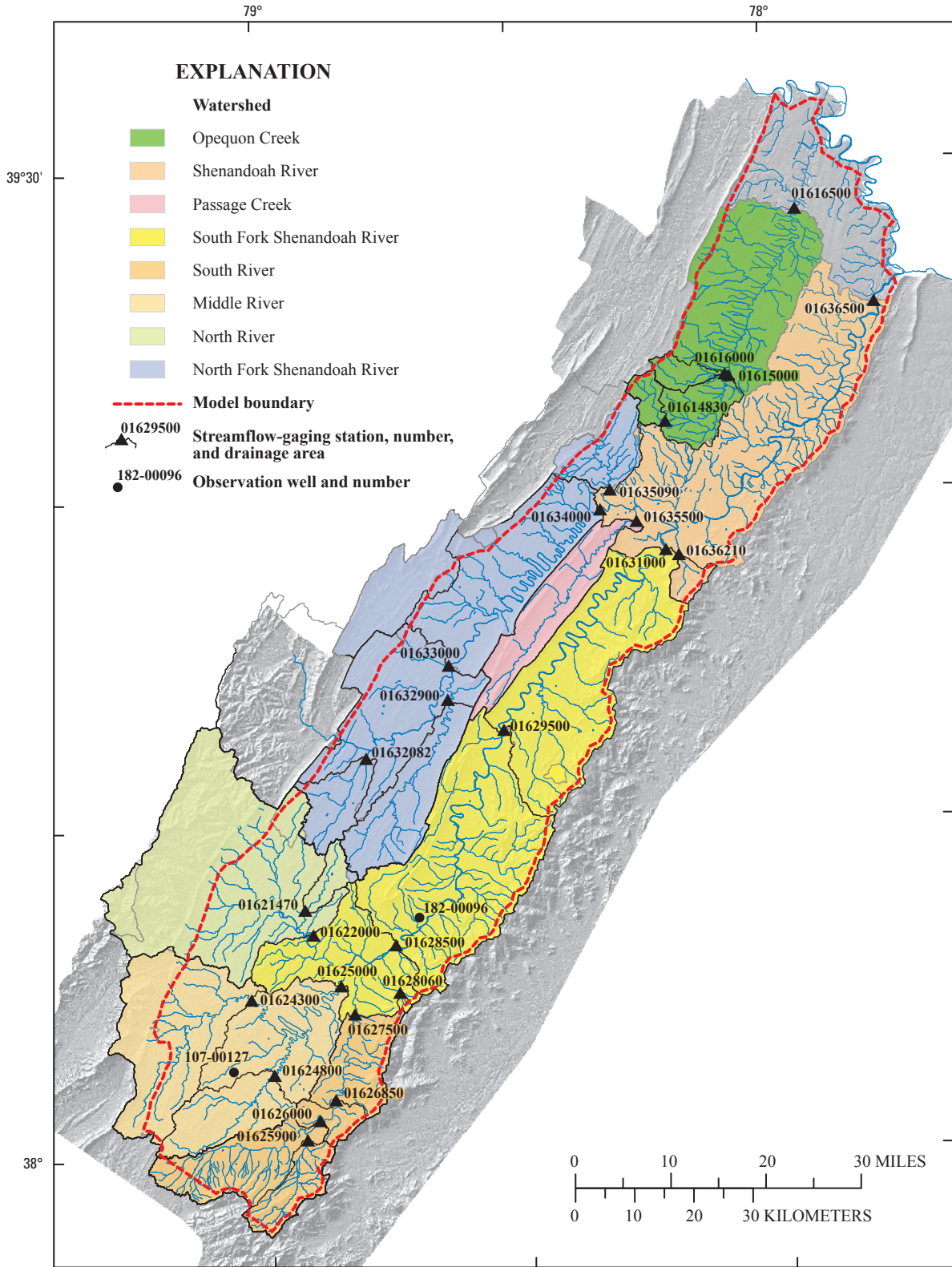


Figure 6. Watersheds and streamflow-gaging stations where base flow was estimated, and locations of wells with long-term hydrographs.

Table 3. Base flow and basin characteristics for streamflow-gaging stations used in linear regressions.[Base flow from Nelms and others (1997). Shading indicates base-flow values not included in linear regression for recharge. km², square kilometers; m³/d, cubic meters per day; cm/yr, centimeters per year]

U.S. Geological Survey streamflow-gaging station		Drainage area (km ²)	Period of record (years)	Percentage of basin by rock unit ^b				Base flow (m ³ /d × 1,000)	Recharge (cm/yr)	
Station name	Station number			Metamorphic	Carbonate	Clastic	Western-toe carbonate		Measured	Computed by linear regression
Opequon Creek near Stephens City, Va.	1614830	39.4	1	0.00	93.70	1.12	0.00	8.61 ^a	8.00	24.02
Opequon Creek near Berryville, Va.	1615000	148.4	52	0.00	42.37	56.28	0.00	54.96	13.51	18.48
Abrams Creek near Winchester, Va.	1616000	42.7	13	0.00	71.83	27.67	0.00	47.00	40.18	21.66
Opequon Creek at Martinsburg, W.Va.	1616500	707.1	55	0.00	62.43	34.11	0.00	471.08	21.59	20.64
Blacks Run at RT 704 near Mount Crawford, Va.	1621470	50.2	1	0.00	90.13	9.87	0.00	12.38 ^a	8.99	23.63
North River near Burkettown, Va.	1622000	981.6	44	0.00	41.23	4.12	0.00	587.00	21.94	18.35
Middle River near Verona, Va.	1624300	461.0	18	0.00	65.29	0.10	0.00	316.33	25.07	20.95
Christians Creek near Fishersville, Va.	1624800	181.6	28	0.00	67.10	22.31	10.58	126.33	25.40	23.85
Middle River near Grottoes, Va.	1625000	971.3	74	0.00	61.81	18.73	2.88	537.77	20.22	21.31
Back Creek at Lyndhurst, Va.	1625900	106.7	2	85.56	0.00	0.00	13.44	101.91 ^a	34.87	25.13
South River near Waynesboro, Va ^a	1626000	328.9	49	40.05	4.97	0.00	54.61	264.75 ^a	29.4	32.06
South River near Dooms, Va.	1626850	385.9	20	41.41	5.14	0.00	53.10	372.97	35.31	31.82
South River at Harriston, Va.	1627500	549.1	33	40.64	3.60	0.00	55.42	420.17	27.94	32.17
White Oak Run near Grottoes, Va. ^a	1628060	5.0	15	99.56	0.00	0.00	0.00	3.16 ^a	22.89	22.96

Table 3. Base flow and basin characteristics for streamflow-gaging stations used in linear regressions.—Continued[Base flow from Nelms and others (1997). Shading indicates base-flow values not included in linear regression for recharge. km², square kilometers; m³/d, cubic meters per day; cm/yr, centimeters per year]

U.S. Geological Survey streamflow-gaging station		Drainage area (km ²)	Period of record (years)	Percentage of basin by rock unit ^b				Base flow (m ³ /d × 1,000)	Recharge (cm/yr)	
Station name	Station number			Metamorphic	Carbonate	Clastic	Western-toe carbonate		Measured	Computed by linear regression
S F Shenandoah River near Lynnwood, Va.	1628500	2,807.6	71	9.31	40.81	10.35	14.72	1695.93	22.07	22.92
S F Shenandoah River near Luray, Va.	1629500	3,566.4	22	14.71	34.04	14.04	17.68	2370.58	24.28	23.44
S F Shenandoah River at Front Royal, Va.	1631000	4,252.8	71	19.85	29.65	15.09	18.96	2603.50	22.35	23.76
Linnville Creek at Broadway, Va.	1632082	117.8	26	0.00	71.23	27.94	0.00	63.10	19.56	21.59
Smith Creek near New Market, Va.	1632900	241.4	41	0.00	60.84	39.16	0.00	132.37	20.02	20.47
N F Shenandoah River at Mount Jackson, Va.	1633000	1,310.5	58	0.00	42.11	12.06	0.00	583.52	17.24	18.45
N F Shenandoah River near Strasburg, Va.	1634000	1,989.1	76	0.00	43.05	15.31	0.00	943.28	17.32	18.55
Cedar Creek above HWY 11 near Middletown, Va.	1635090	396.3	2	0.00	28.24	0.36	0.00	158.38 ^a	14.61	16.95
Passage Creek near Buckton, Va.	1635500	227.4	69	0.00	0.00	100.00	0.00	101.84	16.36	13.90
Happy Creek at Front Royal, Va.	1636210	36.3	27	99.39	0.00	0.00	0.00	23.12	23.29	22.94
Shenandoah River at Millville, W.Va.	1636500	7,876.2	104	14.27	35.32	17.17	10.19	4052	18.80	21.62

^aBase-flow value not included in calibration of ground-water flow model.^bBasins where the percentage of rock units do not sum to 100 include rocks outside the portion of the Shenandoah Valley included in the model domain.

$$Rch = 13.9 + 10.8Carb + 9.07Meta + 25.6West, \quad (1)$$

where the explanatory variables are the percentages of the basin underlain by the following rock units: carbonate (*Carb*), metamorphic (*Meta*), and western-toe carbonate (*West*). Only three of the four rock units are included in this equation because the percentages of all rock units in a basin must sum to 1.0, so the percentage of clastic rock is included implicitly. The correlation coefficient (r^2) between recharge values computed with equation 1 and from measured base flows was 0.785. The linear regression indicates that the recharge rate is lowest in areas underlain by clastic rocks (13.9 cm/yr) and highest in areas underlain by the western-toe carbonates (39.5 cm/yr) (table 4). The regression predicts the measured base flows reasonably well, except for two of the four stations with periods of record less than 10 years and Abrams Creek (fig. 7).

Table 4. Recharge rates for different rock units in the Shenandoah Valley estimated by linear regression of base flow.

[cm/yr, centimeters per year]	
Rock class	Recharge rate, cm/yr
Metamorphic	23
Carbonate	24.7
Clastic	13.9
Western-toe carbonate	39.5

Transmissivity

Estimates of transmissivity for the four rock units were computed from specific-capacity data measured at nearly 500 wells in the Shenandoah Valley, of which nearly 80 percent were completed in carbonate rocks (U.S. Environmental Protection Agency, 2002, STORET Legacy Data Center, accessed March 15, 2002, at <http://www.epa.gov/storpubl/legacy/gateway.htm>; Kozar and Mathes, 2001). Specific capacity (Q/s) is the ratio of pumping rate to drawdown in a well, from which the transmissivity (T) can be calculated from the following relation:

$$Q/s = \frac{1}{(2.3/4\pi T)\log(2.25Tt/r^2S)}, \quad (2)$$

where

- r is the well radius [L],
- t is the time of pumping [T], and
- S is the storage coefficient (Todd, 1980).

The value of the storage coefficient was assumed to be 1×10^{-4} —an order of magnitude variation in S causes the estimated T values to vary by about 10 percent. The specific-capacity data indicate that transmissivity generally is highest

in the western-toe carbonate rocks, where the median value is 110 m²/d. The highest values were estimated in the other carbonate rocks, however, where transmissivity ranges more than 5 orders of magnitude from 0.2 to more than 7,000 m²/d, and has a median value of 25 m²/d (fig. 8). Transmissivity values generally are lower in clastic and metamorphic rocks, where the median values are 10 and 5 m²/d, respectively, although the ranges of values for all rock units largely overlap.

Anisotropy in Inclined, Fractured Sedimentary Rocks

Anisotropic hydraulic properties have long been observed in inclined, fractured sedimentary rocks, and a number of studies have documented anisotropy in Mesozoic rift basins and watersheds in the Valley and Ridge Province in eastern North America (fig. 1). Vecchioli (1967) noted that pumping from gently dipping fractured shale in the Newark Basin in New Jersey produced larger drawdowns in wells aligned along the strike of the rock than in wells aligned perpendicular to strike. A later study by Lewis (1992) in the Newark Basin determined that ground water flowed preferentially along the strike of dipping rocks and that, as a consequence, streams aligned perpendicular to strike directions received more base flow than did streams aligned parallel to the strike. More recently, Burton and others (2002) measured ground-water ages in piezometers in a small watershed in the Valley and Ridge Province in Pennsylvania. A transect of wells was placed perpendicular to a stream that flowed parallel to the strike of inclined beds of clastic rocks. Water flowing toward the stream was younger along paths aligned with the dip direction, and older along paths aligned opposite the dip direction.

The anisotropic properties of ground-water flow are a consequence of the orientation of bedding planes and fractures that provide preferential flow paths through the sedimentary rocks, which generally have little primary permeability. Preferential flow along bedding planes has been extensively documented in studies of flat-lying sedimentary rocks, notably in Silurian dolostone in New York (Yager, 1996), Ontario (Zanini and others, 2000), and Wisconsin (Muldoon and others, 2001). Bedding planes also provide the principal flow paths in inclined sedimentary rocks, as was shown for clastic rocks in the Newark Basin in New Jersey by Michalski and Britton (1997) and Carleton and others (1999). In both flat-lying and inclined sedimentary rocks, at least two orthogonal sets of fractures (joints) typically cut the bedding and provide hydraulic connection between adjacent bedding planes (Michalski and Britton, 1997; Carleton and others, 1999; Burton and others, 2002). The density and spacing of the joint sets determines the degree of cross-bedding anisotropy in the fracture network. The direction of maximum hydraulic conductivity is oriented within the bedding plane, and the direction of minimum hydraulic conductivity is perpendicular

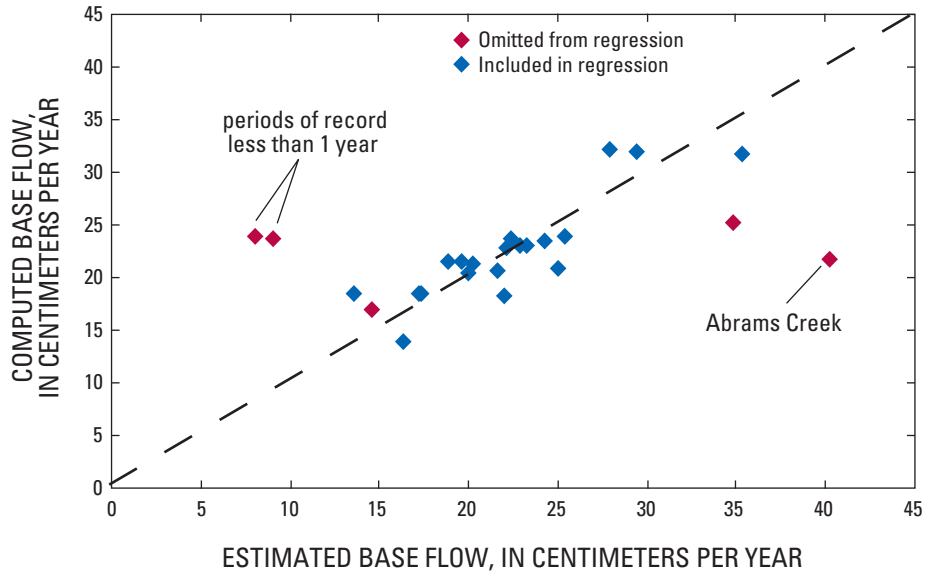


Figure 7. Relation between base flow estimated from streamflow measurements and computed as a function of the percentages of the basin area underlain by rock unit.

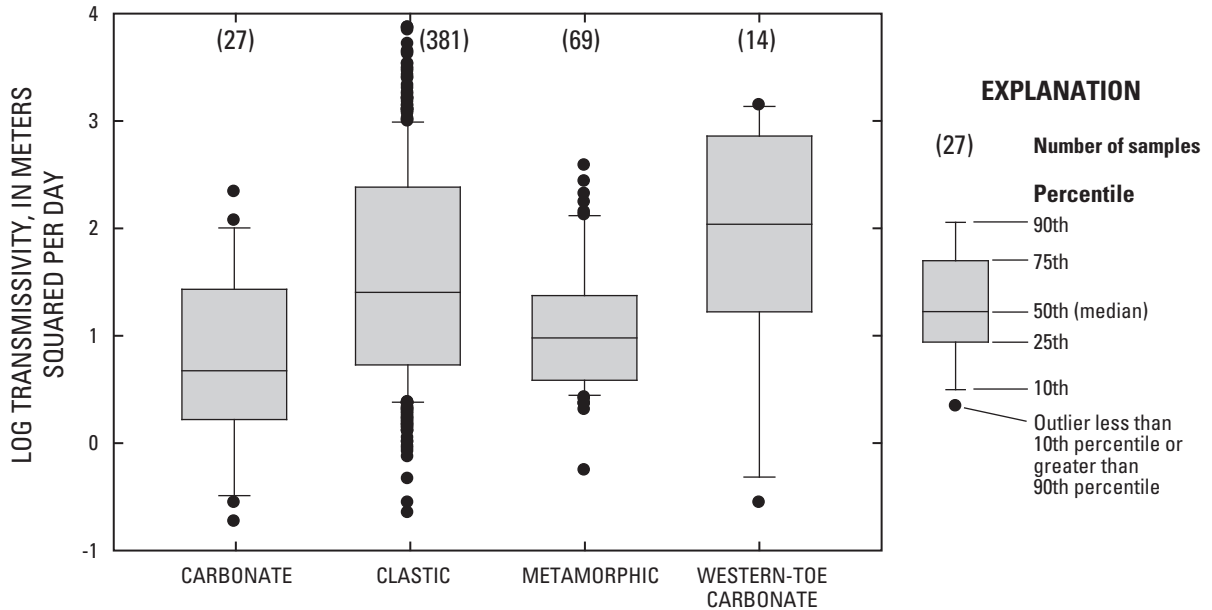


Figure 8. Box plots showing transmissivity values by rock unit estimated from specific capacity of pumped wells.

to the bedding. In flat-lying rocks, the resulting conductivity tensor is oriented horizontally and vertically. In inclined rocks, the tensor can be oriented horizontally along strike, but it is rotated in the downdip direction so that the direction of minimum hydraulic conductivity is oriented normal to the dip. Extensive through-going fractures or faults can cut through numerous bedding planes at high angles and serve as preferential flow paths, barriers to flow, or both.

Simulation of Flow in Inclined, Fractured Sedimentary Rocks

Simulation studies of inclined, fractured-rock aquifers have used three basic approaches to represent anisotropic properties. These studies generally use three-dimensional models constructed with MODFLOW (Harbaugh and others, 2000), a finite-difference (FD) model that is based on an orthogonal grid. The simplest approach has been to align the FD grid parallel to strike and specify horizontal anisotropy to decrease hydraulic conductivity parallel to the dip direction. Vertical hydraulic connections under this approach are controlled by specifying vertical anisotropy to decrease the hydraulic conductivity in the vertical direction. The simulated conductivity tensor is, therefore, oriented horizontally and vertically, and does not conform to the actual dip of the rock. This approach can neither simulate the anisotropic hydraulic properties within the plane of dipping beds nor accurately represent the vertical movement of ground water along bedding planes. Examples of this approach for simulating ground-water flow in inclined sedimentary rock include

Senior and Goode (1999) in the Newark Basin, and Haugh (2002) and Lindsey and Koch (2004) in the Valley and Ridge Province (table 5). Each of these studies found evidence for increased hydraulic conductivity along the strike of the bedding. Estimated values of horizontal anisotropy (ratio of strike-parallel to strike-perpendicular hydraulic conductivity) ranged from 2:1 to 11:1. Vertical anisotropy (ratio of strike-parallel to cross-bed hydraulic conductivity) was generally an insensitive parameter in model calibration and was set to values ranging from 1:1 to 24:1.

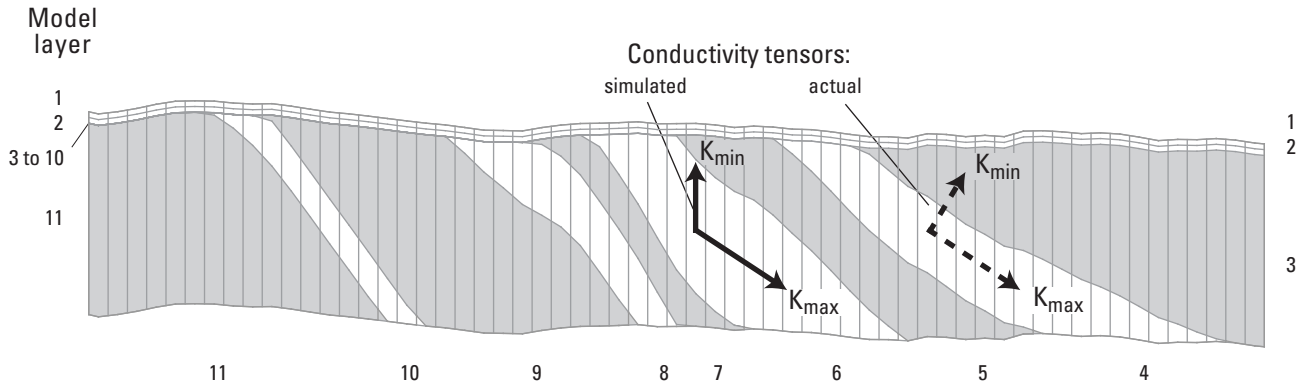
Two alternative FD approaches to simulating flow in inclined, fractured rocks involve either aligning the grid layers with the dip of the bedding or representing each fracture by specifying a stair-step configuration of high-permeability cells (fig. 9). Flow across low-permeability interbeds that separate adjacent fractures is computed using a vertical-conductance term with an inclined grid, while the interbeds are represented explicitly in a stair-step grid. These approaches are best suited to relatively simple geologic structures, such as homoclines and monoclines, although the stair-step approach could be applied to more complex geologic structures if the spacing of the FD grid was sufficiently small. A number of studies have used one of these approaches to simulate flow on local and regional scales in the Newark Basin (table 5). Flow within model layers representing fracture zones is typically assumed to be isotropic, although values of anisotropy (ratio of strike-parallel to strike-perpendicular hydraulic conductivity) were estimated by Carleton and others (1999) to be 2:1 and specified by Risser and Bird (2003) to be 5:1. In these alternative approaches, vertical anisotropy (ratio of strike-parallel to cross-bedding hydraulic conductivity) was a

Table 5. Finite-difference models constructed to simulate ground-water flow through inclined, fractured sedimentary rocks.

[Shading indicates models in which low-permeability interbeds are represented explicitly]

Model design	Geologic setting	State	Dip of bedding (degrees)	Anisotropy		Reference
				Horizontal (within layer)	Vertical (between layers)	
A. Oriented grid						
	Newark Basin	PA	11	11	1	Senior and Goode (1999)
	Valley and Ridge Province	TN	20	2 to 8	10	Haugh (2002)
	Valley and Ridge Province	PA	60 to 80	5	24	Lindsey and Koch (2004)
B. Inclined grid						
	Newark Basin	NJ	27	2	1.8×10^5	Carleton and others (1999)
	Newark Basin	PA	8	1	138 to 7,500	Goode and Senior (2000)
	Newark Basin	NJ	15 to 70	1	10	Lewis-Brown and Rice (2002)
	Newark Basin	PA	10 to 30	5	10	Risser and Bird (2003)
	Newark Basin	NJ	8	1	190 to 660	Lewis-Brown and others (2005)
C. Stair-step grid						
	Newark Basin	PA	12	1	3.8×10^4	Goode and Senior (2000)

A Inclined grid



B Stair-step arrangement of high-permeability cells

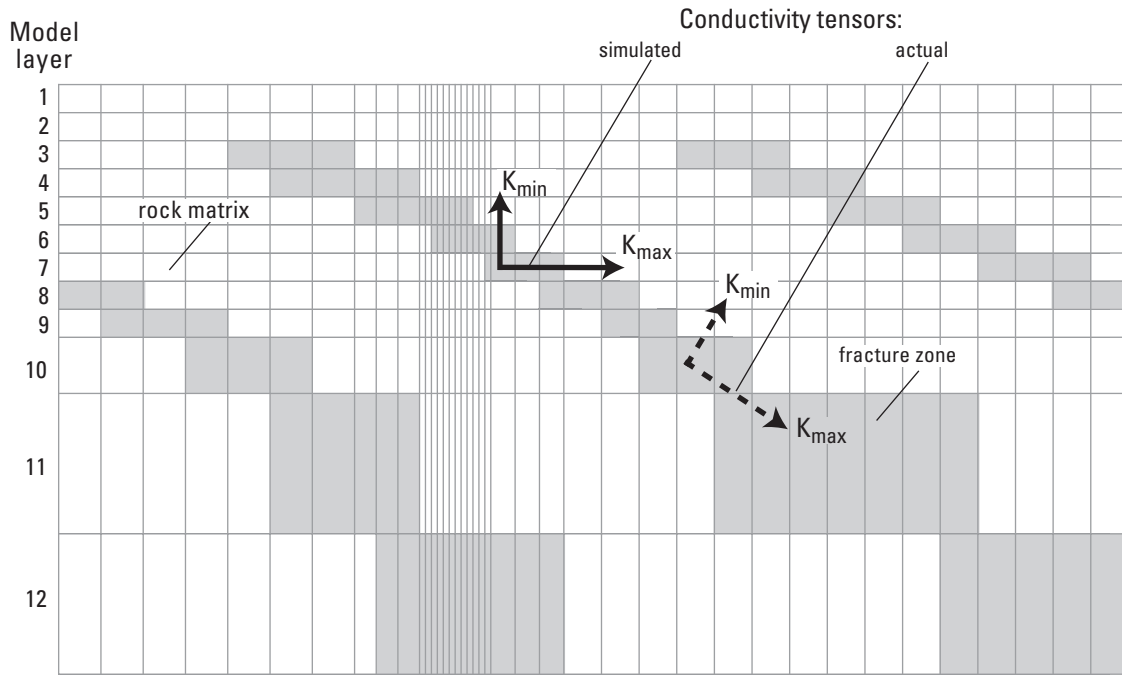


Figure 9. Schematic diagram showing alternative designs to represent ground-water flow through inclined fractured sedimentary rocks with an orthogonal finite-difference grid. (Modified from Goode and Senior, 2000, figs. 11 and 24.)

generally insensitive parameter in model calibration, except in models that simulated aquifer tests (Carleton and others, 1999; Goode and Senior, 2000) in which estimated values ranged from 138:1 to more than 1×10^5 :1.

The accuracy of simulations using an orthogonal FD grid with MODFLOW is limited by the assumption that the principal directions of the conductivity tensor are parallel to the coordinate axes used to define the grid. Hoaglund and Pollard (2003) showed that significant errors in flow can result if the orientation of the conductivity tensor does not coincide with the model coordinate axis. The resulting errors in flow are a function of the dip angle, the direction of the hydraulic gradient, and anisotropy (ratio of bedding-parallel to cross-bedding hydraulic conductivity). The errors are small (< 20 percent) for dip angles less than 10° , but can reach 100 percent for dip angles greater than 50° (Hoaglund and Pollard, 2003). Weiss (1985) had previously developed an FD numerical method to address this issue by using a nonorthogonal, curvilinear coordinate system, but the method has not been incorporated in widely used FD models such as MODFLOW. Recently, Anderman and others (2002) added a package to MODFLOW to represent variable-direction anisotropy within a two-dimensional plane. Although this same method could be extended, in principle, to three dimensions, it is not currently available in MODFLOW.

In finite-element (FE) models, such as SUTRA, the principal directions of the conductivity tensor can be specified independently of the model coordinate axes and the FE mesh. As a result, SUTRA is particularly applicable to the simulation of flow through folded and faulted fractured-rock terranes, like the Shenandoah Valley, where directions of strike and dip are variable. Bedrock structure in these terranes can be represented by varying the orientation of the conductivity tensor in each element to reflect variations in the strike and dip of the bedding. In this study, directions of strike and dip were computed from a three-dimensional representation of bedrock structure that was interpolated from generalized sections that show the orientation and attitude of the bedding in rocks that underlie the Shenandoah Valley.

Representation of Bedrock Structure in Shenandoah Valley

The sedimentary rocks of the Shenandoah Valley contain foliations that serve as conduits for ground-water flow. The rocks were deposited as horizontal strata along bedding planes, but were deformed during the late Paleozoic Alleghanian orogeny. Contractual forces were directed to the northwest from the southeast (current geography) and resulted in folded strata with the axes and hinges of the anticlines (concave down) and synclines (concave up) oriented northeast to southwest. Two sets of prominent fractures (joints) developed perpendicular to the bedding when the rocks were folded (fig. 10). Fractures that parallel the northeast-southwest-

trending fold axes are called longitudinal joints, and fractures that are perpendicular to the axes are called cross joints.

The clay-rich clastic rocks also developed cleavage, another type of foliation, through contractional deformation. Cleavage associated with folding is oriented parallel to the fold axes and, in cross section, appears to fan about the fold (fig. 10D). In tightly folded strata, cleavage can be more strongly developed than bedding and serves as the primary conduits for ground-water flow. In the Shenandoah Valley, for example, cleavage is locally well developed in the shale of the Martinsburg Formation where it strikes northeast and dips consistently to the southeast, parallel to the axial planes of the folds (Drew and others, 2004).

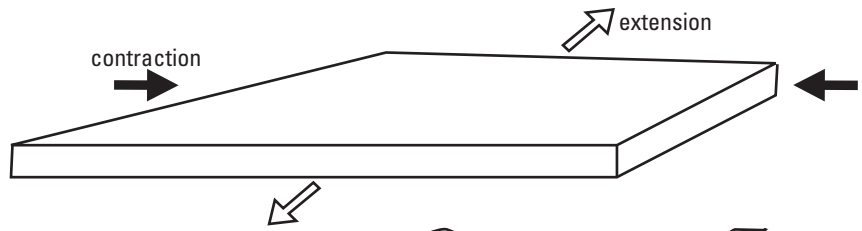
These conceptual foliations are illustrated in a section through the north-central part of the Shenandoah Valley (see fig. 10E). Horizontal bedding is folded into a syncline. Beds on the east limb and the west limb of the fold dip downward toward one another, and the beds are nearly horizontal along the hinge axis at the center of the fold. Steeply dipping longitudinal and cross joints provide hydraulic connections across the bedding. Locally, several steep, northwest-dipping thrust faults cut the east limb of the syncline, providing steep through-going pathways across bedding. These five types of foliations (bedding, longitudinal and cross joints, thrust faults, and cleavage) provide conduits for ground-water flow (Kozar and others, 2007; Weary and others, 2004).

Conceptual Fracture Framework

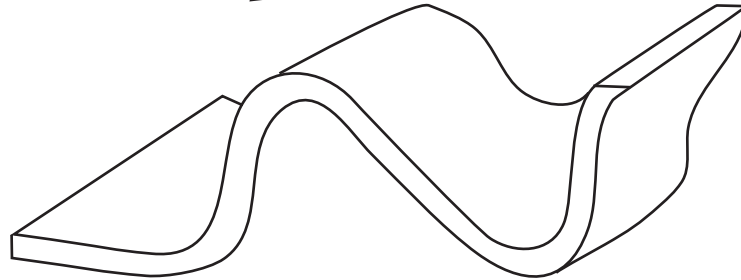
Ground water flows in the Shenandoah Valley through a set of interconnected flow systems. The foliations described above form a three-dimensional network of fractures that is approximately orthogonal and aligned with the bedding of the rock in areas of carbonate and clastic rocks; in metamorphic rocks, the network is more irregular. This pervasive fracture network forms a regional flow system throughout the valley. This regional flow system is intersected by faults that offset the bedding and can act as barriers to flow. Intense fracturing and cleavage associated with some faults provides conduits for vertical flow, however, and have been correlated with spring locations in some carbonate rocks of the valley (Harlow and others, 2005). In addition, dissolution along fractures in some carbonate rocks has created narrow karst channels that funnel ground-water flow. Sinkholes provide discrete points of recharge, and springs serve as discrete points of discharge. Faults and karst features create local flow systems that are hydraulically connected to the regional flow system and can either collect or distribute water.

The approach chosen to simulate ground-water flow through the folded, fractured rock of the Shenandoah Valley was based on the resolution of the simulation model and the capability of available modeling programs. A lateral-mesh spacing of 1 km was chosen to provide a model that could represent the entire valley with a computation time that was sufficiently short to allow model calibration. The 1-km lateral-mesh resolution is fine enough to represent

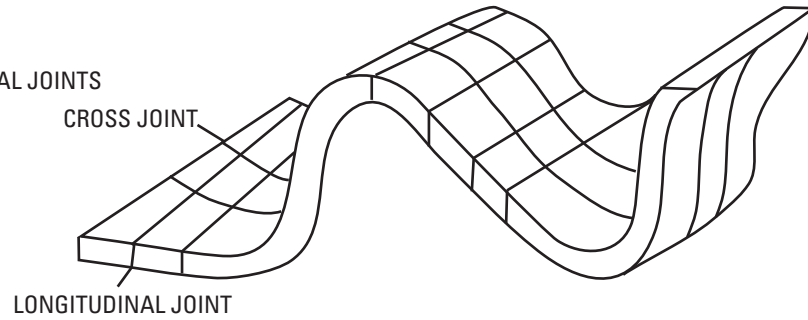
A HORIZONTAL STRATA



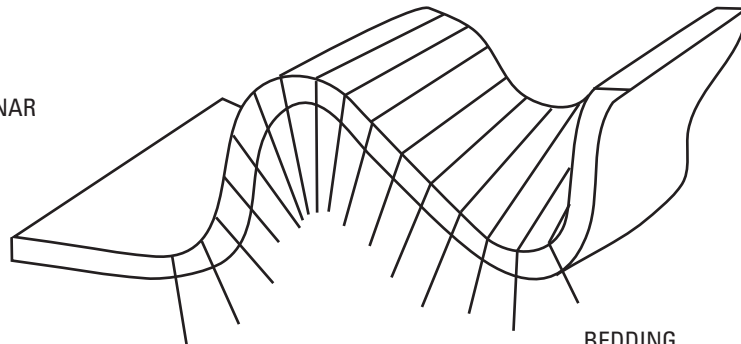
B FOLDED STRATA



C CROSS AND LONGITUDINAL JOINTS



D FANNING CLEAVAGE AXIAL PLANAR TO FOLDS



E BEDDING AND FOLDS BLOCK DIAGRAM ALONG SECTION G-G' (LOCATION OF SECTION SHOWN IN FIG. 3)

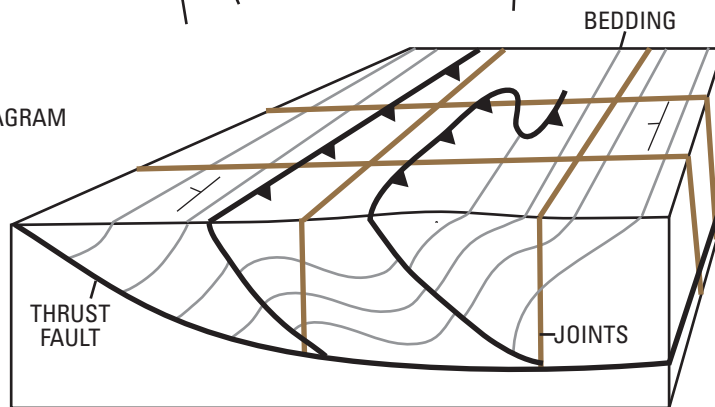


Figure 10. Formation of fractures in response to contractional deformation and folded bedding.

regional trends in topography and drainage, but is too coarse to represent karst features and minor faults that may be locally important. The representation of these features also is limited by the lack of available comprehensive field data from geologic mapping. The choice of lateral-mesh spacing was, therefore, a compromise that considered both the regional nature of the model and the available data.

Computer programs used to develop ground-water models (including MODFLOW and SUTRA) are based on the theory of flow through porous media, but are commonly applied to fractured-rock aquifer systems, especially at a regional scale, by accounting for anisotropy in the hydraulic properties of fractured rock. Computer programs are available to simulate flow in discrete fractures embedded in porous media (for example, Therrien and Sudicky, 1996), but have not been applied to regional-scale models where the geometry of discrete fractures is poorly defined. One exception is a field-scale model of flow through gold-bearing veins near a shear zone in the Canadian Shield in Ontario where the geologic structure has been extensively mapped (Beaudoin and others, 2006). The ground-water model of the Shenandoah Valley was designed to only represent the regional flow system because the lateral-mesh spacing was not fine enough to resolve discrete features. This decision is supported by geochemical evidence from springs in carbonate rock that indicate ground-water discharge generally is near saturation with respect to calcite (L.N. Plummer, U.S. Geological Survey, oral commun., 2007). In contrast, ground water in areas dominated by discrete flow typically is undersaturated with respect to calcite, because travel times are too short to allow dissolution reactions to reach saturation (White, 1988). Thus, discharge to springs in carbonate rock in the Shenandoah Valley appears to be dominated by the regional flow system, rather than by discrete fractures.

Form Lines, Form Surfaces, and Computation of Conductivity Tensor

Seven geologic sections were constructed across the Shenandoah Valley, from the Potomac River (A–A') at the north to the southern watershed divide (G–G') (fig. 11). The sections begin at the North Mountain Fault at the western boundary of the valley, continue eastward to the drainage divide in the Blue Ridge, and extend to a depth of about 5 km below sea level. The sections show the spatial distribution of major rock units, form lines of bedding, and mapped thrust faults. Contacts at land surface were projected to depth using available structural data for strike and dip of the bedding. The thicknesses of units at the surface were used to project the geometry below land surface.

The internal structure of the folded clastic and carbonate rocks in the Shenandoah Valley is depicted by form lines drawn parallel to bedding. Structure in the metamorphic rocks is highly complex and was not considered in this study because it was not possible to generalize at the maximum

adopted model resolution (1 km). The form lines are generalized because the scale and spacing of the sections are relatively large. Bedding can be considerably more complex in areas where the folds are very tight or the beds are overturned. The Staunton-Pulaski thrust fault, which divides the valley into two structural blocks, is shown on the sections, but many minor faults are not.

The form lines of bedding on each cross section were connected along strike to create "form surfaces," deformed planar surfaces that provide spatial continuity throughout the rock mass. Form surfaces were interpolated from the form lines depicted on the set of sections using procedures (provided by R.B. Winston, U.S. Geological Survey, written commun., 2006) written for SutraGUI (Winston and Voss, 2004), a graphical interface developed for SUTRA that is based on the Argus ONE program (Argus Interware, Inc., 1997). Corresponding points on adjacent sections were linked together to construct an interpolated form surface, from which the elevation, direction of dip, and dip angle could be computed for any point on the surface. A set of three SutraGUI functions uses this information to compute the angles needed to define the conductivity tensor specified in SUTRA. These functions transform the angles into the coordinate system used in SUTRA and require the direction of maximum hydraulic conductivity (i.e. parallel to strike or parallel to dip) as additional data.

The resulting stack of form surfaces provides a three-dimensional representation of bedding within the folded rocks that underlie the Shenandoah Valley. The form surfaces are better defined for the carbonate rocks than for the clastic rocks, because the carbonate rocks underlie a wider area in the valley and penetrate the subsurface to greater depths. The subcrop area of clastic rocks is much narrower and the folding is much tighter, especially near Massanutten Mountain, so the form surfaces are difficult to portray. The form surfaces defined for carbonate rocks in the narrow Page Valley east of Massanutten Mountain (fig. 2) also are highly generalized and might not correspond locally to the actual strike and dip of the rocks.

Anisotropy in the carbonate and clastic rocks that underlie the valley was represented by aligning the principal directions of the conductivity tensor with the bedding, so the components of the conductivity tensor are parallel to the principal fracture orientations. Fractures parallel to bedding, the primary hydraulic paths within the rock, are represented by form surfaces. The bedding planes are generally intersected at high angles by two sets of orthogonal joints: longitudinal joints that parallel the strike of the bedding and cross joints that are perpendicular to the bedding. Locally, cleavage planes strike parallel to longitudinal joints and bedding. The directions of maximum and medium hydraulic conductivity are assumed to lie within the form surface (bedding plane), whereas the minimum hydraulic conductivity is oriented normal to the form surface (parallel to the joint sets). It is possible that fracture apertures become wider as a result of dissolution along the intersections of the joint sets

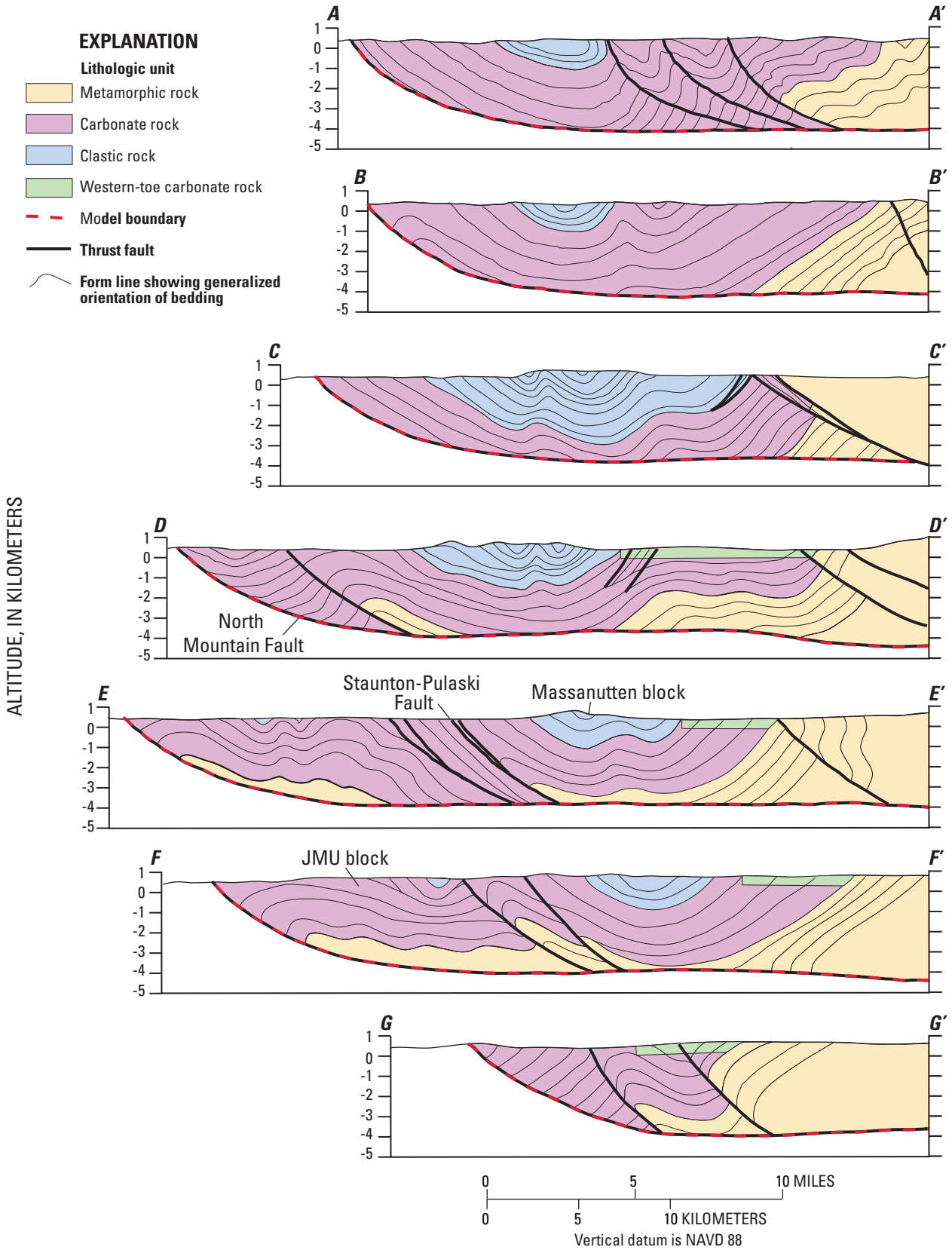


Figure 11. Generalized geologic sections showing rock units and form lines of bedding and faults in rocks underlying the Shenandoah Valley, Virginia and West Virginia. (Location of section lines shown on figure 3.)

with bedding-plane fractures. The wider apertures could channel flow and impart preferential flow directions within the bedding plane. The direction of maximum hydraulic conductivity within bedding planes could, therefore, be aligned either along strike (parallel to longitudinal joints) or cross-strike (parallel to cross-strike joints), with the medium hydraulic conductivity having a lower value.

Ground-Water Flow Model

Ground-water flow in the Shenandoah Valley was simulated with three-dimensional models constructed using SUTRA. Steady-state simulations were used to compute the hydraulic-head distribution and to estimate the rate of ground-water flow because the aquifer system is assumed to be near equilibrium, as indicated by long-term water-level hydrographs (fig. 5) and the relatively small rate of ground-water withdrawals. The models represent the aquifer system in fractured bedrock with a constant saturated thickness, and downward flow from the saturated overburden is represented as recharge to the underlying fractured bedrock. Three alternative models (A, B, and C) were constructed to assess the effects of specified boundary conditions and different conceptual models of bedrock structure.

Model Design

The top surface of the model represents the water table and was interpolated from the elevations of land surface using a 30-m DEM because the available information was insufficient to map the water table. The top surface was constrained to coincide with perennial stream channels and was specified below land surface in areas between channels to form a subdued reflection of the land-surface topography. The bottom surface of the model coincides with the North Mountain Fault, which underlies the entire valley (fig. 3 and fig. 11).

Mesh and Layering

The model domain covers an area of 7,120 km² and includes the watersheds of the Shenandoah River and Opequon Creek, with the exception of areas west of the North Mountain Fault. The model domain is discretized using a three-dimensional FE mesh consisting of an irregularly connected mesh in the areal plane that is extended vertically to the bottom of the model domain. Areal, the mesh appears as a set of quadrilateral elements with maximum lateral lengths of 1 km (fig. 12). Smaller elements with maximum lateral lengths of 500 m are used to better represent the bedrock geology in the Page Valley and in parts of the JMU block. A generalized stream network was delineated and used to constrain the mesh generation.

The rock mass represented by the model is as much as 5 km thick and is divided into four units. Most of the ground water is assumed to flow within the top 300 m of the fractured bedrock, based on the assumption that the number of water-bearing fractures declines with depth and the fact that most wells are completed within this depth below land surface. The top unit is, therefore, assigned a thickness of 300 m and discretized vertically into 10 equally spaced layers of elements (fig. 13). The remaining three units correspond to the major rock units used to partition the bedrock: fine-grained clastic (referred to as clastic below), carbonate, and metamorphic rocks. The western-toe carbonate rocks are distinguished as a separate zone within the carbonate unit. Maps of the top and bottom of the carbonate rocks were interpolated from the geologic sections presented earlier and were used to divide the rock mass into these three units. The layering in each unit conforms to the top and bottom of the unit. In areas where the metamorphic rock overlies the carbonate rock (see, for example, section C–C', fig. 11)—all rock underlying the metamorphic subcrop area is assumed to be metamorphic rock. Each rock unit is subdivided into five layers of finite elements using a factor of 1.3 to increase the layer thickness with depth. The resulting mesh contains 25 layers with 342,300 elements and 364,264 nodes.

Boundary Conditions

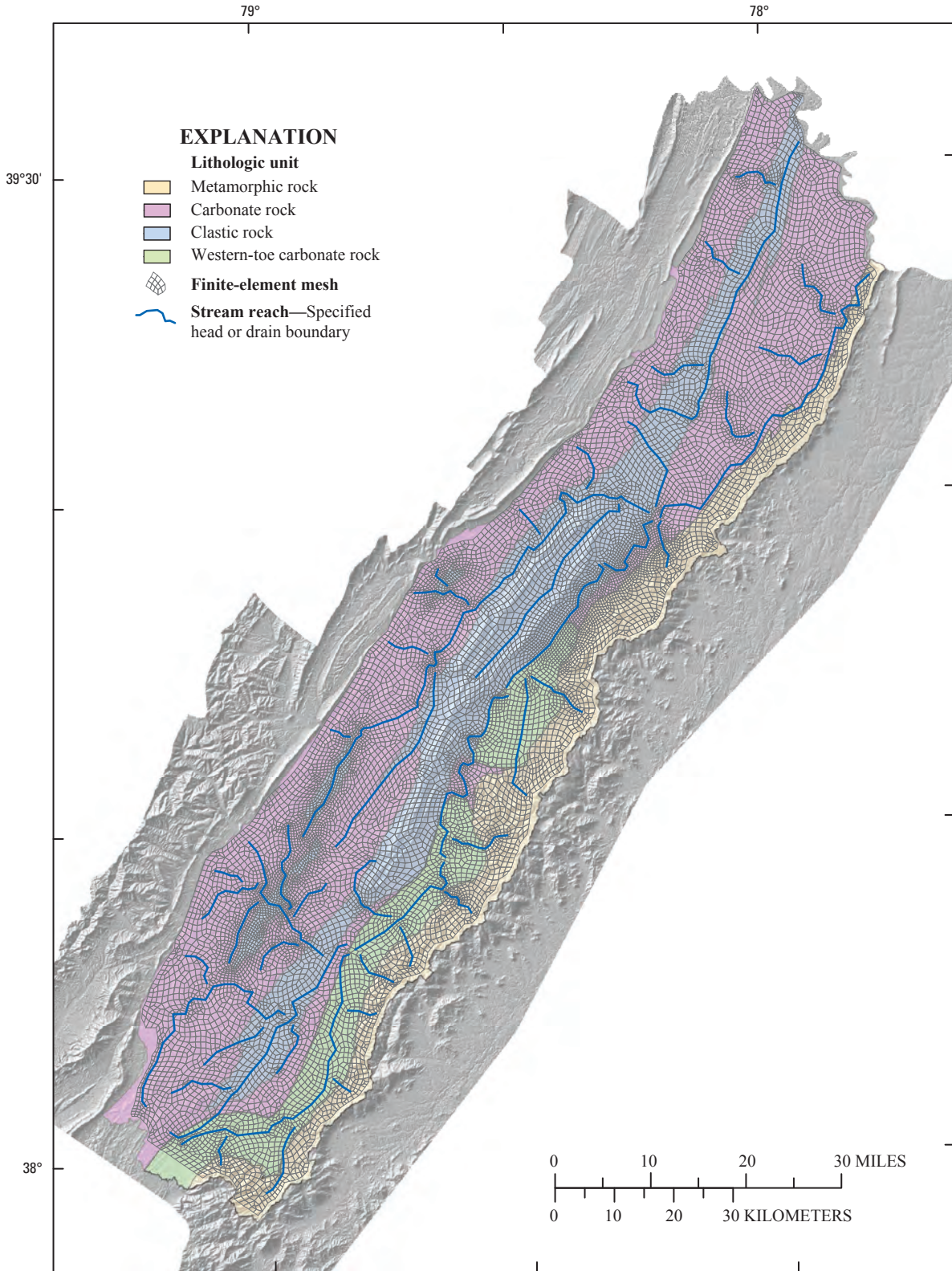
All the lateral and bottom boundaries of the model domain are assumed to be no-flow (impervious to flow). Stream channels, including the Potomac River and the Shenandoah River and its tributaries, are represented by head-dependent flow boundaries. These boundaries use two modifications of the specified-pressure boundary provided in SUTRA (referred to as specified head for the uniform density simulations described herein), as described in appendix 1 (provided by A.M. Provost, U.S. Geological Survey, written commun., 2006). The first modification allows a separate conductance term C to be specified for each node:

$$C = \frac{KLW}{l}, \quad (3)$$

where

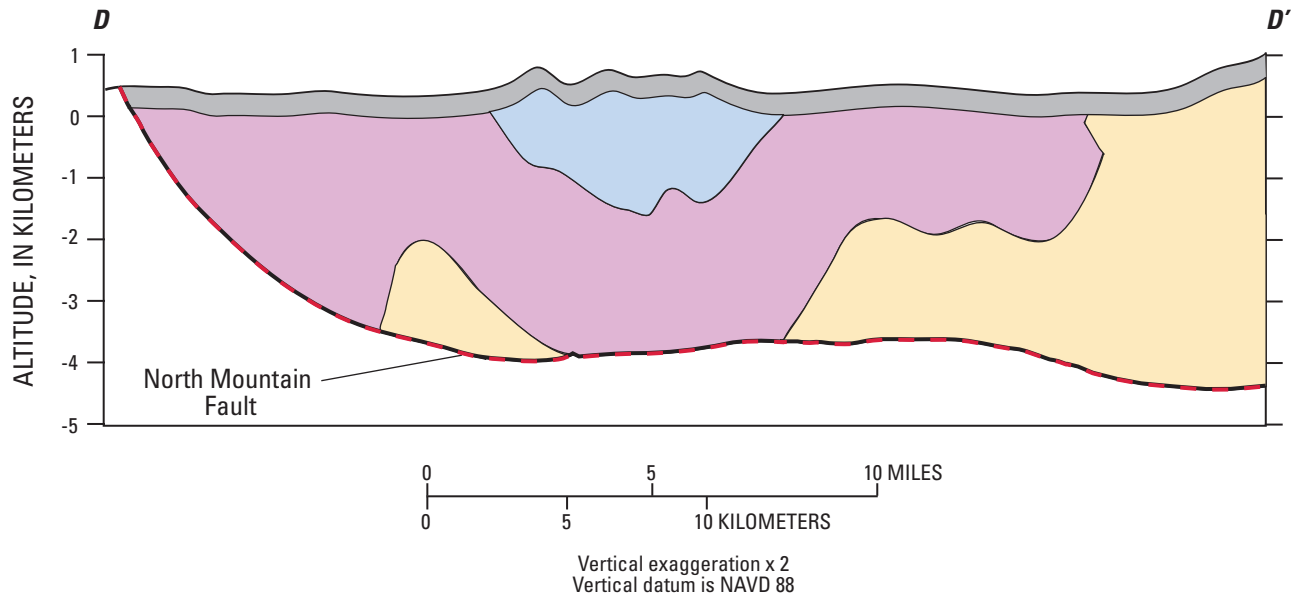
K	is hydraulic conductivity [L/T],
L	is length of stream reach [L],
W	is width of stream reach [L], and
l	is thickness of the streambed [L].

Two leakage terms (K/l) are used in the model, one for nodes representing the Potomac River and the other for nodes representing the remainder of the stream network. The Potomac River is deeply incised along the northern boundary of the model, and a relatively small leakage value was estimated to limit flow through the boundary and match the observed heads, which are elevated above the river. A larger leakage value is specified for the other nodes so that outflow is controlled by the hydraulic conductivity of



Base from U.S. Geological Survey, Seamless Data Distribution System
 Accessed in 2006 at URL <http://seamless.usgs.gov>
 Universal Transverse Mercator projection, Zone 17

Figure 12. Model domain showing map view of finite-element mesh and four rock units represented by the model.



EXPLANATION

- Unit 1: Near-surface rocks (300-m thickness),
10 equally spaced layers
- Unit 2: Clastic rocks,
5 layers with increasing thickness
- Unit 3: Carbonate rocks,
5 layers with increasing thickness
- Unit 4: Metamorphic rocks,
5 layers with increasing thickness

Figure 13. Generalized section D–D' showing units used to define model layers. (Location of section line shown in fig. 3.)

elements adjacent to the boundary. The second modification to SUTRA allows the specified-head boundary to function in a manner similar to a drain boundary in MODFLOW by preventing inflow from the boundary. Outflow from a drain boundary only occurs when the head at the node is larger than the specified head, and is proportional to the conductance term C ; when the head at the node is lower than the specified head, the drain boundary has no effect. Stream boundaries are represented by drain nodes in models A and C, and by specified-head nodes in model B (table 6).

The top model boundary condition provides recharge from the overburden and uses rates estimated with the linear regression that relates base flow to the four rock units, as discussed previously (table 4). Recharge is specified as a fluid source applied to nodes on the top surface of the model, except those that represent stream boundaries. The uniform recharge rate applied to nodes in each rock unit is increased slightly to take into account the additional area associated with nodes

that are used to represent stream boundaries and for which recharge is not represented directly.

Ground-water withdrawals from 50 wells with rates greater than 1 L/s are represented by fluid sinks assigned to node locations that are nearest to each well. At each node location, the pumpage is distributed over a vertically stacked set of nodes that falls within the open interval of the well. For wells lacking this information, a mean depth (110 m) and open-interval length (45 m) are assumed. Well fields containing several closely grouped wells are represented as combined pumpage from a single well when these would be represented by the same column of nodes in the mesh.

Hydraulic Conductivity

Hydraulic-conductivity values were estimated for each of the four rock units through model calibration. In the upper model unit (top 10 model layers of elements), the elements

Table 6. Parameter values in alternative models of ground-water flow specified or estimated through nonlinear regression.

[Optimized values are shaded. m/d, meters per day; m, meters; d, day]

Parameter	MODEL			
	A		B	C
	Value	Approximate individual confidence interval	Value	Value
Maximum hydraulic conductivity, m/d:				
Carbonate rock	3.4	2.8 - 4.0	2	3.7
Clastic rock	0.26	0.18 - 0.36	0.19	0.26
Metamorphic rock	0.13	0.10 - 0.16	0.1	0.17
Western-toe carbonate rock	1.1	0.78 - 1.6	0.8	1.3
Anisotropy ratios:				
Maximum:medium ^a				
Carbonate rock	1		1	1
Clastic rock	1		1	1
Metamorphic rock	1		1	1
Western-toe carbonate rock	1		1	1
Maximum:minimum ^b				
Carbonate rock	17	11 - 23	11	7.8
Clastic rock	17 ^c		11 ^c	7.8 ^c
Metamorphic rock	1		1	1
Western-toe carbonate rock	1		1	1
Power function:				
Decay factor: m ⁻¹	1.1E-03	0.82e-03 - 1.3e-03	6.8E-04	1.3E-03
Depth threshold, m				
Carbonate rock	150		150	150
Clastic rock	50		50	50
Metamorphic rock	70		70	70
Western-toe carbonate rock	150		150	150
Stream leakance, d ⁻¹ :				
Potomac River	4.E-03		4.E-03	4.E-03
Other stream channels	40		40	40
Conductivity tensor		variable strike and dip	variable strike and dip	uniform strike
Stream boundary condition		drain	specified head	drain

^a Models A and B: strike-parallel to dip-parallel conductivity; model C: horizontal to vertical conductivity.^b Models A and B: strike-parallel to cross-bedding conductivity; model C: strike-parallel to strike-perpendicular conductivity.^c Equals value estimated for carbonate rock.

belonging to each rock unit are defined from the bedrock geology at land surface (fig. 3). Elements associated with the lower three units (bottom 15 model layers) correspond to clastic rocks in unit 2, either carbonate or western-toe carbonate rocks in unit 3, and metamorphic rocks in unit 4. A minimum unit thickness of 1 m is specified in parts of the model domain where a rock unit is absent to maintain hydraulic continuity of each unit throughout the domain; this 1-m unit is assigned the value of hydraulic conductivity of the unit below it.

The hydraulic-conductivity values are computed for elements in each rock unit using a conductivity tensor and a function that relates hydraulic conductivity to increasing depth below land surface. Three scalar values (herein referred to as conductivity) and two angles are required to define the conductivity tensor in this study. Although in general three angles are required, only two are required here, because it is assumed that the K_{\max} direction is parallel to the horizontal plane, so the third angle is always zero. The scalar values K_{\max} , K_{med} , and K_{\min} correspond to the directions of maximum, medium, and minimum conductivity, respectively. Values of K_{\max} , K_{med} , and K_{\min} were estimated by nonlinear regression (inverse modeling) for the clastic and carbonate rocks. The conductivity tensors for western-toe carbonate and metamorphic rocks were assumed to be isotropic ($K_{\max} = K_{\text{med}} = K_{\min}$), so only the K_{\max} value was estimated.

The conductivity tensors for clastic and carbonate rocks are assumed to be aligned with the strike and dip of the bedding in models A and B (herein referred to as variable-strike-and-dip models). In the variable-strike-and-dip models, the following definitions of the conductivity tensor are made: the maximum conductivity (K_{\max}) is oriented along the direction of strike, the medium conductivity (K_{med}) is oriented along the direction of dip, and the minimum conductivity (K_{\min}) is perpendicular to the bedding. Two angles were required to define the conductivity tensor: the first defines the strike of bedding as measured counterclockwise from east (from the +X coordinate direction), and the second is the declination of bedding as measured from the horizontal plane in the dip direction (the direction perpendicular to strike).

The angles described above were derived for each element representing clastic or carbonate rocks by interpolation using the stack of form surfaces described previously. The model domain is subdivided by the Staunton-Pulaski Fault into two structural blocks, the Massanutten block and the JMU block. In the Massanutten block, five form surfaces were used to define the conductivity tensors for carbonate rocks, whereas only three form surfaces were used to define the conductivity tensor for clastic rocks where the form surfaces are poorly defined. A separate stack of three form surfaces was prepared for the JMU block. Elements are assigned to either block according to their position relative to a surface representing the Staunton-Pulaski Fault. As a result, adjacent conductivity tensors on either side of the fault are not aligned, but flow along the fault is not represented explicitly.

In model C (herein referred to as uniform strike), the conductivity tensor in carbonate and clastic rocks was oriented horizontally and vertically, with the K_{\max} direction parallel to the N. 30° E. axis of the valley. The strike-direction angle was fixed at a uniform value throughout the model domain and the dip angle was set to zero. Model C is equivalent to using an orthogonal FD grid with grid rows parallel to the strike of the bedding while specifying horizontal anisotropy to decrease permeability in the grid-column direction. The conductivity tensor is assumed to be horizontal with the K_{med} direction oriented vertically and the maximum and minimum conductivities (K_{\max} and K_{\min}) parallel and perpendicular to strike, respectively.

The distributions of angles in models A and B are shown in perspective three-dimensional views of the model domain cropped along sections C–C' and E–E' (fig. 14). The predominant strike direction of the bedding is N. 30° E., but the strike directions in the model range from N. 30° W. to S. 30° W. These are mostly uniform within the Massanutten block (section C–C' block). The directions N. 30° E. (yellow) and S. 30° W. (blue) are parallel and distinguish bedding that is inclined southeastward from bedding that is inclined northwestward, respectively. These areas cover most of the model domain and are associated with either clastic or carbonate rocks. Narrow bands of equal strike direction correspond to undulations in the bedding. The area with a strike direction of 90° E. (green) corresponds to the western-toe carbonate and metamorphic rocks, which are assumed isotropic. The relatively complicated pattern visible in the block cropped along section E–E' corresponds to the JMU block (fig. 14A). Dip angles range from 0° to 60° and are generally steepest in carbonate rocks along the flanks of the basin (fig. 14B). Dip angles of 0° (red) are assigned to western-toe carbonate and metamorphic rocks, and areas where the bedding is horizontal. Dip angles in the JMU block are generally less steep than in the Massanutten block.

A power function similar to that applied to the Death Valley area in Nevada and California by Belcher (2004) is used to relate the decrease in hydraulic conductivity K below a threshold depth D :

$$K_{\text{depth}} = K10^{-\lambda d}, \quad (4)$$

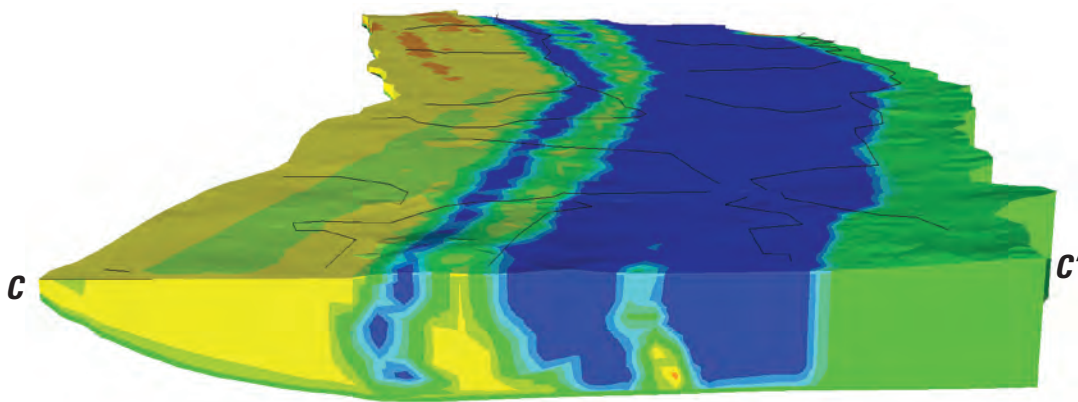
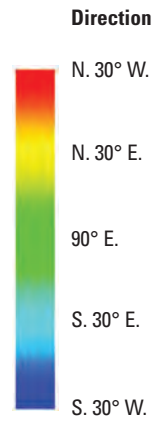
where

$$\begin{aligned} K_{\text{depth}} & \text{ is the hydraulic conductivity [L/T] at depth } d \\ & \text{ [L] below the threshold } D \text{ and} \\ \lambda & \text{ is a decay factor [L}^{-1}\text{].} \end{aligned}$$

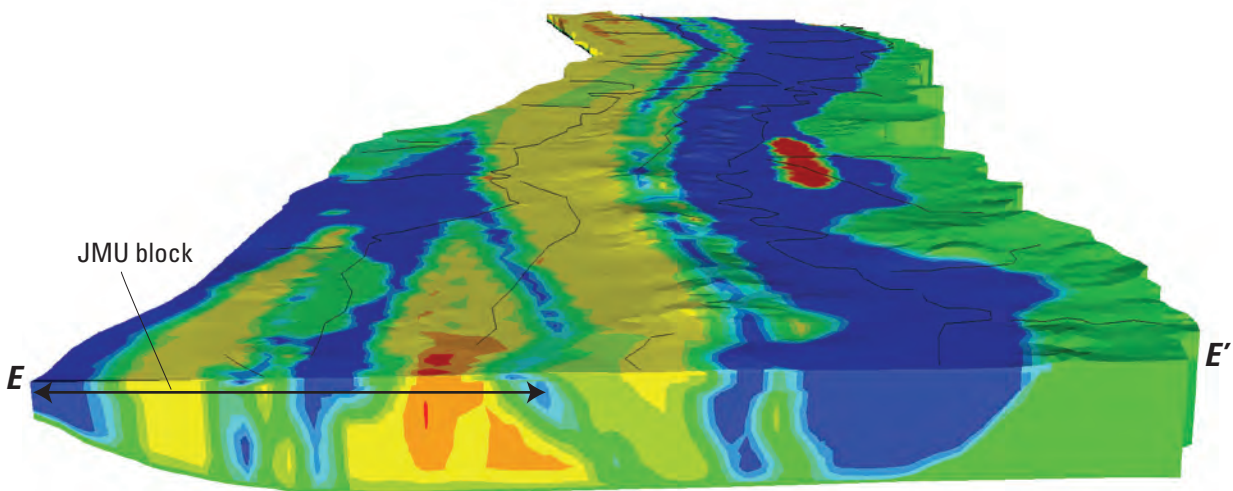
Threshold depths D were assigned for each rock unit based on the mean depth of wells completed in the unit (table 6). The depth decay factor λ was estimated through nonlinear regression and the minimum value of K_{depth} was limited to 10^{-12} m/s.

A Strike direction and maximum conductivity direction, K_{max}

EXPLANATION



Block cropped along section *C-C'*



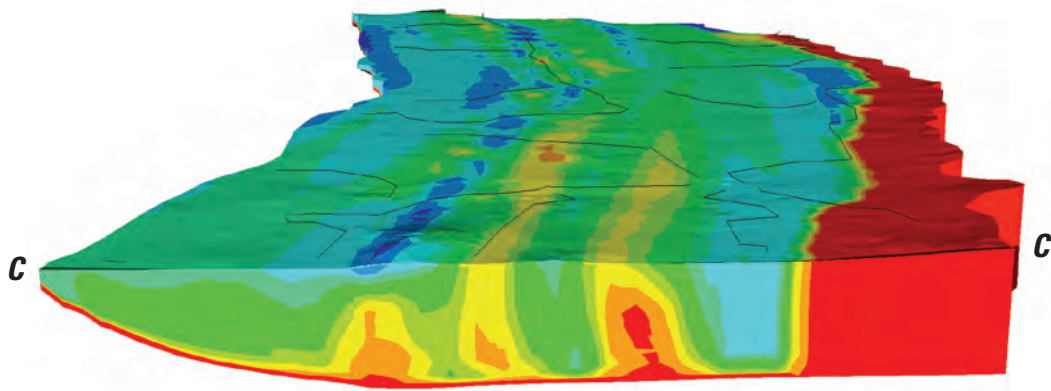
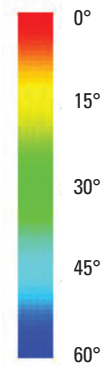
Block cropped along section *E-E'*

Figure 14. Perspective three-dimensional views along sections C–C' and E–E' showing attitude of bedding represented in ground-water flow models A and B: (A) strike direction (maximum conductivity direction, K_{max}), and (B) dip angle (medium conductivity direction, K_{med}). (Location of section lines shown in fig. 3.)

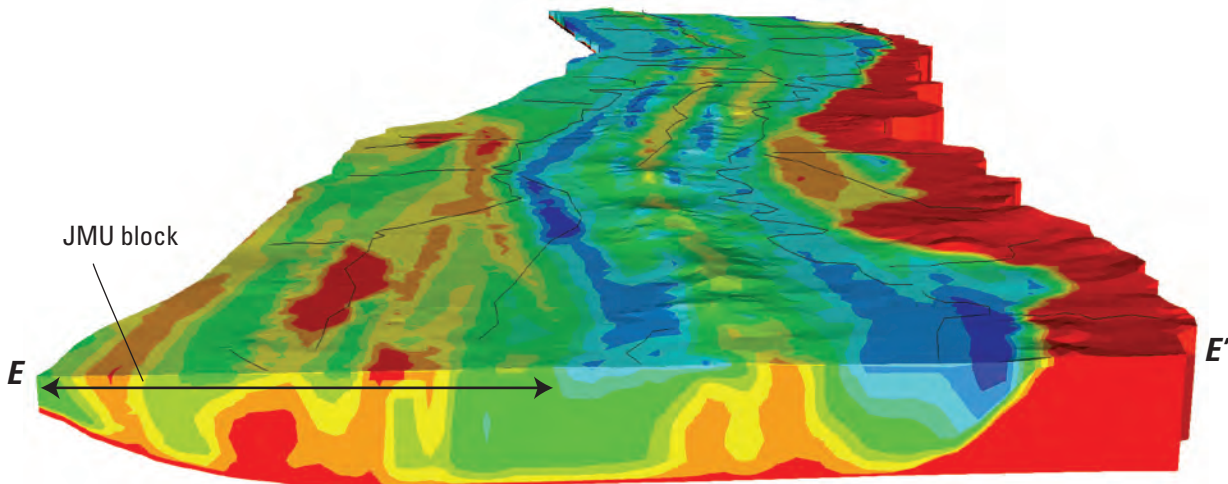
B Dip angle of medium conductivity direction, K_{med}

EXPLANATION

Angle



Block cropped along section *C-C'*



Block cropped along section *E-E'*

Figure 14. Perspective three-dimensional views along sections C–C' and E–E' showing attitude of bedding represented in ground-water flow models A and B: (A) strike direction (maximum conductivity direction, K_{max}), and (B) dip angle (medium conductivity direction, K_{med}). (Location of section lines shown in fig. 3).—Continued

Model Calibration

The ground-water flow models were calibrated by adjusting hydraulic-conductivity values to minimize the difference between ground-water levels and discharges simulated by the model and those observed in wells and streams in the Shenandoah Valley. Optimum parameter values were obtained through nonlinear regression using UCODE (Poeter and Hill, 1998), a computer program that uses weighted least squares to minimize model residuals (difference between observed and simulated data).

Observations

The nonlinear regression compared the simulated data with water levels measured in 354 wells and estimates of base flow at 23 streamflow-gaging stations (see table 3). Water-level measurements were obtained from the USGS's National Water Information System (NWIS) database for well data. This included information on the measurement interval, defined by the top and bottom water-bearing zones intercepted by the well, or the open interval in the well, if water-bearing zones were not noted. The measurement depth in the model was assumed to be midway between the top and bottom of the measurement interval, unless the water level was below the top of the interval, in which case the measurement depth was set midway between the water level and the bottom. The depth to water-bearing zones was noted for the 249 wells in Virginia, with an average measurement-interval length of 4 m and average measurement depth of 55 m. The measurement date was unknown for about 60 percent of the wells, while the rest of the measurements were made in 1984 or 1985 when water levels were near the long-term average (see fig. 5). Information for the 105 wells in West Virginia only included the open-interval location, however, so the average measurement-interval length was longer (68 m) and the average measurement depth was 31 m. Nearly all the measurements in West Virginia were made in 2003 or 2004 when water levels were lower than normal.

Base flow was estimated for 19 of the streamflow-gaging stations with a period of record that exceeded 10 years; flow data were available for less than 2 years at the other 4 stations (see table 3). The smaller watersheds are nested within the larger watersheds, and drainage-area sizes range from 36 km² for Happy Creek at Front Royal, Va., to 7,876 km² for the Shenandoah River at Millville, W.Va. Ground-water discharge simulated by the model was summed for all the nodes associated with the reaches contained in each watershed, and discharges from smaller watersheds were summed to compute discharges for larger watersheds.

Weights assigned to the head and flow observations in the regression were chosen to reflect measurement error, and to insure that the weighted head residuals and weighted flow residuals influenced the regression equally. Weights assigned to head observations were based on Hill and Tiedeman's

(2007, p. 295) suggestion that error values represent a 95-percent confidence interval, and were equivalent to a 3-m standard deviation in measurement error. Weights assigned to flow observations were proportional to the estimated base flow, under the assumption that the rating curves for larger watersheds are more accurate than for smaller watersheds and, therefore, produce better estimates (D.C. Hayes, U.S. Geological Survey, oral commun., 2007). Weights assigned to flow observations were equivalent to coefficients of variation ranging from 1 to 4 percent, which is smaller than the actual rating-curve error, but served to increase the influence of flow measurements in the regression. As a result, inferences made from the statistics generated by the regression are qualitative because the weights do not accurately reflect observation error.

Parameters

A total of 19 parameter values were specified in model A, 6 of which were optimized through nonlinear regression. Coefficients of variation range from 1 to 18 percent for the six estimated parameters, indicating that the regression is sensitive to the parameters and that the values are reasonably well estimated. The estimated value of the decay constant λ is the most uncertain because the parameter is correlated ($r^2 = 0.92$) with the estimated K_{\max} value for carbonate rock. Anisotropy ratios for maximum to medium conductivity ($K_{\max} : K_{\text{med}}$) were relatively insensitive parameters and were specified as 1.0 for all rocks, as was the $K_{\max} : K_{\min}$ ratio for metamorphic rocks. The $K_{\max} : K_{\min}$ ratios for clastic and western-toe carbonate rocks were specified equal to the ratio estimated for carbonate rock (17:1). Threshold depths used to compute the decline in conductivity with depth were specified for each rock unit as discussed above. Values for the two stream-leakance parameters were estimated through regressions that improved overall measures of model fit, but did not converge because the sensitivity of the regression to these parameters was too low.

Optimized K_{\max} values for the four rock units differ by about an order of magnitude, with the largest values estimated for carbonate rocks and the smallest value estimated for metamorphic rock (table 6). Although the estimated K_{\max} value for western-toe carbonates rocks (1.1 m/d) is less than that estimated for other carbonate rocks (3.4 m/d), the K_{\min} value is larger (1.1 m/d and 0.2 m/d, respectively) because the western-toe carbonate is assumed to be isotropic in model simulations. The estimated decay factor λ results in about an order of magnitude decline in hydraulic conductivity within 1 km of land surface for each rock unit (fig. 15). The distribution of hydraulic conductivity is illustrated in block diagrams showing estimated values of K_{\max} along two sections within the Shenandoah Valley (fig. 16). The largest values (orange and yellow) are assigned near land surface in areas underlain by carbonate rocks, while lower values (green) correspond to areas underlain by clastic and metamorphic rocks. Hydraulic conductivity decreases with depth beneath all rock units, but values decrease more slowly beneath the carbonate-rock

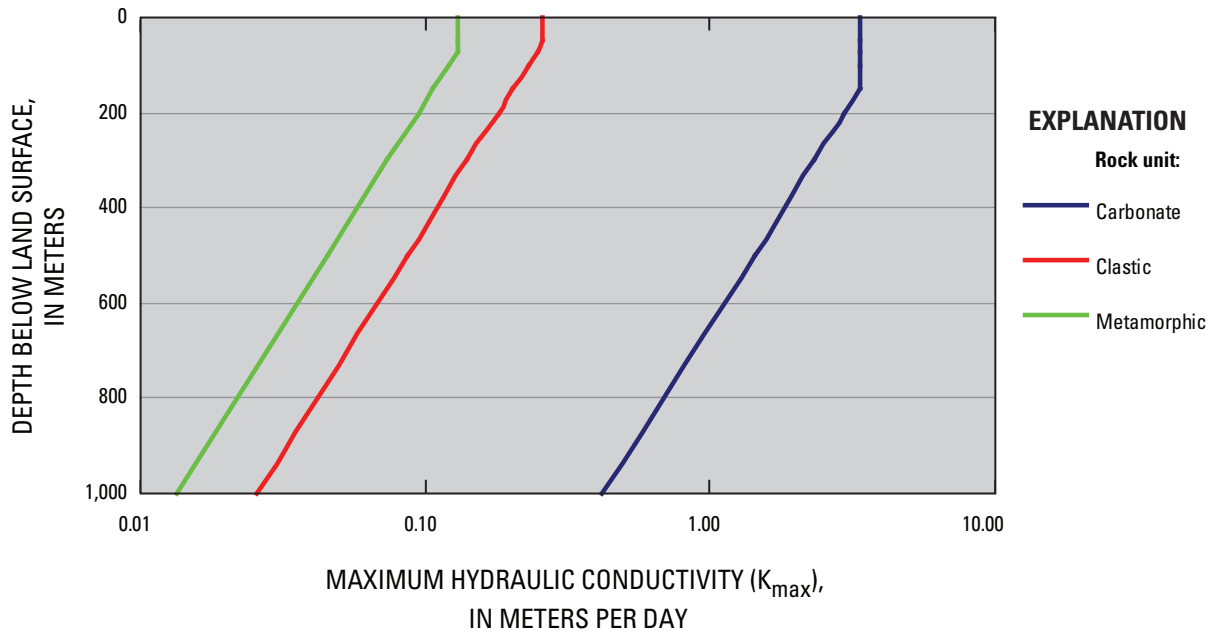


Figure 15. Estimated relations used to compute maximum hydraulic conductivity with depth in carbonate, clastic, and metamorphic rocks in model A.

areas where K_{max} is larger and the threshold depth is deeper. Simulated ground-water velocities are higher (greater than 5 m/d) in lowlands within carbonate areas and lower (less than 1 m/d) in uplands in clastic and metamorphic areas (fig. 17). Simulated velocities generally decline to less than 0.5 m/d within 1 km of land surface, except beneath carbonate areas where velocities of 0.5 m/d persist to depths greater than 2 km. Velocities were computed using an effective porosity estimated with ground-water age simulations, as discussed in the following section.

Replacing drain boundaries used to represent streams in model A by specified-head boundaries in model B resulted in smaller values of K_{max} and a smaller $K_{max}:K_{min}$ ratio, but all the parameter values generally fall within the approximate 95-percent confidence intervals associated with model A, or are close to the lower limit (table 6). The use of specified-head boundaries created an additional source of water in model B and increased the inflow rate by 10 percent. Infiltration from streams has not been shown to be a significant source of recharge in the valley, however, and the spacing of the FE mesh used in the model does not permit the precise placement of stream boundaries, so elevations of the specified heads at streams are approximate. For these reasons, model A is assumed to better represent the aquifer system than model B, although the model fit is slightly worse (table 7). In contrast, differences in the parameter sets obtained by replacing the variable-strike-and-dip conductivity tensor in model A with the uniform-strike tensor in model C are small, with the exception of the ratio of hydraulic conductivity parallel and perpendicular to bedding ($K_{max}:K_{min}$, 7.8:1), which was less than one-half the corresponding ratio ($K_{max}:K_{min}$, 17:1)

estimated for model A (table 6). There was little difference in model error between models A and C.

Comparison of K_{max} values estimated through model calibration with transmissivity values estimated from specific-capacity tests in the field is not straightforward. Field tests in fractured rock measure the water-transmitting properties of the local fracture network that surrounds a pumped well and, therefore, can display a wide range of values. In contrast, the model-derived values represent the properties of hydraulic connections among local fracture networks that control regional flow. These effective regional values typically fall within the range of values measured by field tests (Shapiro and others, 2007). In addition, comparison requires that the field-estimated transmissivity values (T) be converted to hydraulic conductivity (K) via knowledge of the saturated thickness b ($T = Kb$). The choice of saturated thickness is somewhat arbitrary because water in fractured rock flows through discrete intervals that are separated by rock layers that yield negligible flow, so only a small portion of the total thickness of the rock contributes water to a well. For the purpose of comparison, K values were calculated from the T values shown previously (fig. 8) by assuming that the saturated thickness is equal to the height of the water column above the bottom of the well. This strategy preserved the relative transmissivity rankings of the four rock units. Values of hydraulic conductivity estimated with model A fall within the interquartile ranges of field-derived values and are near the median values obtained for clastic and metamorphic rocks (fig. 18).

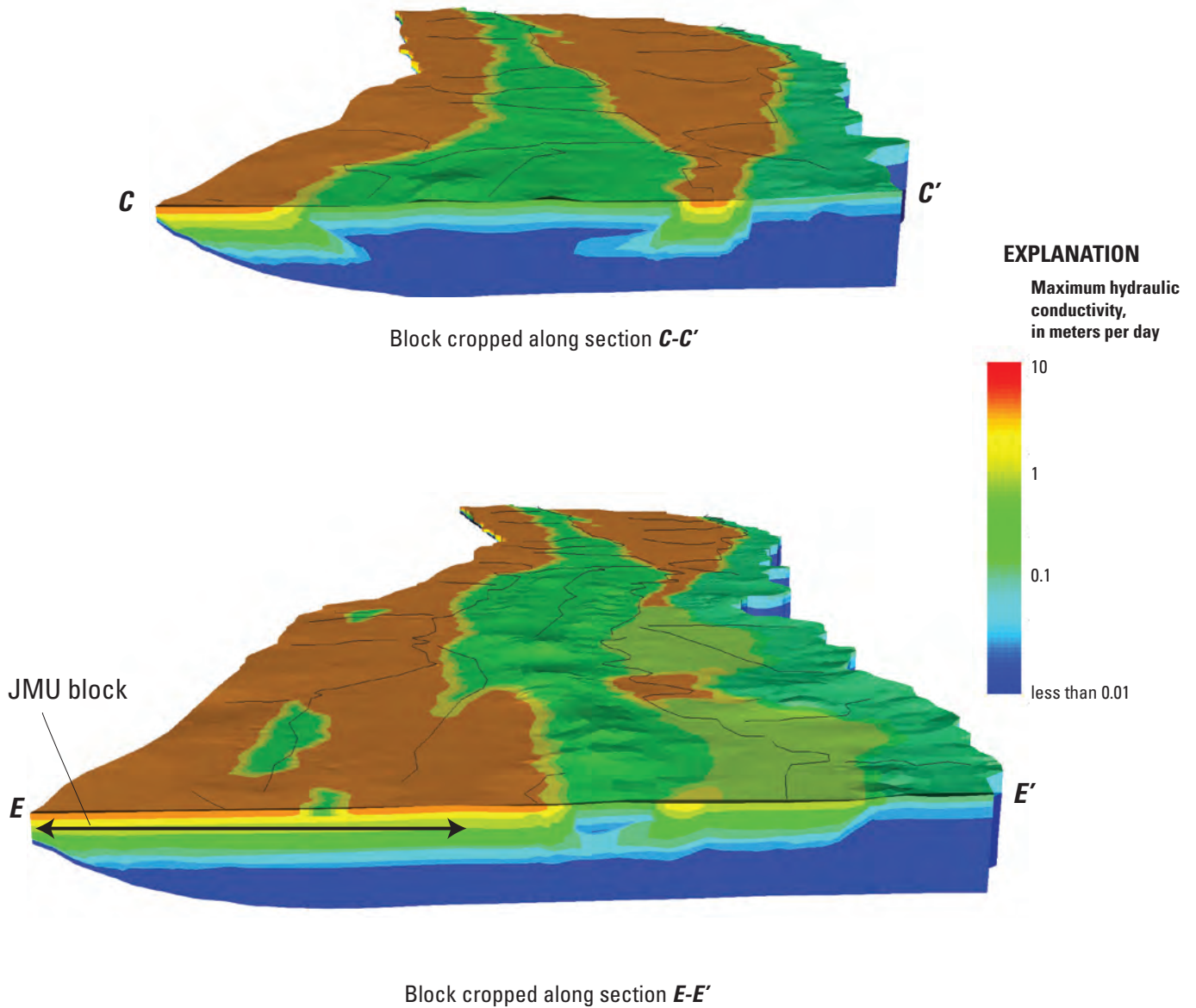


Figure 16. Block diagrams along sections C–C' and E–E' showing spatial distribution of maximum hydraulic conductivity (K_{max}) used in models A and B. (Location of section lines shown in fig. 3.)

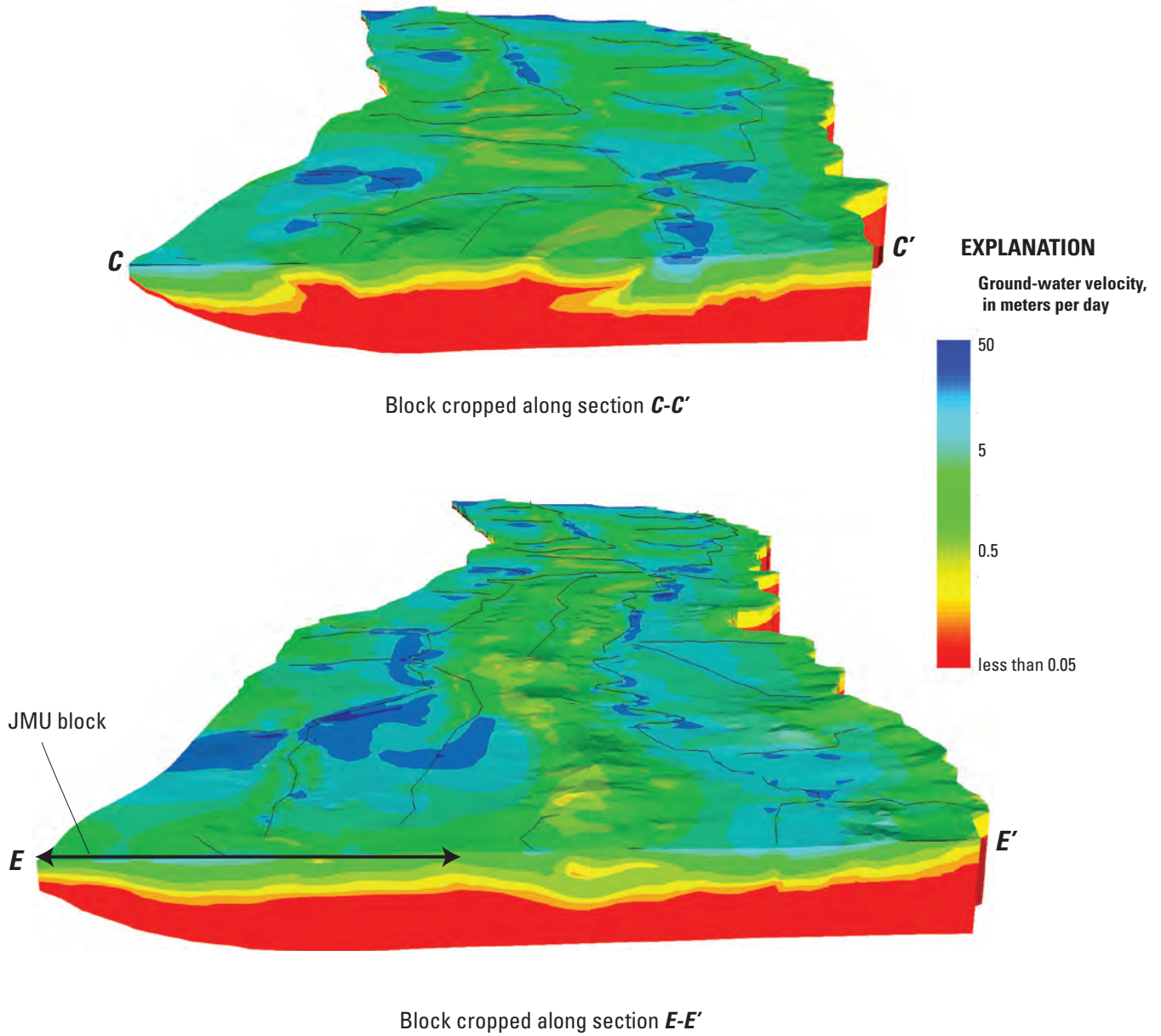


Figure 17. Block diagrams along sections C–C' and E–E' showing spatial distribution of simulated ground-water velocity in model A. (Location of sections shown in figure 3.)

Table 7. Standard error in meters in ground-water flow models of the Shenandoah Valley.

Rock unit	Number of observations	Model		
		A	B	C
Carbonate	226	21.1	19.8	20.6
Clastic	63	18.2	16.6	19.7
Metamorphic	16	22.0	20.4	23.0
Western-toe	49	18.2	21.5	18.1
All	354	20.2	19.5	20.2

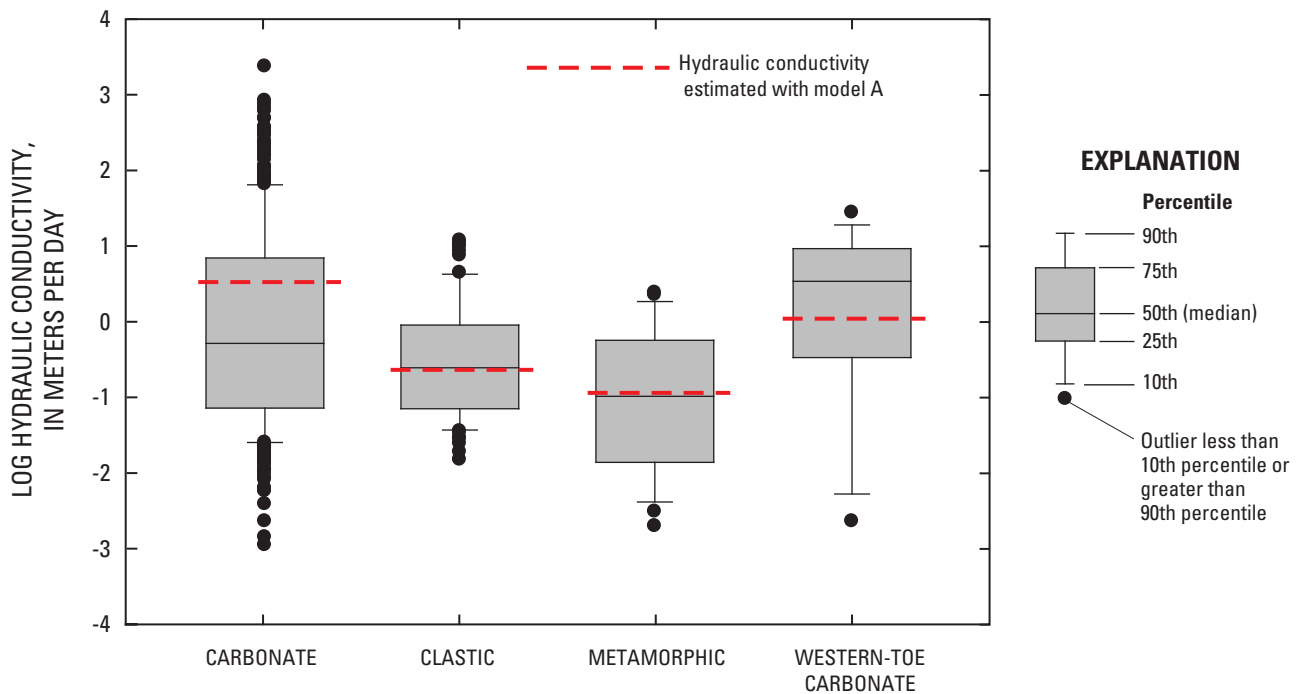


Figure 18. Box plots of hydraulic-conductivity values by rock unit estimated from specific capacity of pumped wells and through calibration with model A.

Model Fit

Residual plots for heads and flows (measured minus simulated values) indicate that model A simulates the ground-water flow system reasonably well. Residual plots for heads show little bias in model error with the mean residual near zero (fig. 19). The standard error in head is 20.2 m or 4 percent of the 480-m measurement range (table 7). There are 10 outliers, however, where the simulated heads underpredict the actual value by more than 45 m; these observations are located at higher elevations along the North Mountain Fault and the Blue Ridge Mountains, and on Massanutten Mountain in Shenandoah County and at the southern end of the watershed in Augusta County. The standard errors in models B and C are equivalent to those in model A (table 7), indicating a similar model fit.

Simulated flows in model A are generally within 40 percent of the observed value, but are less than one-half the observed flow for two streams that drain metamorphic rocks (Back Creek and Happy Creek) and one that drains clastic rocks (Passage Creek) (fig. 6 and table 3). A plot of weighted residuals indicates a bias in model error, with mostly positive residuals (underprediction) (fig. 20A). The underprediction of flow could result from the lack of detail in the simulated stream network, or from the omission of features (like karst channels) that increase ground-water discharge from the aquifer system. The largest absolute error in simulated flow (3.4 m³/s) is for the reach of the South Fork of the Shenandoah River in the Page Valley south of Front Royal. The model representation of the highly complex geologic structure in this area is not sufficiently detailed to accurately simulate ground-water discharge along this reach of the river. The simulated

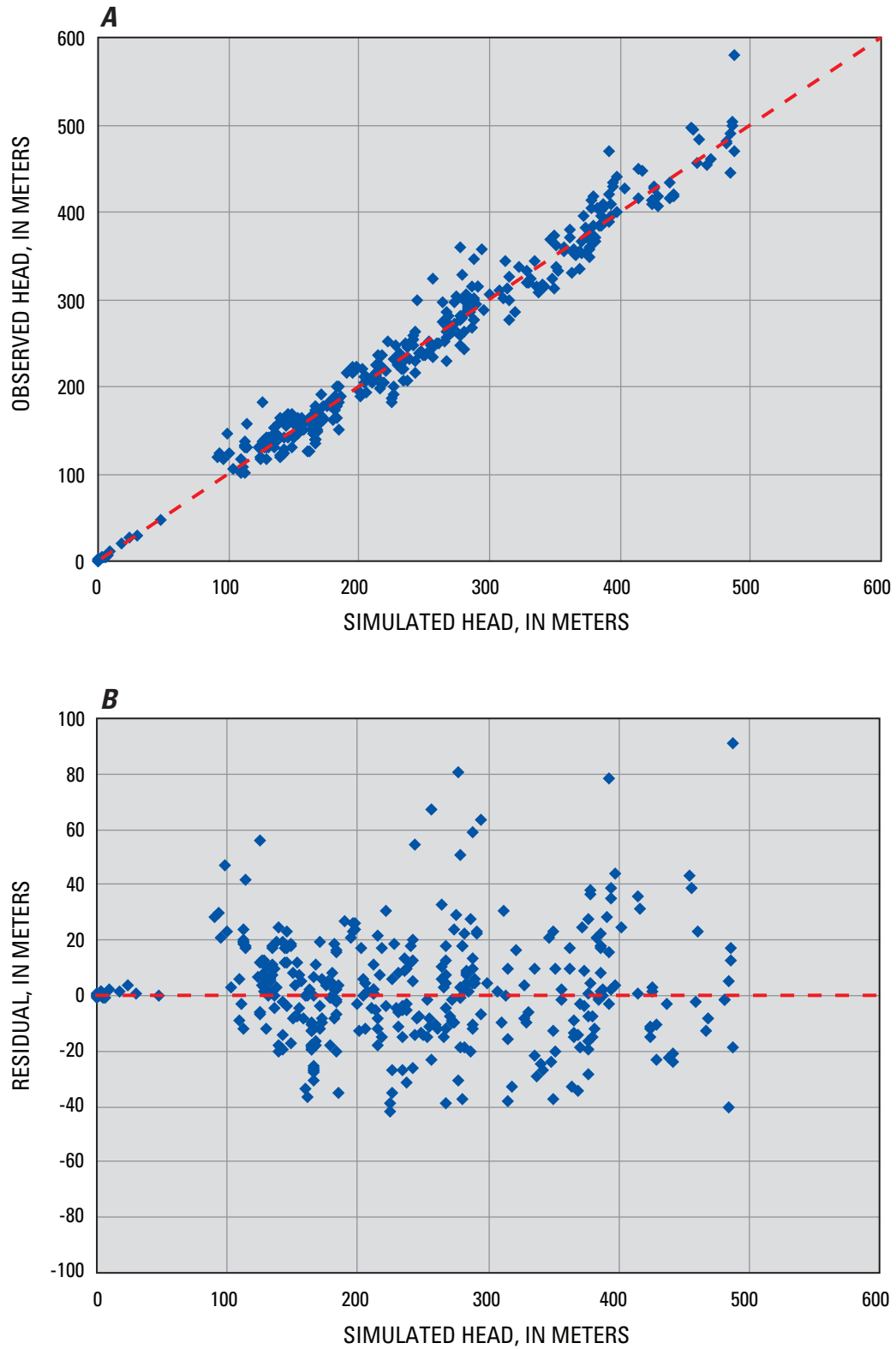


Figure 19. Residual plots for simulated heads in model A: (A) relation between simulated and observed values, and (B) relation between simulated values and residuals.

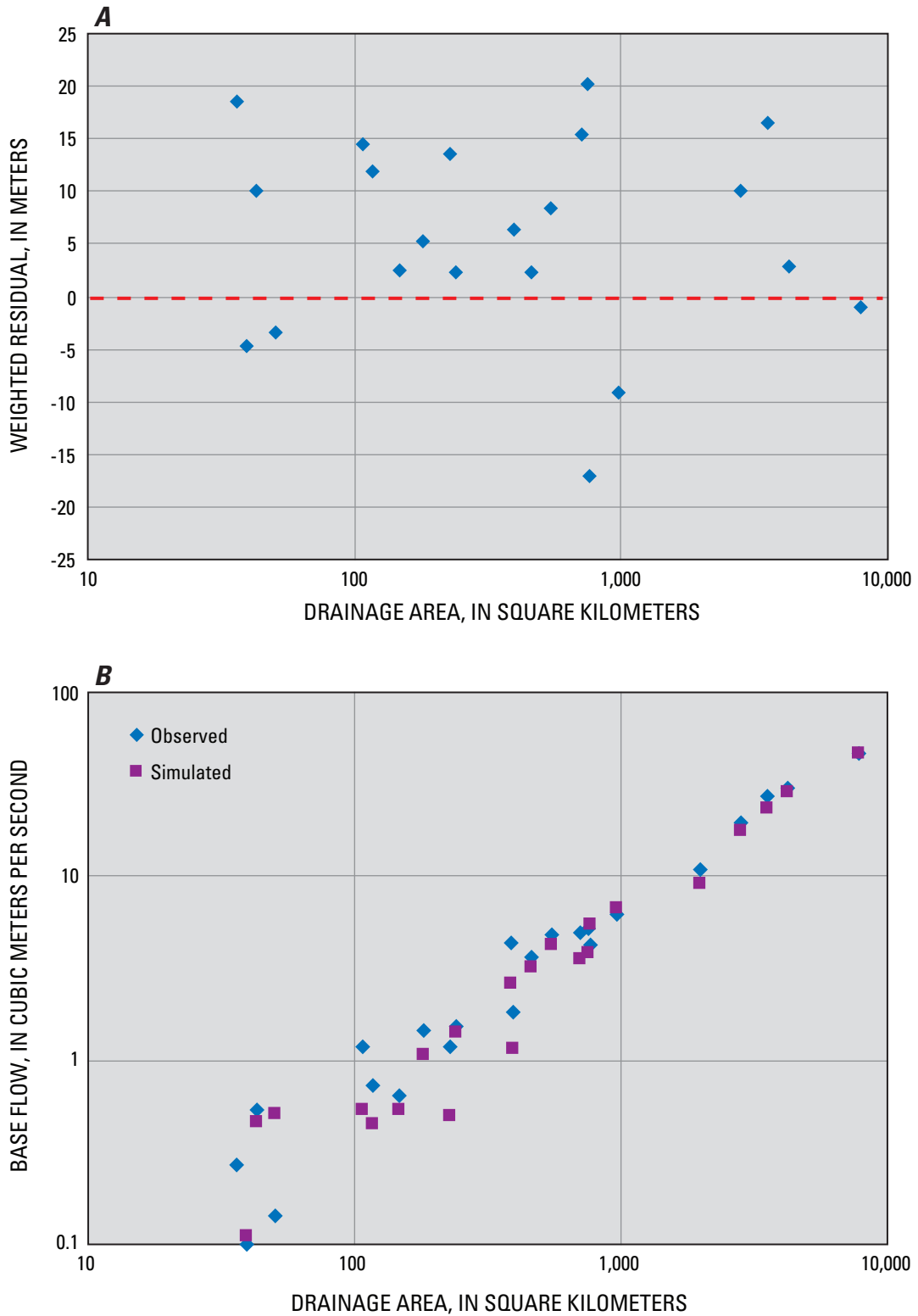


Figure 20. Residual plots for simulated flows in model A: (A) relation between residuals and drainage-area size, and (B) relation between simulated and observed base flow and drainage-area size.

results generally reproduce the reduced variability in flow with increasing drainage-area size, as observed in the actual estimates of base flow (fig. 20B).

The sensitivity of model A to the estimated parameter values was assessed by comparing the composite-scaled sensitivities (CSS), which indicate the amount of information provided by all observations on each parameter (Hill, 1998). The CSS statistics indicate that the parameter sensitivities are nearly equal, but are slightly larger for the K_{\max} value for carbonate rocks and the decay factor λ used in the function relating hydraulic conductivity with depth (fig. 21). The parameter sensitivities for the K_{\max} value for western-toe carbonate rocks and the anisotropy ratio $K_{\max}:K_{\min}$ are slightly lower.

The sensitivity of the regression to specified parameter values was explored through the parameter error ratio, which is the ratio of the percent change in an optimal parameter value to the percent change in a specified value. Four variations of model A were tested in which a single parameter value was fixed near the value specified in the optimal regression, but perturbed by an arbitrary amount, and then the remaining parameters were obtained by recalibrating the model using the same observations and weights as in the original calibration. The K_{\max} value of carbonate rock was increased by 5 percent in variant A-1 to serve as a basis for comparison for the other three variants. The recharge rate was increased by 5 percent for all rock units in variant A-2, and the strike direction and dip angles defining the conductivity-tensor orientation were increased by 5 percent for the clastic and carbonate rocks in variant A-3. The threshold depth D below which the maximum hydraulic conductivity decreases with depth was increased by 100 percent for all rock units in variant A-4.

Error ratios associated with the specified-recharge rates (variant A-2) are all larger than 6.0, indicating that error in the recharge rate would strongly affect the estimates of all parameters in the regression (table 8). Error ratios are largest for the K_{\max} value of clastic rocks (21) and the $K_{\max}:K_{\min}$ ratio of carbonate and clastic rocks (14), the parameters that are the most sensitive to errors in specified recharge. Error ratios associated with the K_{\max} value of carbonate rock (variant A-1) are also largest for these two parameters (6.5 and 6.7, respectively). Error ratios for other parameters are less than 2.5 in variant A-1. Error ratios associated with the strike direction and dip angles (variant A-3) are less than 3.5, and error ratios associated with threshold depths (variant A-4) are less than 0.3, indicating that these parameters have relatively little effect on regression estimates. These results suggest that acquiring additional information concerning recharge rates would increase confidence in the estimated parameter values.

Model Applications

Conservative solute-transport simulations were conducted with two alternative models (model A: variable strike and dip,

and model C: horizontally anisotropic with uniform strike) to simulate ground-water age in the flow system and the capture zones of production wells. Capture zones were delineated through backward tracking using reverse-flow simulations that track migration of a tracer solute injected at the production wells to discharge points at land surface. Reverse-flow simulations are achieved by multiplying all specified heads and all sources by negative one (-1). This means that water production wells become injection wells in the reverse-flow simulation and recharge rates are specified as negative values. Further, the drain boundaries representing discharge to streams are replaced by specified-head boundaries with negative head values. These changes have the effect of routing flow in a reverse direction from inflow points at production wells and along streams to discharge points at land surface. Longitudinal and transverse dispersivities were specified as 800 m and 30 m, respectively, to facilitate convergence of the transport solution and reduce numerical oscillations.

Ground-Water Age Distributions

Ground-water age was computed through steady-state simulations in which the solute concentration was interpreted as age. The initial concentration (age) of ground water and concentration of recharge were specified as zero, and a zero-order (linear increase in time) production of solute of unit strength (1 concentration unit/year) was used to represent aging. The simulated ages are inversely proportional to the value of effective porosity specified in the models, which is not well known for the model area. The age distribution can be examined qualitatively, however, to distinguish younger water from older water. In addition, the age of simulated ground-water discharge can be compared with estimated age of base flow from the Shenandoah watershed. Michel (1992) estimated the ground-water residence time in the Potomac River Basin to be 20 years, based on long-term tritium records. His approach assumed that base flow was derived from two ground-water sources—recent flow (within 1 year) and older flow from long-term storage. The residence time computed for the Potomac River Basin was the longest of those for seven moderate-sized basins (4,500–75,000 km²) studied in the United States (Michel, 1992). Recently, the ages of ground water discharged from more than 50 springs in the Shenandoah Valley were computed (L.N. Plummer, U.S. Geological Survey, oral commun., 2007) from measured radiocarbon ages. The computed ages range from less than 10 years to several decades, and are consistent with the estimated residence time of ground water in the Potomac River Basin, which is an integrated mixture of ages from all the tributary watersheds within the basin.

A basin-wide effective-porosity value was estimated by adjusting the flow-weighted mean age of ground-water discharge computed from the SUTRA budget calculation for model A to the 20-year residence time computed by Michel (1992). This calculation yields an effective porosity of

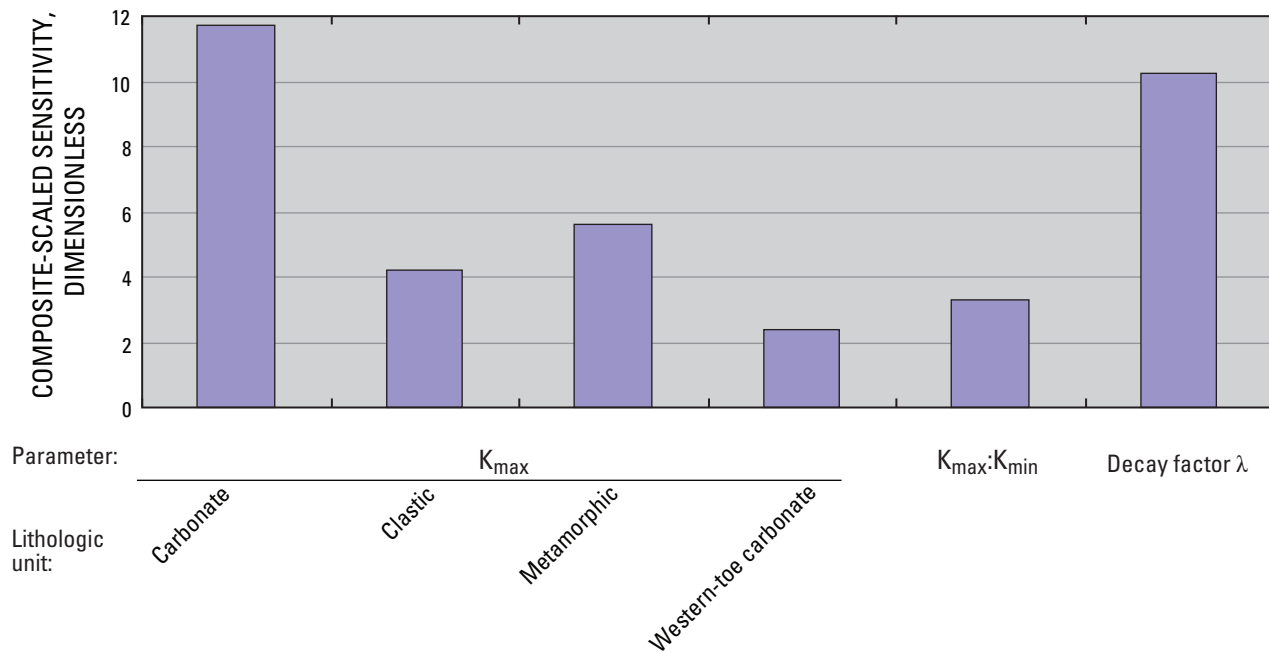


Figure 21. Composite-scaled sensitivities of optimal parameters in model A. (K_{max} : maximum hydraulic conductivity, K_{med} : medium hydraulic conductivity, K_{min} : minimum hydraulic conductivity.)

Table 8. Parameter error ratios associated with variations of model A.

[--, not applicable]

Parameter	Error ratio for variant ^a			
	A-1 ^b	A-2 ^c	A-3 ^d	A-4 ^e
Maximum conductivity, K_{max} :				
Carbonate rock	--	8.1	-3.2	-0.29
Clastic rock	6.5	21	-0.24	-0.03
Metamorphic rock	2.1	7.6	-0.91	-0.13
Western-toe carbonate rock	0.61	6.4	-2.5	-0.21
Maximum:minimum conductivity ratio, $K_{max}:K_{min}$:				
Carbonate and clastic rocks	6.7	14	2.7	0.01
Power function decay factor, λ :	2.3	8.5	-2.5	-0.02

^a Ratio of percent change in optimal parameter value to percent change in modified value.

^b K_{max} of carbonate rock increased by 5 percent.

^c Recharge rate for all rock units increased by 5 percent.

^d Strike direction and dip angles for clastic and carbonate rocks increased by 5 percent.

^e Threshold depths D in power function (eq. 4) increased by 100 percent for all rock units.

1.3×10^{-4} for the flow system, which is dominated by the upper 300 m of the fractured-rock aquifer. This value is useful when considering movement of environmental tracers on a regional scale (kilometers), but is not necessarily applicable to the prediction of contaminant migration at a local scale (hundreds of meters or less). This value is about one order of magnitude less than that obtained through numerical simulation of a tracer test (1.4×10^{-3}), which was conducted over 180 m in inclined fractured mudstone in the Newark Basin (Carleton and others, 1999).

The simulated distribution of ground-water age in model A (variable strike and dip) indicates that most shallow ground water is less than 10 years old (fig. 22A). The absolute ages are dependent on the assumed values of effective porosity and transverse dispersivity, but relative ages in different parts of the flow system can be compared qualitatively. Older water (more than 20 years old) discharges into the major stream channels. In carbonate areas, the depth of recent flow (less than 10 years) typically is within 150 m of land surface, except in areas adjacent to high relief where the bedding is steeply dipping. In these areas, such as along the North Mountain Fault and between Massanutten Mountain and the Blue Ridge Mountains, the depth of recent flow is as much as 500 m. Ground water that penetrates to these depths flows northeastward along the strike of the bedding toward the Potomac River. Simulated ground-water ages increase with depth towards the bottom of the model domain, where the older water has simulated ages greater than 50 years. Unfortunately, it is not possible to compare the simulated results with observed data because information concerning ground-water levels and age at discrete depth intervals in the aquifer system is not available.

The simulated pattern of ground-water flow with depth in model A is depicted by flow vectors projected onto a vertical plane that corresponds to section D–D' (fig. 22A). The direction of flow is towards the rounded tips of the vectors. Ground water deep within the basin discharges upward to both the North and South Forks of the Shenandoah River, and flows from west to east beneath Massanutten Mountain, parallel to the bedding of the carbonate rocks. In contrast, Massanutten Mountain coincides with a ground-water divide in the flow distribution simulated by model C (uniform strike), partitioning westward flow to the North Fork from eastward flow to the South Fork (fig. 22B). The ground-water age distribution simulated with model C is similar to that simulated with model A, except along the Passage Creek valley, where simulated ground-water ages are up to 50 years old. Flow is isotropic in the vertical plane in model C and the degree of vertical hydraulic connection is uniform throughout the model domain, so flow is largely controlled by topography, rather than by the dip of bedding, as in model A. The differences in simulated flow resulting from the different representations of bedrock structure in models A and C for this regional-scale model are only important at large depths (greater than 1 km). Differences at shallower depths could also be significant, however, in local-scale models where the dip

of the bedding is variable and, therefore, controls the depth of recent ground-water flow.

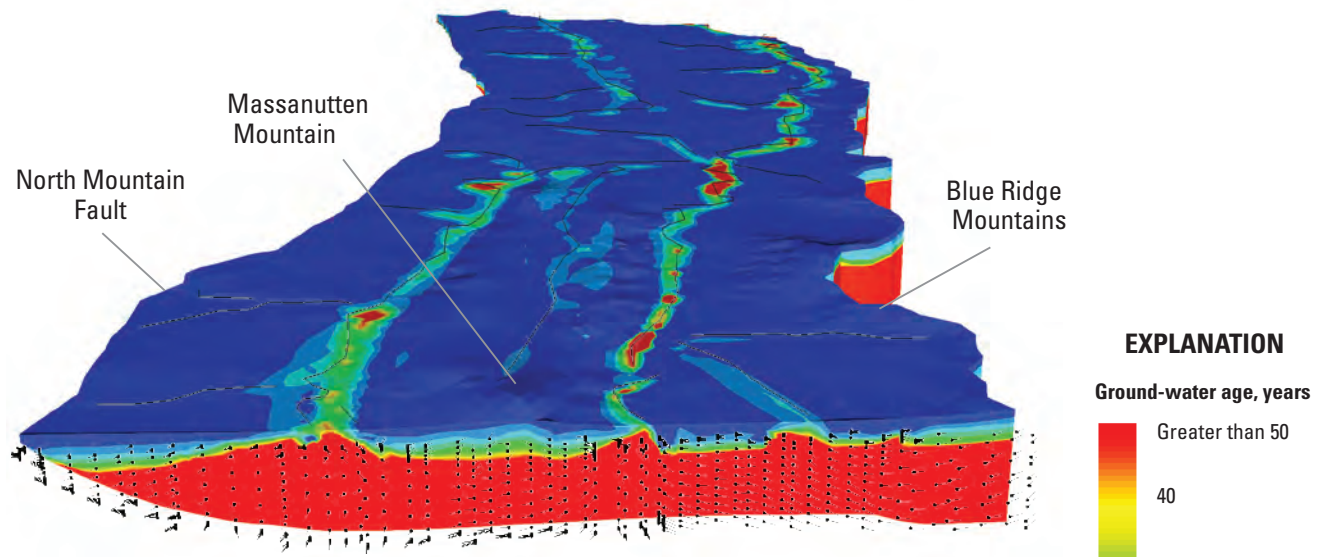
Capture Zones of Well Fields

Three-dimensional capture zones of six major water supplies in the Shenandoah Valley with withdrawal rates greater than 4,000 m³/d were delineated through reverse-flow simulations using both model A (variable strike and dip) and model C (uniform strike). Inflow from wells was labeled with a conservative tracer of unit concentration, and steady-state transport simulations delineated approximate capture zones. This procedure is similar to backward tracking using particles (for example, Zheng and Bennett, 2002), but simulation of dispersion results in larger delineated areas. The dispersion coefficient represents heterogeneity in aquifer hydraulic conductivity that creates uncertainty in the position of the capture zone. A normalized concentration distribution can be strictly interpreted as a location-probability distribution (Neupauer and Wilson, 2004) for a similar simulation with somewhat different boundary conditions. Qualitatively, the simulated concentration distributions presented herein can be interpreted as relative certainties that water recharging parts of the capture zone will reach the well. Water in locations of higher concentrations is more likely to reach the well at the field site than water in locations of lower concentrations. The steady-state simulations did not represent release of ground water from storage due to declining water levels, which would have resulted in smaller areas.

Plan views of the capture zones delineated with models A and C for three of the largest producing water supplies, the Martinsburg water supply in Berkeley County, W.Va., and industrial well fields in Rockingham County, Va., are shown in figs. 23 and 24. The Martinsburg water supply, derived from ground-water withdrawals from springs and pumpage from an abandoned quarry, was treated as a well field for this application. These plan views are analogous to contributing recharge areas typically delineated in other studies. Simulated flow vectors drawn on the plots are projected onto a horizontal plane and show the direction and relative magnitude of ground-water flow near the well fields. The coloring of the capture zones indicates the relative likelihood that water in the capture zone will be discharged by the well. The width of the capture zone is related to the specified value of transverse dispersivity (30 m), and would be larger for larger dispersivity values that reflect more heterogeneity in hydraulic conductivity. Three-dimensional perspective views (fig. 25) indicate the relative depths of the capture zones simulated for the Martinsburg water supply by each model.

The capture zone delineated with model A for the Martinsburg water supply is wider and shallower than that delineated with model C (figs. 23A and 24A). The model-A capture zone extends downdip along the bedding of carbonate rock and its vertical extent is limited by a low K_{\min} value (0.2 m/d) that limits cross-bedding flow (fig. 25A). In contrast,

A Model A: variable strike and dip



B Model C: uniform strike

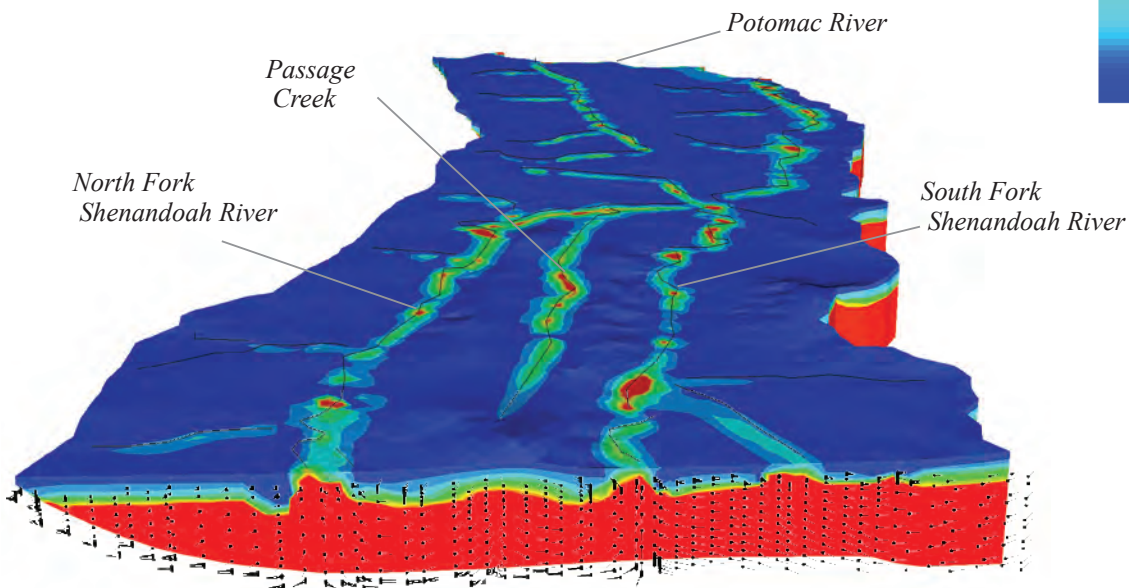
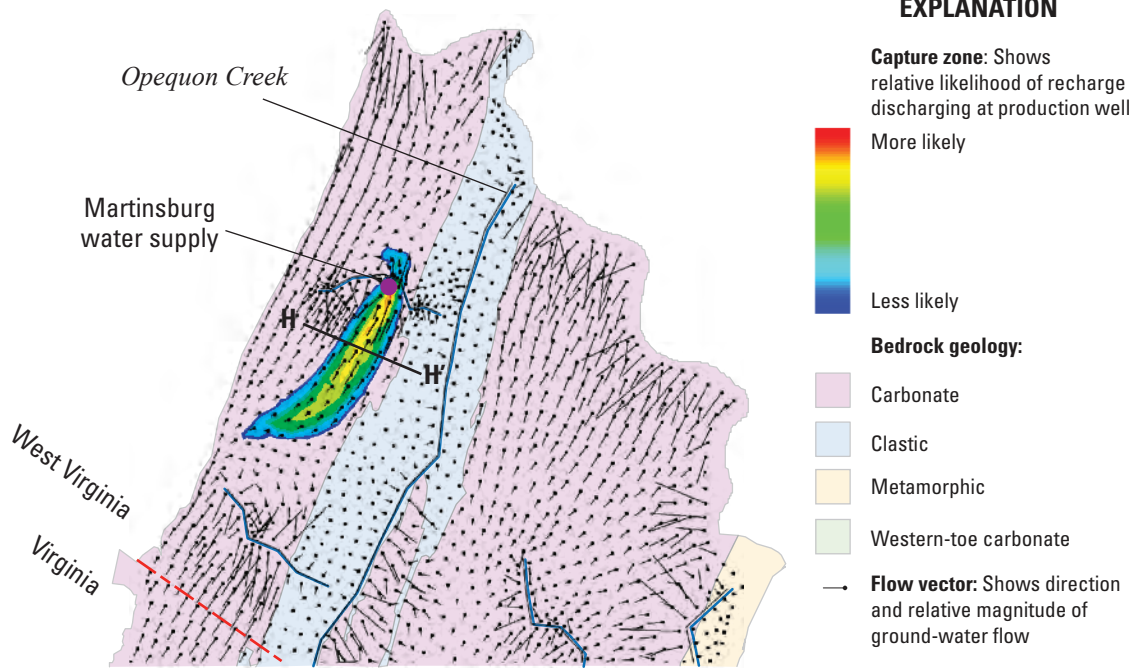


Figure 22. Block diagram along section D–D’ showing spatial distribution of simulated ground-water age and flow directions with (A) model A (variable strike and dip), and (B) model C (uniform strike). (Location of section line shown in fig. 3. Rounded tips of vectors denote direction of ground-water flow.)

the capture zone delineated with model C (in which flow is vertically isotropic) extends to the bottom of the flow system and does not reflect the dip of the bedding (fig. 25B). Although most of the simulated flow to the Martinsburg water supply is through the upper 150 m of the model domain, it is unreasonable to assume that water from depths of 5 km will

discharge to wells, as predicted by model C. Capture zones simulated for the industrial well fields in Rockingham County by both models are similar because simulated flow is isotropic through metamorphic rocks and the western-toe carbonate. Capture zones of all wells extend beneath adjacent streams and collect recharge from the opposite side. Stream infiltration

A



B

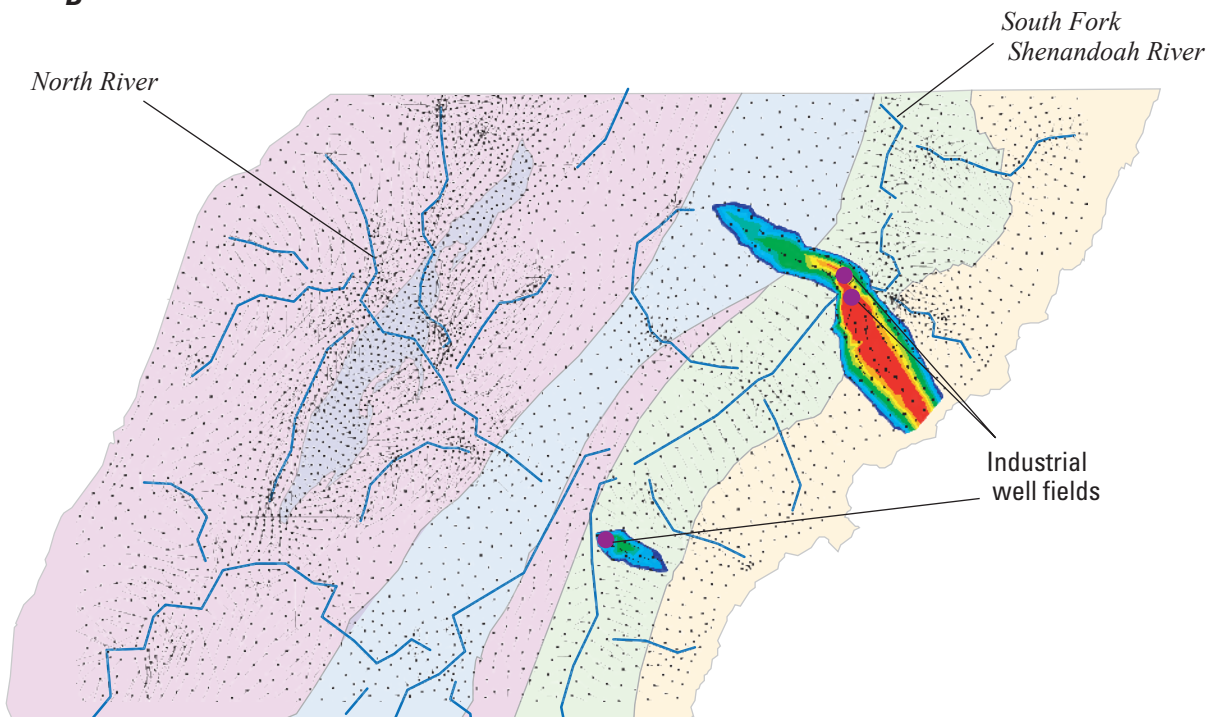
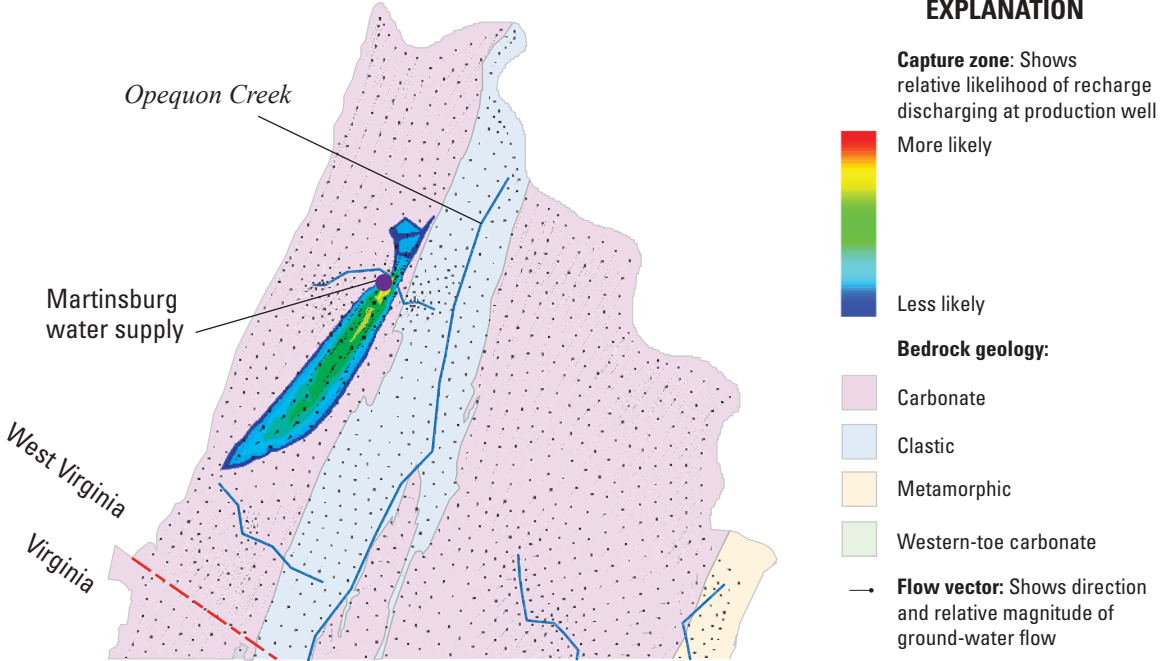


Figure 23. Capture zones (plan view of contributing area) delineated with model A (variable strike and dip) to (A) the Martinsburg water supply in Berkeley County, W.Va., and (B) industrial well fields in Rockingham County, Va. (Locations shown in fig. 3. Rounded tips of vectors denote direction and relative magnitude of ground-water flow.)

A



B

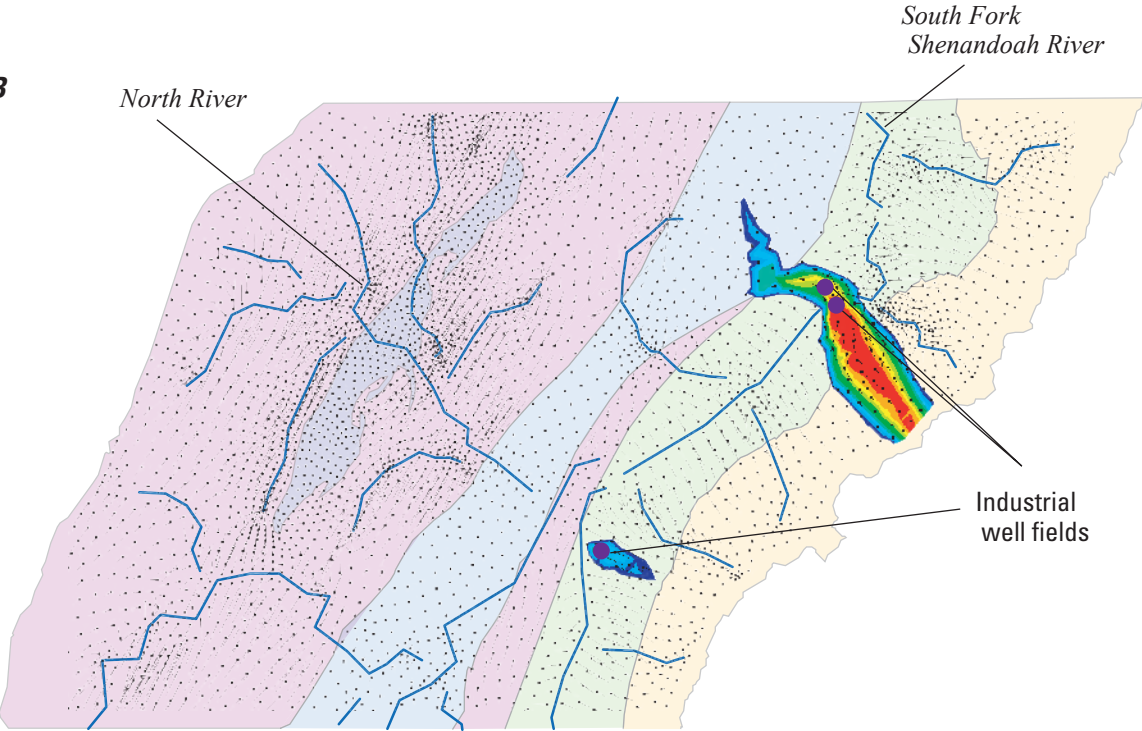
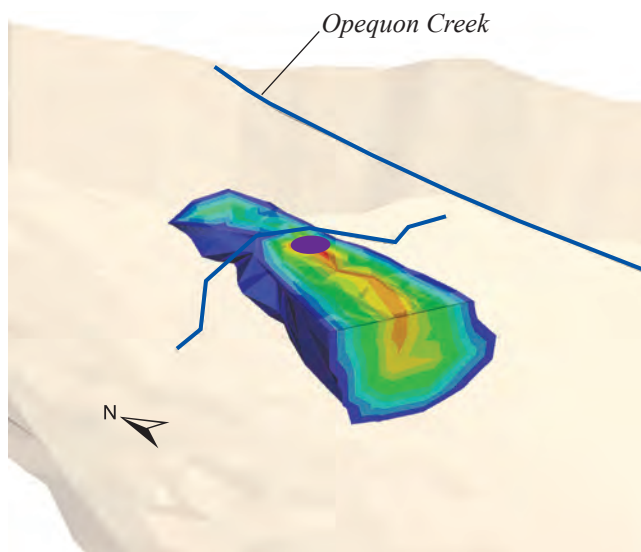
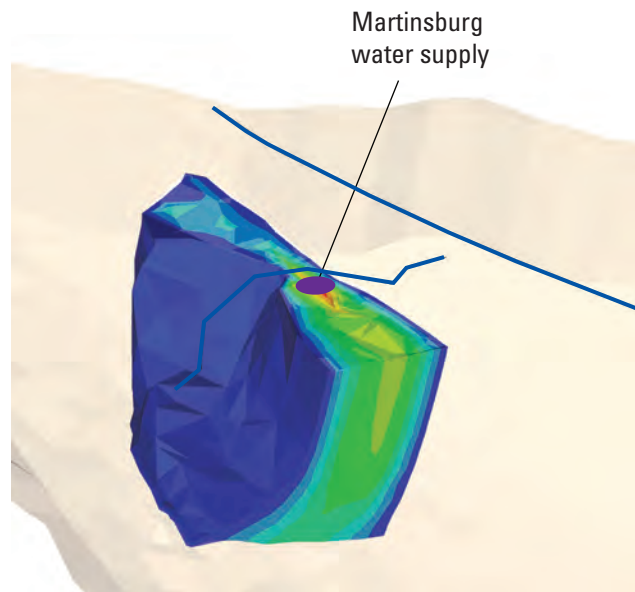


Figure 24. Capture zones (plan view of contributing area) delineated with model C (uniform strike) to (A) the Martinsburg water supply in Berkeley County, W.Va., and (B) industrial well fields in Rockingham County, Va. (Locations shown in fig. 3. Rounded tips of vectors denote direction and relative magnitude of ground-water flow.)

A Model A: variable strike and dip

No vertical exaggeration
Oblique view, not to scale

B Model C: uniform strike

No vertical exaggeration
Oblique view, not to scale

EXPLANATION

Capture zone: Shows relative likelihood of recharge discharging at production well

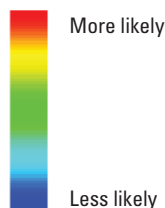


Figure 25. Three-dimensional perspective views of capture zones to the Martinsburg water supply in Berkeley County, W.Va., delineated with (A) model A (variable strike and dip), and (B) model C (uniform strike). (Vertical slice along section H–H'. Location of section line shown in fig. 23.)

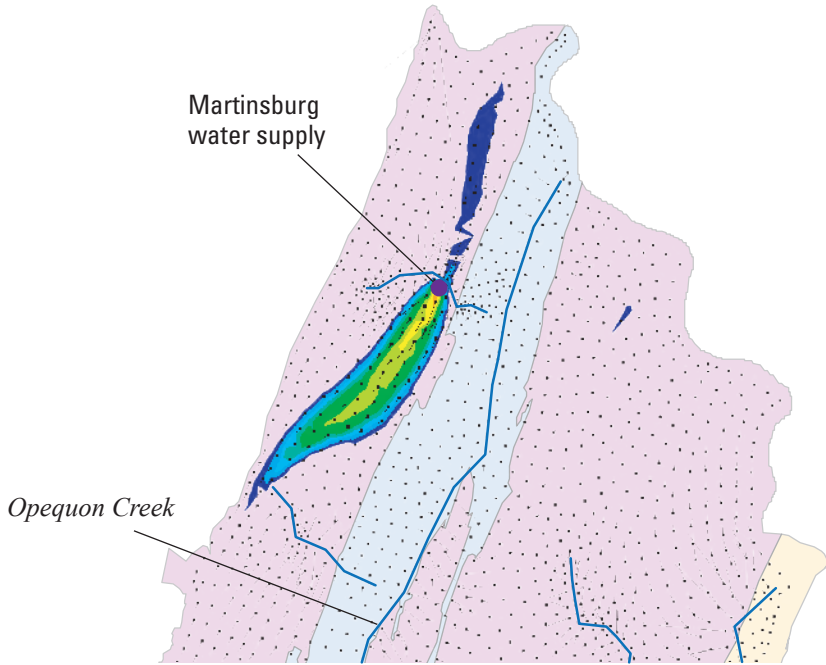
provides approximately 7 percent of the total discharge simulated from the six water supplies in model A and about 9 percent of the total discharge in model C.

Flow vectors simulated with both models A and C indicate more base flow to tributary streams that flow perpendicular to the N. 30° E. strike of the bedding and less base flow to the larger streams that are aligned parallel to strike. These results are consistent with the pattern of base flow observed by Lewis (1992) in the Newark Basin. Flow vectors simulated by both models are similar in areas where the strike of bedding is relatively uniform (as in the northern part of the valley, figs. 23A and 24A) and where flow is isotropic (eastern part of valley, figs. 23B and 24B). Flow vectors simulated in areas near North River differ, however,

because the strike of bedding is variable in model A, but treated as uniform in model C (figs. 23B and 24B).

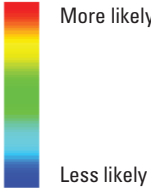
An additional simulation was run with model A to represent the effect of drought by decreasing the recharge rate by 50 percent and decreasing the leakance value K/l (see eq. 3 and table 6) by a factor of 1,000 to limit infiltration from streams. These changes were meant to reflect low water conditions, such as the drought from 1999 to 2002 (Harlow and others, 2005). The simulated drought resulted in larger capture zones for all six well fields that, in some cases, extended into adjacent tributary watersheds (fig. 26). The relative magnitude of flow vectors is generally smaller with the lower recharge rate, although this difference is less obvious in the southern part of the valley where the topography is steeper (fig. 26B).

A



EXPLANATION

Capture zone: Shows relative likelihood of recharge discharging at production well



Bedrock geology:

- Carbonate
- Clastic
- Metamorphic
- Western-toe carbonate

Flow vector: Shows direction and relative magnitude of ground-water flow

B

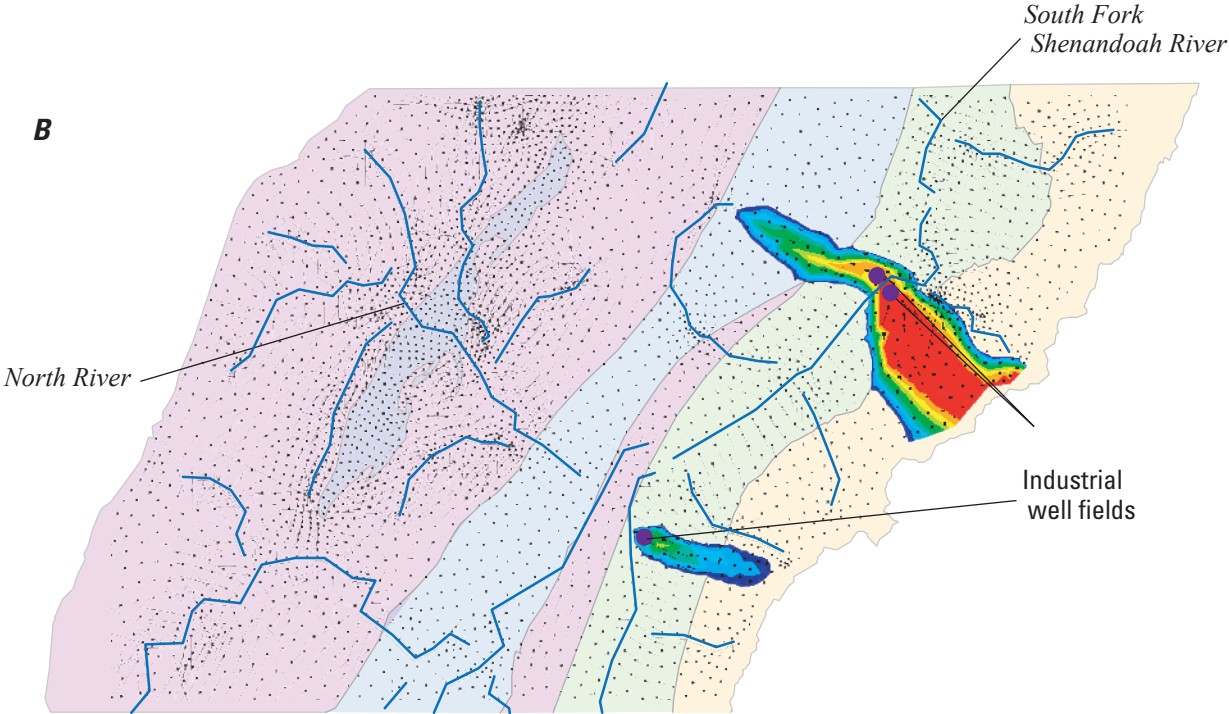


Figure 26. Capture zones (plan view of contributing area) delineated with model A (variable strike and dip) with recharge decreased by one-half to simulate drought conditions at (A) the Martinsburg water supply in Berkeley County, W.Va., and (B) industrial well fields in Rockingham County, Va. (Locations shown in fig. 3. Rounded tips of vectors denote direction and relative magnitude of ground-water flow.)

Summary

A hydrogeologic study was undertaken to assess the ground-water resources of the Shenandoah Valley, which provide about two-thirds of the current (2008) water supply for a rapidly expanding population. Ground water flows through fractures in sedimentary rocks that underlie the 7,100-km² Shenandoah Valley, part of the Great Valley section that extends from southern New York to central Alabama in the Central Appalachian Valley and Ridge Physiographic Province. The valley is underlain by Cambrian to Devonian sedimentary rocks that were contractionally deformed and folded during the Alleghanian orogeny about 300 m.y. ago. The Massanutten synclinorium occupies the central part of the valley and contains a section of strata as much as 5 km thick with a core of clastic rocks that form Massanutten Mountain. The clastic rocks are underlain by carbonate rocks that crop out on the eastern and western sides of the synclinorium. The valley is bounded to the east by Neoproterozoic metamorphic rocks of the Blue Ridge anticlinorium and to the west by the North Mountain Fault. Bedding is the dominant foliation in the sedimentary rocks and generally strikes N. 30° E. Rocks on the western limb of the synclinorium generally dip gently southeast, whereas the rocks on the eastern limb dip to the northwest, are near vertical, or locally are overturned. The east and west limbs converge in the core beneath Massanutten Mountain and are nearly flat-lying. The bedding is intersected by cross and longitudinal joints related to folding that are steep and strike northwest and northeast, respectively. The regional Staunton-Pulaski Fault divides the valley into two large structural blocks.

The Shenandoah Valley is drained by the Shenandoah River and Opequon Creek, which are tributaries to the Potomac River. Although numerous karst features, such as sinkholes and springs, occur locally in carbonate areas, ground-water flow is not assumed to be dominated by these fractures based on analyses of ground water discharged from springs that are nearly saturated with respect to calcite. The aquifer system appears to be near equilibrium based on long-term water-level hydrographs, and ground-water withdrawals account for less than 3 percent of the total recharge to the valley. Base flow from drainage basins in the valley was found by linear regression to be related to the underlying bedrock. Recharge rates are lowest in clastic rocks (13.9 cm/yr) and highest in western-toe carbonates (39.5 cm/yr), an area of carbonate rock overlain by colluvial deposits as much as 150 m thick that enhance recharge and dissolution of the rock. Specific-capacity data indicate that the western-toe carbonate is the most transmissive rock unit (110 m²/d), followed by other carbonate rocks (25 m²/d) and clastic and metamorphic rocks (10 and 5 m²/d, respectively).

Deformation of the carbonate and clastic rocks in the valley created a three-dimensional fracture network consisting of bedding partings and two orthogonal sets of joints developed perpendicular to the bedding when the rocks

were folded. The orientations of bedding planes and fractures provide preferential flow paths through the rock, such that the direction of maximum hydraulic conductivity is oriented within the bedding plane and the direction of minimum hydraulic conductivity is perpendicular to the bedding. This arrangement causes anisotropic hydraulic behavior that has been observed in tracer and aquifer tests in the inclined, fractured sedimentary rocks in the valley. The regional fracture network is intersected by discrete faults and karst features, creating local flow systems that can either distribute or collect water to or from the regional system. The ground-water model of the Shenandoah Valley was designed to only represent the regional flow system because most karst features and minor faults have not been located through geologic mapping, and the mesh resolution was too coarse to represent these relatively small features.

Steady-state flow simulations of the fractured-rock aquifer system in the Shenandoah Valley were conducted using the finite-element model SUTRA to specify variable directions of strike and dip in order to represent changes in the orientation of the bedding throughout the valley. The model domain was discretized using an irregularly connected mesh of quadrilateral elements with maximum lateral lengths of 1 km. The bedrock was divided into four units: a 300-m-thick top unit with 10 equally spaced layers through which most ground water is assumed to flow, and three lower units each containing 5 layers of increasing thickness that correspond to the major rock units in the valley: clastic, carbonate, and metamorphic rocks. The western-toe carbonate rocks were distinguished as a separate zone in the carbonate unit.

All the lateral and bottom boundaries of the model domain were assumed to be impervious to ground-water flow, and recharge was introduced through the top model boundary using rates estimated for each rock unit by linear regression. Stream channels were represented by head-dependent flow boundaries that functioned as drains (outflow only) and for which unique conductance terms were specified (these conditions required modification of the SUTRA code). Three alternative models were constructed to assess the effects of specified boundary conditions and different conceptual models of bedrock structure. Stream boundaries were represented by drain nodes in two alternative models (A and C), and by specified-head nodes in the third alternative model (B).

Hydraulic-conductivity values were estimated through model calibration for each of the four rock units and a power function was used to decrease hydraulic conductivity with increasing depth below a specified threshold. Conductivity tensors for metamorphic and western-toe carbonate rocks were assumed to be isotropic, while conductivity tensors for carbonate and clastic rocks were assumed to be anisotropic. Conductivity tensors for carbonate and clastic rocks were aligned with the strike and dip of the bedding in models A and B (variable strike and dip), with maximum and medium conductivity (K_{\max} and K_{med}) parallel to bedding and minimum conductivity (K_{\min}) perpendicular to bedding. The directions of the conductivity tensor in models A and B were interpolated

for each mesh element from a stack of “form surfaces” that provided a three-dimensional representation of bedding in the folded rocks underlying the valley. Conductivity tensors were assumed to be horizontally anisotropic in model C (uniform strike) with the K_{\max} direction parallel to the N. 30° E. axis of the valley and the K_{\min} direction perpendicular to the strike.

The models were calibrated through nonlinear regression using UCODE to optimize hydraulic-conductivity values using ground-water levels in 354 wells and discharge at 23 streamflow-gaging stations in the Shenandoah Valley. The optimized parameters included K_{\max} of each of the four rock units, the $K_{\max}:K_{\min}$ ratio of carbonate and clastic rock, and the decay factor used in the power functions. Residual plots for heads indicate good model fit with little bias and a standard error in head of 20.2 m, about 4 percent of the 480-m measurement range. Simulated flows were generally within 40 percent of the observed values with a slight bias toward underprediction at higher flows, which could result from either lack of detail in the simulated stream network, or omission of discrete features that increase ground-water discharge.

Replacing drain nodes in model A by specified-head nodes in model B produced parameter estimates that generally fell within or near the lower limit of the approximate 95-percent confidence intervals associated with model A. Infiltration from streams in model B increased the simulated inflow rate by 10 percent, however, so model A was assumed to better represent the aquifer system because the resolution of the finite-element mesh does not permit the precise assignment of head at stream boundaries. Replacing the variable-strike-and-dip tensor in model A with the uniform-strike tensor in model C produced a parameter set similar to that of model A, with the exception of the ratio of hydraulic conductivity parallel and perpendicular to bedding, which was 50 percent lower in model C. Sensitivity analyses indicate that acquiring additional information concerning recharge rates would increase confidence in the estimated parameter values.

Steady-state, solute-transport simulations were conducted with models A (variable strike and dip) and C (uniform strike) to delineate the depth of recent ground-water flow from the simulated distribution of ground-water age, which was obtained by interpreting the solute concentration as age and including a zero-order production term. Longitudinal and transverse dispersivities were specified as 800 m and 30 m, respectively, to facilitate convergence of the transport solution, and a basin-wide effective porosity (1.3×10^{-4}) was estimated by adjusting the flow-weighted average age of ground-water discharge to a 20-year residence time previously computed for the Potomac River Basin. The simulated age distributions indicated that most shallow ground water is less than 10 years old. Ground-water age distributions computed by models A and C were similar, but the flow patterns deep in the basin differed, especially beneath Massanutten Mountain in the center of the valley. Model A simulated flow from west to east beneath Massanutten Mountain, parallel to the bedding of the carbonate rocks, while in model C Massanutten Mountain coincided with an east-west ground-water divide

that partitioned flow to the South and North Forks of the Shenandoah River. This difference is a consequence of isotropic flow in the vertical plane in model C that is largely controlled by topography, rather than by the dip of bedding, as in model A.

Qualitative, probabilistic capture zones of six major water supplies were delineated through backward tracking in reverse-flow simulations that routed flow from inflow points at production wells and along streams to discharge points at land surface. Inflow from wells was labeled with a conservative tracer and tracked backward through steady-state transport simulations to produce normalized concentration distributions that were interpreted qualitatively as a location probability. Capture zones delineated with both models are similar in plan view, but differ in vertical extent. The capture zone simulated for a municipal well field by model A extends downdip with the bedding of carbonate rock and is relatively shallow. The capture zone simulated by model C, however, extends to the bottom of the flow system and does not reflect the dip of the bedding, which is unrealistic. Flow vectors simulated by both models were similar in areas where the strike of bedding is relatively uniform and where flow is isotropic, but differed where the strike of bedding is variable and flow is anisotropic.

Although the ground-water age distributions and capture zones simulated by the variable-strike-and-dip and uniform-strike models are similar, the simulated results differ at depth, especially in areas where the depth of flow is limited by horizontal bedding. These differences are only important at large depths (greater than 1 km) for this regional-scale model, but differences could be significant at shallower depths in local-scale models where the dip of the bedding is variable and controls the depth of recent ground-water flow. Simulations of ground-water flow through folded fractured rock can be constructed using SUTRA to represent variable orientations of the hydraulic-conductivity tensor and produce a physically realistic flow system that accurately reflects the pattern of bedrock structure.

Acknowledgments

Information required to construct and calibrate the ground-water flow models described in this report was provided by George Harlow, John Eggleston, Donald Hayes, and Jennifer Krstolic (USGS, Richmond, Va.); and Mark Kozar, Kurt McCoy, and John Atkins (USGS, Charleston, W. Va.). Alden Provost (USGS, Reston, Va.) wrote the appendix describing his modifications to SUTRA, and Richard Winston (USGS, Reston, Va.) wrote procedures for SutraGUI that generated the strike direction and dip angles used to define conductivity tensors specified in the ground-water flow models. David Eckhardt (USGS, Ithaca, N.Y.) conducted the linear regression that related base flow to bedrock units.

References Cited

- Anderman, E.R., Kipp, K.L., Hill, M.C., Valstar, Johan, and Neupauer, R.M., 2002, MODFLOW-2000, The U.S. Geological Survey modular ground-water model—Documentation of the model-layer variable-direction horizontal anisotropy (LVDA) capability of the hydrogeologic-unit flow (HUF) package: U.S. Geological Survey Open-File Report 02–409, 29 p.
- Argus Interware, Inc., 1997, User's guide Argus ONE, Argus open numerical environments—A GIS modeling system, version 4.0: Jericho, N.Y., Argus Holdings, Ltd., 506 p.
- Beaudoin, Georges, Therrien, Rene, and Savard, Catherine, 2006, 3D numerical modelling of fluid flow in the Val-d'Or orogenic gold district—Major crustal shear zones drain fluids from overpressured vein fields: *Miner Deposita*, v. 41, p. 82–98.
- Belcher, W.R., ed., 2004, Death Valley regional ground-water flow system, Nevada and California—Hydrogeologic framework and transient ground-water flow model: U.S. Geological Survey Scientific Investigations Report 2004–5205, 408 p.
- Bieber, P.P., 1961, Ground-water features of Berkeley and Jefferson Counties, West Virginia: *West Virginia Geological and Economic Survey Bulletin* 21, 81 p.
- Burbey, T.J., 2003, Water-management model—Frederick County Sanitation Authority: Thomas J. Burbey, PhD, Blacksburg, Va., 11 p.
- Burton, W.C., Plummer, L.N., Eurybiades, Lindsey, B.D., Gburek, W.J., 2002, Influence of fracture anisotropy on ground water ages and chemistry, Valley and Ridge Province, Pennsylvania: *Ground Water*, v. 40, no. 3, p. 242–257.
- Cady, R.C., 1938, Ground-water resources of northern Virginia: *Virginia Geological Survey, Bulletin* 50, 200 p.
- Cardwell, D.H., Erwin, R.B., and Woodward, H.P., 1968, Geologic map of West Virginia: Morgantown, W. Va., West Virginia Geological and Economic Survey, 2 sheets, scale 1:250,000.
- Carleton, G.B., Welty, Claire, and Buxton, H.T., 1999, Design and analysis of tracer tests to determine effective porosity and dispersivity in fractured sedimentary rocks, Newark Basin, New Jersey: U.S. Geological Survey Water-Resources Investigations Report 98–4126A, 80 p.
- Drew, L.J., Southworth, Scott, Sutphin, D.M., Rubis, G.A., Schuenemeyer, J.H., and Burton, W.C., 2004, Validation of the relation between patterns in the structure of fractured bedrock and structural information interpreted from two-dimensional variogram maps of water-well yields: *Natural Resources Research*, v. 13, no. 4, p. 255–264.
- Golder Associates Inc., 2005, Groundwater resource exploration study Stonewall Well No. 7, Shenandoah Brewing Project: Richmond Va., prepared for Jacobs Engineering, Inc., 28 p.
- Goode, D.J., and Senior, L.A., 2000, Simulation of aquifer tests and ground-water flowpaths at the local scale in fractured shales and sandstones of the Brunswick Group and Lockatong Formation, Lansdale, Montgomery County, Pennsylvania: U.S. Geological Survey Open-File Report 00–97, 46 p.
- Hack, J.T., 1965, Geomorphology of the Shenandoah Valley Virginia and West Virginia and origin of the residual ore deposits: U.S. Geological Survey Professional Paper 484, 84 p.
- Hack, J.T., and Young, R.S., 1959, Entrenched meanders of the North Fork of the Shenandoah River, Virginia: U.S. Geological Survey Professional Paper 354–A, p. 1–10.
- Harbaugh, A.W., Banta, E.R., Hill, M.C., and McDonald, M.G., 2000, MODFLOW-2000, the U.S. Geological Survey modular ground-water model—User guide to modularization concepts and the ground-water flow process: U.S. Geological Survey Open-File Report 00–92, 121 p.
- Harlow, G.E., Jr., Orndorff, R.C., Nelms, D.L., Weary, D.J., and Moberg, R.M., 2005, Hydrogeology and ground-water availability in the carbonate aquifer system of Frederick County, Virginia: U.S. Geological Survey Scientific Investigations Report 2005–5161, 30 p.
- Haug, C.J., 2002, Hydrogeology and ground-water-flow simulation of the Cave Springs Area, Hixson, Tennessee: U.S. Geological Survey Water-Resources Investigations Report 02–4091, 57 p.
- Hill, M.C., 1998, Methods and guidelines for effective model calibration: U.S. Geological Survey Water-Resources Investigations Report 98–4005, 90 p.
- Hill, M.C., and Tiedeman, C.R., 2007, Effective groundwater model calibration, with analysis of data, sensitivities, predictions, and uncertainty: New York, John Wiley and Sons, 456 p.
- Hinkle, K.R., and Sterrett, R.M., 1976, Rockingham County groundwater, present conditions and prospects: Virginia State Water Control Board Planning Bulletin 300, 88 p.

- Hinkle, K.R., and Sterrett, R.M., 1977, Shenandoah County groundwater, present conditions and prospects: Virginia State Water Control Board Planning Bulletin 306, 67 p.
- Hinkle, K.R., and Sterrett, R.M., 1978, Augusta County groundwater, present conditions and prospects: Virginia State Water Control Board Planning Bulletin 310, 119 p.
- Hoaglund, J.R., III, and Pollard, David, 2003, Dip and anisotropy effects on flow using a vertically skewed model grid: *Ground Water*, v. 41, no. 6, p. 841-846.
- Hutson, S.S., Barber, N.L., Kenny, J.F., Linsey, K.S., Lumia, D.S., and Maupin, M.A., 2004, Estimated use of water in the United States in 2000: U.S. Geological Survey Circular 1268, 46 p., accessed October 20, 2006, at <http://pubs.usgs.gov/circ/2004/circ1268/>
- Jones, W.K., 1991, The carbonate aquifer of the northern Shenandoah Valley of Virginia and West Virginia, *in* Kastning, E.H., and Kastning, K.M., eds., *Appalachian Karst: Proceedings of the Appalachian Karst Symposium*, Huntsville, Ala., National Speleological Society, p. 217-222.
- King, P.B., 1950, Geology of the Elkton area, Virginia: U.S. Geological Survey Professional Paper 230, 82 p.
- Kozar, M.D., Hobba, W.A., Jr., and Macy, J.A., 1991, Geohydrology, water availability, and water quality of Jefferson County, West Virginia, with emphasis on the carbonate area: U.S. Geological Survey Water-Resources Investigations Report 90-4118, 93 p.
- Kozar, M.D., and Mathes, M.V., 2001, Aquifer-characteristics data for West Virginia: U.S. Geological Survey Water-Resources Investigations Report 01-4036, 74 p.
- Kozar, M.D., Weary, D.J., Paybins, K.S., and Pierce, H.A., 2007, Hydrogeologic setting and ground-water flow in the Leetown Area, West Virginia: U.S. Geological Survey Scientific Investigations Report 2007-5066, 70 p.
- Krstolic, J.L., and Hayes, D.C., 2004, Water-quality synoptic sampling, July 1999—North Fork Shenandoah River, Virginia: U.S. Geological Survey Scientific Investigations Report 2004-5153, 88 p.
- Lewis, J.C., 1992, Effect of anisotropy on ground-water discharge to streams in fractured Mesozoic basin rocks: American Water Resources Association Monograph Series 17, p. 94-105.
- Lewis-Brown, J.C., and Rice, D.E., 2002, Simulated ground-water flow, Naval Air Warfare Center, West Trenton, New Jersey: U.S. Geological Survey Water-Resources Investigations Report 02-4019, 44 p.
- Lewis-Brown, J.C., Rice, D.E., Rosman, Robert, and Smith, N.P., 2005, Hydrogeologic framework, ground-water quality, and simulation of ground-water flow at the Fair Lawn Well Field Superfund Site, Bergen County, New Jersey: U.S. Geological Survey Scientific Investigations Report 2004-5280, 109 p.
- Lindsey, B.D., and Koch, M.L., 2004, Determining sources of water and contaminants to wells in a carbonate aquifer near Martinsburg, Blair County, Pennsylvania, by use of geochemical indicators, analysis of anthropogenic contaminants, and simulation of ground-water flow: U.S. Geological Survey Scientific Investigations Report 2004-5124, 46 p.
- McCoy, K.J., Podwysoki, M.H., Crider, E.A., and Weary, D.J., 2005a, Fracture trace map and single-well aquifer test results in a carbonate aquifer in Berkeley County, West Virginia: U.S. Geological Survey Open-File Report 2005-1040, 1 pl.
- McCoy, K.J., Podwysoki, M.H., Crider, E.A., and Weary, D.J., 2005b, Fracture trace map and single-well aquifer test results in a carbonate aquifer in Jefferson County, West Virginia: U.S. Geological Survey Open-File Report 2005-1407, 1 pl.
- Michalski, Andrew, and Britton, Richard, 1997, The role of bedding fractures in the hydrogeology of sedimentary bedrock—Evidence from the Newark Basin, New Jersey: *Ground Water*, v. 35, no. 2, p. 318-327.
- Michel, R.L., 1992, Residence times in river basins as determined by analysis of long-term tritium records: *Journal of Hydrology*, v. 130, p. 367-378.
- Morgan, B.A., Eaton, L.S., and Wieczorek, G.F., 2004, Pleistocene and Holocene colluvial fans and terraces in the Blue Ridge region of Shenandoah National Park, Virginia: U.S. Geological Survey Open-File Report 03-410, 25 p.
- Muldoon, M.A., Simo, J.A., and Bradbury, K.R., 2001, Correlation of hydraulic conductivity with stratigraphy in a fractured-dolomite aquifer, northeastern Wisconsin, USA: *Hydrogeology Journal*, v. 9, issue 6, p. 570-583.
- Nelms, D.L., Harlow, G.E., Jr., and Hayes, D.C., 1997, Base-flow characteristics of streams in the Valley and Ridge, the Blue Ridge, and the Piedmont physiographic provinces of Virginia: U.S. Geological Survey Water-Supply Paper 2457, 48 p.
- Neupauner, R.M., and Wilson, J.L., 2004, Numerical implementation of a backward probabilistic model of ground water contamination: *Ground Water*, v. 42, no. 2, p. 175-189.

- Poeter, E.P., and Hill, M.C., 1998, Documentation of UCODE, a computer code for universal inverse modeling: U.S. Geological Survey Water-Resources Investigations Report 98-4080, 116 p.
- Rankin, D.W., Drake, A.A., Jr., and Ratcliffe, N.M., 1989, Geologic map of the U.S. Appalachians showing the Laurentian margin and Taconic orogen, *in* Hatcher, R.D., Jr., Thomas, W.A., and Viele, G.W., eds., *The Appalachian-Ouachita orogen in the United States*, v. F-2 of *The Geology of North America*: Boulder, Colo., Geological Society of America, plate 2.
- Risser, D.W., and Bird, P.H., 2003, Aquifer tests and simulation of ground-water flow in Triassic sedimentary rocks near Colmar, Bucks and Montgomery Counties, Pennsylvania: U.S. Geological Survey Water-Resources Investigations Report 03-4159, 79 p.
- Rutledge, A.T., 1993, Computer programs for describing the recession of ground-water discharge and for estimating ground-water recharge and discharge from streamflow records: U.S. Geological Survey Water-Resources Investigations Report 93-4121, 45 p.
- Senior, L.A., and Goode, D.J., 1999, Ground-water system, estimation of aquifer hydraulic properties, and effects of pumping on ground-water flow in Triassic sedimentary rocks in and near Lansdale, Pennsylvania: U.S. Geological Survey Water-Resources Investigations Report 99-4228, 112 p.
- Shapiro, A.M., Hsieh, P.A., Burton, W.C., and Walsh, G.J., 2007, Integrated multi-scale characterization of ground-water flow and chemical transport in fractured crystalline rock at the Mirror Lake Site, New Hampshire, *in* Hyndman, D.W., Day-Lewis, F.D., and Singha, K., eds., *Subsurface hydrology: Data integration for properties and processes*: American Geophysical Union Geophysical Monograph Series, v. 171, p. 201-225.
- Shultz, R.A., Hobba, W.A., Jr., and Kozar, M.D., 1995, Geohydrology, ground-water availability, and ground-water quality of Berkeley County, West Virginia, with emphasis on the carbonate-rock area: U.S. Geological Survey Water-Resources Investigations Report 93-4073, 88 p.
- Southworth, Scott, Brezinski, D.K., Drake, A.A., Jr., Burton, W.C., Orndorff, R.C., Froelich, A.J., Reddy, J.E., and Denenny, Danielle, 2007, Geologic map of the Frederick 30 x 60 minute quadrangle, Maryland, Virginia, and West Virginia: U.S. Geological Survey Scientific Investigations Map 2889, 1:100,000-scale and pamphlet.
- Swain, L.A., Mesko, T.O., and Hollyday, E.F., 2004, Summary of the hydrogeology of the Valley and Ridge, Blue Ridge, and Piedmont physiographic provinces in the eastern United States: U.S. Geological Survey Professional Paper 1422-A, 31 p.
- Therrien, Rene, and Sudicky, E.A., 1996, Three-dimensional analysis of variably-saturated flow and solute transport in discretely-fractured porous media: *Journal of Contaminant Hydrology*, v. 23, p. 1-44.
- Todd, D.K., 1980, *Groundwater hydrology*: New York, John Wiley & Sons, 535 p.
- Vecchioli, John, 1967, Directional hydraulic behavior of a fractured-shale aquifer in New Jersey, *in* International symposium on hydrology of fractured rocks, Dubrovnik, Yugoslavia, 1965, *Proceedings: International Association of Scientific Hydrology, Publication 73*, v. 1, p. 318-326.
- Virginia Division of Mineral Resources, 1993, *Geologic map of Virginia*: Virginia Division of Mineral Resources, scale 1:500,000.
- Voss, C.I., and Provost, A.M., 2002, SUTRA—A model for saturated-unsaturated variable-density ground-water flow with solute or energy transport: U.S. Geological Survey Water-Resources Investigations Report 02-4231, 250 p.
- Weary, D.J., Harlow, G.E., Jr., Orndorff, R.C., and Alemán-González, W., 2004, Interdisciplinary cooperative geologic mapping and ground-water resource analyses of Frederick County, Virginia, by the U.S. Geological Survey: *Geological Mapping—Providing for successful water and land resource planning (Posters)*, 2004 Denver Annual Meeting (November 7-10, 2004), Geological Society of America.
- Weiss, Emmanuel, 1985, Evaluating the hydraulic effects of changes in aquifer elevation using curvilinear coordinates: *Journal of Hydrology*, v. 81, p. 253-275.
- White, W.B., 1988, *Geomorphology and hydrology of karst terrains*: New York, Oxford University Press, 464 p.
- Winston, R.B., and Voss, C.I., 2004, SutraGUI, A graphical user interface for SUTRA, a model for ground-water flow with solute or energy transport: U.S. Geological Survey Open-File Report 03-285, 114 p.
- Yager, R.M., 1996, Simulated three-dimensional ground-water flow in the Lockport Group, a fractured-dolomite aquifer near Niagara Falls, New York: U.S. Geological Survey Water-Supply Paper 2487, 42 p.
- Zanini, Lavinia, Novakowski, K.S., Lapcevic, P.A., Bickerton, G.S., Voralek, John, and Talbot, Charlie, 2000, Ground water flow in a fractured carbonate aquifer inferred from combined hydrogeological and geochemical measurements: *Ground Water*, v. 38, no. 3, p. 350-360.
- Zheng, Chunmiao, and Bennett, G.D., 2002, *Applied contaminant transport modeling*: New York, John Wiley & Sons, 621 p.

Appendix 1. Modifications to SUTRA

Appendix 1. **Modifications to SUTRA**

This appendix describes the changes made to the SUTRA code to (1) enable simulation of drains-boundary nodes at which water can exit the model but cannot enter the model, and (2) force storage of the last solution in the restart (RST) file even if the solution did not converge. These features are not available in the standard version of SUTRA (Voss and Provost, 2002, version of 2007).

At a drain node, the flow q_{drn} [M/T] in or out of the model is $v(p_{bc} - p)$ if $p > p_{bc}$ and zero if $p \leq p_{bc}$, where p [M/(LT²)] is the last computed value of pressure at the node, p_{bc} [M/(LT²)] is a specified external pressure, and v [LT] is the conductance of the hydraulic connection between pressures p and p_{bc} . Thus, when the pressure at the boundary node, p , exceeds the external pressure, p_{bc} , a negative flow (out of the model) results. When p is less than or equal to p_{bc} , there is no flow in or out of the model at that node.

Drain-boundary conditions are implemented as a variation on specified-pressure boundary conditions. Input of drain-boundary conditions is through SUTRA dataset 19. The input format for this dataset has been modified by adding two parameters. Details of how this dataset is read by SUTRA are described in “Subroutine BOUND” below.

Main program SUTRA_MAIN

Arrays ISDRAIN, GNUG, and CMNT19 were allocated by including the following statements in the section of code in which most of the allocations are performed:

```
ALLOCATE ( ISDRAIN (NBCN) , CMNT19 (NBCN) )
ALLOCATE ( GNUG (NBCN) )
```

See “Module ALLARR” and “Subroutine BOUND” below for more information about these three arrays.

In the calls to subroutines BOUND and SUTRA, arrays ISDRAIN, GNUG, and CMNT19 were added to the end of each argument list.

Module ALLARR

The following declarations for arrays ISDRAIN and GNUG were added:

```
LOGICAL, DIMENSION (:), ALLOCATABLE ::
1  ISDRAIN
DOUBLE PRECISION, DIMENSION (:), ALLOCATABLE ::
1  GNUG
CHARACTER*100, DIMENSION (:), ALLOCATABLE ::
1  CMNT19
```

Subroutine BC

Arrays ISDRAIN, GNUG, and PITER were added to the end of the argument list and were dimensioned as follows:

```
LOGICAL ISDRAIN (NBCN)
DOUBLE PRECISION GNUG (NBCN) , PITER (NNVEC)
```

The section of code that computes the contributions of a specified-pressure boundary condition to the left- and right-hand sides of the matrix equation for flow was changed from

```
100 GPINL=-GNUG
    GPINR=GNUG*PBC (IP)
```

to

```

100 IF ((.NOT.ISDRAIN(IP)).OR.(PITER(I).GT.PBC(IP))) THEN
    GPINL=-GNUG(IP)
    GPINR=GNUG(IP)*PBC(IP)
ELSE
    GPINL=0D0
    GPINR=0D0
END IF

```

If the node in question is not a drain or the pressure last computed at that node exceeds the external pressure, then the original formula for flow out of a specified-pressure node is used to compute the left- and right-hand-side contributions. Otherwise, the contributions to both sides are set to zero.

Subroutine BCTIME

Arrays ISDRAIN and GNUG were added to the end of the argument list and were dimensioned as follows:

```

LOGICAL ISDRAIN(NBCN)
DOUBLE PRECISION GNUG(NBCN)

```

These changes were made to allow coding in BCTIME to use the values of ISDRAIN and GNUG in setting time-dependent boundary conditions. However, time-dependent boundary conditions were not used in this work.

Subroutine BOUND

Arrays ISDRAIN, GNUG, and CMNT19 were added to the end of the argument list and were declared as follows, along with local variables CDUM and SPTYPE:

```

LOGICAL ISDRAIN(NBCN)
DOUBLE PRECISION GNUG(NBCN)
CHARACTER CMNT19(NBCN)*100, CDUM*4, SPTYPE*5

```

The section of code that reads in dataset 19 was changed from

```

READ(INTFIL,*,IOSTAT=INERR(1)) IPBC(IPU),PBC(IPU),UBC(IPU)
IF (INERR(1).NE.0) CALL SUTERR(ERRCOD,CHERR,INERR,RLERR)
WRITE(K3,160) IPBC(IPU),PBC(IPU),UBC(IPU)

```

to

```

1 READ(INTFIL,*,IOSTAT=INERR(1)) IPBC(IPU),PBC(IPU),UBC(IPU),
  CMNT19(IPU)
IF (INERR(1).NE.0) CALL SUTERR(ERRCOD,CHERR,INERR,RLERR)
READ(CMNT19(IPU),*) CDUM,CDUM,IDUM,SPTYPE,GNUG(IPU)
IF (SPTYPE.EQ.'DRAIN') THEN
  ISDRAIN(IPU) = .TRUE.
ELSE
  ISDRAIN(IPU) = .FALSE.
END IF
WRITE(K3,160) IPBC(IPU),PBC(IPU),UBC(IPU),SPTYPE,GNUG(IPU)

```

52 Simulation of Ground-Water Flow in the Shenandoah Valley, Virginia and West Virginia

The format for the write statement above was changed from

```
160 FORMAT (7X, I9, 6X, 1PD20.13, 6X, 1PD20.13)
```

to

```
160 FORMAT (7X, I9, 6X, 1PD20.13, 6X, 1PD20.13, 6X, A5, 3X, 1PD20.13)
```

When a line of dataset 19 is read (for example, corresponding to specified-pressure node number IPU), any information following the original three input parameters (IPBC, PBC, and UBC) is stored in entry IPU of a character array called CMNT19. CMNT19(IPU) is then parsed to extract the values of two new parameters, SPTYPE (character string) and GNUG (double precision array). SPTYPE='SPECP' indicates that the node is an ordinary specified-pressure node; SPTYPE='DRAIN' indicates that the node is a drain. Logical array ISDRAIN is defined to permanently store type information for each node in dataset 19: if node IPU is a drain, then ISDRAIN(IPU)=.TRUE.; otherwise, ISDRAIN(IPU)=.FALSE.. GNUG(IPU) holds the value of the conductance v for node IPU.

The parsing of CMNT19 to extract SPTYPE and GNUG assumes that the information following IPBC, PBC, and UBC consists of two character fields (both read into character string CDUM), followed by an integer value (read into integer IDUM), followed by the values of SPTYPE and GNUG. This corresponds to the form of dataset 19 produced by a version of SutraGUI (Winston and Voss, 2004) that has been modified to include a comment field with specified-pressure boundary conditions. The user-specified entry in the comment field in SutraGUI is assumed to be of the form "'SPECP " + *gnug*' for an ordinary specified-pressure node and "'DRAIN " + *gnug*' for a drain, where *gnug* is the numerical value of GNUG for the node.

Subroutine BUDGET

Arrays ISDRAIN, GNUG, PITER, and CMNT19 were added to the end of the argument list and were declared as follows, along with local variable SPTYPE:

```
LOGICAL ISDRAIN(NBCN)  
DOUBLE PRECISION GNUG(NBCN), PITER(NNVEC)  
CHARACTER SPTYPE*5, CMNT19(NBCN)*100
```

Although SPTYPE was declared, it was not used.

The section of code that computes the contribution of each specified-pressure node to the fluid mass budget was changed from

```
TERM = GNUP*(PBC(IP)-PVEC(I))
```

to

```
IF ((.NOT.ISDRAIN(IP)).OR.(PITER(I).GT.PBC(IP))) THEN  
  TERM=GNUG(IP)*(PBC(IP)-PVEC(I))  
ELSE  
  TERM=0D0  
END IF
```

If the node in question is not a drain or the pressure last computed at that node exceeds the external pressure, then the original formula for flow out of a specified-pressure node is used. Otherwise, the flow is set to zero.

Similarly, the code that computes and reports the flow in or out of each specified-pressure node was changed from

```
WRITE(K3,450) I, GNUP*(PBC(IP)-PVEC(I))
```

to

```

IF (.NOT.ISDRAIN(IP)) THEN
  TERM=GNUG(IP)*(PBC(IP)-PVEC(I))
ELSE
  IF (PITER(I).GT.PBC(IP)) THEN
    TERM=GNUG(IP)*(PBC(IP)-PVEC(I))
  ELSE
    TERM=0D0
  END IF
END IF
WRITE(K3,677) I, TERM, CMNT19(IP)
677 FORMAT(18X,I9,10X,1PD15.7,5X,A100)

```

Subroutine SUTRA

Arrays ISDRAIN, GNUG, and CMNT19 were added to the end of the argument list and were dimensioned as follows:

```

LOGICAL ISDRAIN(NBCN)
DOUBLE PRECISION GNUG(NBCN)
CHARACTER CMNT19(NBCN)*100

```

The two sections of code that compute and store the flow in or out of each specified-pressure node based on the latest computed values of pressure was changed from

```

DO 2050 IP=1,NPBC
  I=IABS(IPBC(IP))
  QPLITR(IP)=GNUG*(PBC(IP)-PITER(I))
2050 CONTINUE

```

to

```

DO 2050 IP=1,NPBC
  I=IABS(IPBC(IP))
  IF ((.NOT.ISDRAIN(IP)).OR.(PITER(I).GT.PBC(IP))) THEN
    QPLITR(IP)=GNUG(IP)*(PBC(IP)-PITER(I))
  ELSE
    QPLITR(IP)=0D0
  END IF
2050 CONTINUE

```

and from

```

DO 2475 IP=1,NPBC
  I=IABS(IPBC(IP))
  QPLITR(IP)=GNUG*(PBC(IP)-PITER(I))
2475 CONTINUE

```

to

```

DO 2475 IP=1, NPBC
I=IABS (IPBC (IP))
IF ( (.NOT. ISDRAIN (IP)) .OR. (PITER (I) .GT. PBC (IP)) ) THEN
    QPLITR (IP) = GNUG (IP) * (PBC (IP) - PITER (I))
ELSE
    QPLITR (IP) = 0D0
END IF
2475 CONTINUE

```

In the call to subroutine BCTIME, arrays ISDRAIN and GNUG were added to the end of the argument list. In the call to subroutine BC, arrays ISDRAIN, GNUG, and PITER were added to the end of the argument list. In the call to subroutine BUDGET, arrays ISDRAIN, GNUG, PITER, and CMNT19 were added to the end of the argument list.

The section of code that controls storage of results in the restart (RST) file was changed to force storage of the last solution even if it did not converge. The original code read as follows:

```

IF (IERR.EQ.0) THEN
IF ( (ISTORE.NE.0) .AND. (PRNALL.OR. (MOD (IT, ISTORE) .EQ.0)) )
1 CALL OTRST (PVEC, UVEC, PM1, UM1, CS1, RCIT, SW, QINITR, PBC)
IF ( (IERR.EQ.0) .AND. (ISTOP.EQ.0) ) GOTO 1000
END IF

```

In the modified code, the first and last lines were removed so that the call to subroutine OTRST would not be contingent on IERR=0.

For additional information write to:
New York Water Science Center
U.S. Geological Survey
30 Brown Rd.
Ithaca, N.Y. 14850

Information requests:
(518) 285-5602
or visit our Web site at:
<http://ny.water.usgs.gov>

Yager and others—**Simulation of Ground-Water Flow in the Shenandoah Valley, Virginia and West Virginia**,—Scientific Investigations Report 2008-5002
Using Variable-Direction Anisotropy in Hydraulic Conductivity to Represent Bedrock Structure

ISBN 1-4113-2289-4



9 781411 322899